POLITECNICO
MILANO 1863

SCUOLA DI INGEGNERIA INDUSTRIALE
E DELL'INFORMAZIONE

Self-expandable transcatheter aortic valve finite-element models for patient-specific TAVI simulations

Master's Thesis In
Biomedical Engineering - Ingegneria Biomedica

Authors:
Roberto Taino - 966037
Michela Volpi - 968503

Advisor: Prof. Francesco Migliavacca
Co-advisors: Dr. Giulia Luraghi
Academic Year: 2021-22

Abstract

Aortic stenosis (AS) is the most common heart valves' pathology in the Western world. The standard procedure is the surgical aortic valve replacement (SAVR), that is very dangerous. For this reason, transcatheter aortic valve implantation (TAVI), a mini-invasive method, had been developed. Computational simulations of TAVI have become important: several studies can be found in the literature, divided between the ones using idealised or patient-specific geometries. In this thesis work, structural computational simulations were developed to replicate the implant of the ACURATE Neo2 valve in six patients, reproducing their aortas, natural aortic valves and calcifications. A CAD model of the device has been realized, including the skirt and the leaflets, and discretized. The aortic geometries of the six patients were segmented starting from pre-intervention CT images and discretized. These meshed models were implemented in the solver LS-DYNA and completed by assigning material models. Six patient-specific finite elements (FE) simulations were carried out to replicate the device implant, which was positioned following the patients' angiographies. The quantities analysed were the first principal stresses on the aorta, the deformation of the latter, the Von Mises stresses on the stent and the distance between the stent and the aorta. For all these quantities, their distribution was reasonable and similar in the six patients, except for a few differences, due to the patient-specific anatomies. This thesis work showed the importance of reproducing patient-specific geometries and the correct positioning of the device to obtain FE simulations of TAVI. Different geometries and placements are associated with different stress and deformation responses. This work is not without limitations regarding measurements of the actual device, natural valves reconstructions and device positioning. The mechanical properties for some components should be improved by using more accurate models. These simulations could be simplified by creating a one-dimensional model of the device, discretized with beam-type elements. This would make possible the development of fluid-structure models.

Keywords: TAVI, patient-specific, FEM, *in silico* model

Sommario

La stenosi aortica è la patologia delle valvole cardiache più diffusa in occidente. La procedura standard è la sostituzione chirurgica della valvola aortica, che è molto pericolosa. Per questo motivo, è stato sviluppato l'impianto transcatetere (TAVI), un metodo mini-invasivo. Le simulazioni computazionali della TAVI sono diventate importanti: in letteratura si trovano diversi studi, divisi tra quelli che utilizzano geometrie idealizzate o patient-specific. In questo lavoro di tesi, sono state sviluppate simulazioni computazionali strutturali per replicare l'impianto della valvola ACURATE Neo2 in sei pazienti, con le loro aorte, le valvole aortiche naturali e le calcificazioni. È stato creato un modello CAD del dispositivo, comprendente la gonnellina e i foglietti, e discretizzato. Le geometrie aortiche dei sei pazienti sono state segmentate a partire da immagini CT e discretizzate. Questi componenti sono stati implementati in LS-DYNA e completati con l'assegnazione di modelli dei materiali. Sono state eseguite sei simulazioni agli elementi finiti (FE) patient-specific per replicare l'impianto del dispositivo, che è stato posizionato seguendo le angiografie dei pazienti. Le grandezze analizzate sono stati i primi sforzi principali sull'aorta, le deformazioni di quest'ultima, gli stress di Von Mises sullo stent e la distanza tra lo stent e l'aorta. Per tutte queste grandezze, la loro distribuzione è risultata ragionevole e simile nei sei pazienti, salvo alcune differenze, dovute alle anatomie patient-specific. Questo lavoro di tesi ha dimostrato l'importanza di riprodurre le geometrie del paziente e il corretto posizionamento nelle simulazioni FE della TAVI. Geometrie e posizionamenti diversi sono infatti associati a risposte diverse in termini di stress e deformazioni. Questo lavoro non è privo di limitazioni per quanto riguarda le misurazioni del dispositivo reale, le ricostruzioni delle valvole naturali e il posizionamento del dispositivo. Le proprietà meccaniche di alcuni componenti dovrebbero essere migliorate utilizzando modelli più accurati. Queste simulazioni potrebbero essere semplificate creando un modello 1D del dispositivo, discretizzato con elementi di tipo beam, rendendo possibile lo sviluppo di modelli fluido-strutturali.

Keywords: TAVI, patient-specific, FEM, modello *in silico*

Contents

Introduction

Calcific aortic stenosis (AS) is the most common pathology affecting the heart valves in the Western world, and its burden on the health system is bound to increase as the world's population grows and ages. This pathology is characterized by an obstruction of blood flow through the aortic valve during the ventricular systole. The result is an increase in the valve stiffness and in a progressive narrowing of the valve opening. [1]

The standard procedure is the surgical aortic valve replacement (SAVR), that is an open-heart intervention, making it very dangerous for elderly patients or those with other pathologies. For this reason, the transcatheter aortic valve implantation (TAVI), a mini-invasive method, had been developed. The aim is to reach the heart with a catheter with a valve over it, inserted inside the body from a low invasiveness spot. Transcatheter heart valves are mainly divided in balloon-expandable and self-expandable devices.

In the last years, computational simulations of this intervention have become increasingly important. They can be used to help surgeons in pre-operative planning and to predict the possible outcomes, but also to assist the design of a new device.[2] Several studies can be found in the literature, divided between the ones using idealised geometries[3, 4] or patient-specific geometries.[5–12] All these studies will be addressed and described in more detail in the third chapter.

The aim of this thesis work will be the development of structural computational simulations in order to replicate the implant of a particular device already widely used in clinical practice, the Boston Scientific's ACURATE Neo2 valve, in six different patients, thus reproducing the device in all its components, but also the patient-specific aortas, natural aortic valves and calcifications.

Using the Solidworks software (Dassault Systèmes SolidWorks Corporation, Waltham, Massachusetts, USA), a CAD model of the device has to be realized, including the pericardium skirt and the leaflets. This process will be described in chapter four. The structure of the stent can be obtained starting from some fundamental units, which will be repeated exploiting the symmetries. The skirt and the leaflets are obtained as surfaces. This geometry has to be than discretized, as will be described in chapter five, using ANSA Pre Processor v22.1.2 (BETA CAE Systems, Switzerland). For the stent, hexahedral el-

ements will be used. Triangular elements will be chosen for the skirt, and quadrilateral elements for the leaflets.
To develop patient-specific simulations, the aortic geometries of the six patients (including the native aortic valves and the calcifications) will be segmented starting from pre-intervention contrast-enhanced CT images. Then, all the components have to be discretized in ANSA.
These discretized models will be implemented in the solver LS-DYNA (ANSYS, Canonsburg, PA, USA) and completed by assigning adequate material models to each component. Six patient-specific finite elements (FE) structural simulations will be carried out to replicate the Acurate Neo2 valve implant. The device has to be positioned at the correct aortic depth, following the patients' angiographies. The simulations can be divided into two phases, i.e. the crimping phase and the deployment phase inside the patient-specific anatomy, and they will be described accurately in chapter six.
The results of the simulations will be analysed in META v22.1.2 (BETA CAE Systems, Switzerland). In particular, the first principal stresses on the aorta's wall, the deformation of the latter, the Von Mises stresses on the stent and the distance between the stent and the aorta will be analysed.
This thesis work will show the importance of accurately reproducing patient-specific geometries and the correct positioning of the device to obtain correct structural computational simulations of the TAVI procedure, because different geometries and placements are associated with different stress and deformation responses.
However, the work done will not be without limitations. Most of the measurements of the actual device, the basis of CAD development, will be made using a software and not on the actual valve. In the future, it might be interesting to develop a parametric model of this CAD to study the influence of various parameters on the behaviour of the device. In addition to this, the patients' natural valves will be reconstructed following reference points on the aortas as they can not be obtained from CT images. Obviously, the positioning of the device inside the aortic root could also be inaccurate in some cases because the available angiographies don't always allow clear information to be obtained.
Finally, the mechanical properties that will be used for some components could be improved by using more complex and accurate models and data from pathological aortic roots.
The simulations developed in this thesis could eventually be simplified by creating a one-dimensional model of the device, which can be discretized with beam-type elements. this would also make possible the natural continuation of structural simulations, i.e. the development of fluid-structure models.

1 | Anatomy and pathology

In this chapter, some information will be given about the anatomy of the heart, and more specifically the aortic root and the aortic valve, its physiology and the pathologies it bears. It is indeed of great importance to know and understand these aspects in order to tackle the remaining work.

1.1. The heart

The heart is a muscle that assumes the function of a pump. It collects the deoxygenated blood from the body tissues and pumps it into the lungs, then collects the freshly oxygenated blood and pumps it again toward the tissues. It is located in the thorax in an oblique position, to the left of the midline, behind the sternum and the costal cartilage.[13] This organ can be divided into a left and a right part, thus corresponding in two pumps working in series. The right and the left heart are divided by a wall called septum (inter-atrial and inter-ventricular). The right heart pumps blood into the pulmonary circulation, while the left one is responsible for the systemic circulation. The right and the left heart are composed of two chambers each. The superior ones are called atria and collect the blood, while the inferior ones are called ventricles and they have the function to distribute the blood flow.

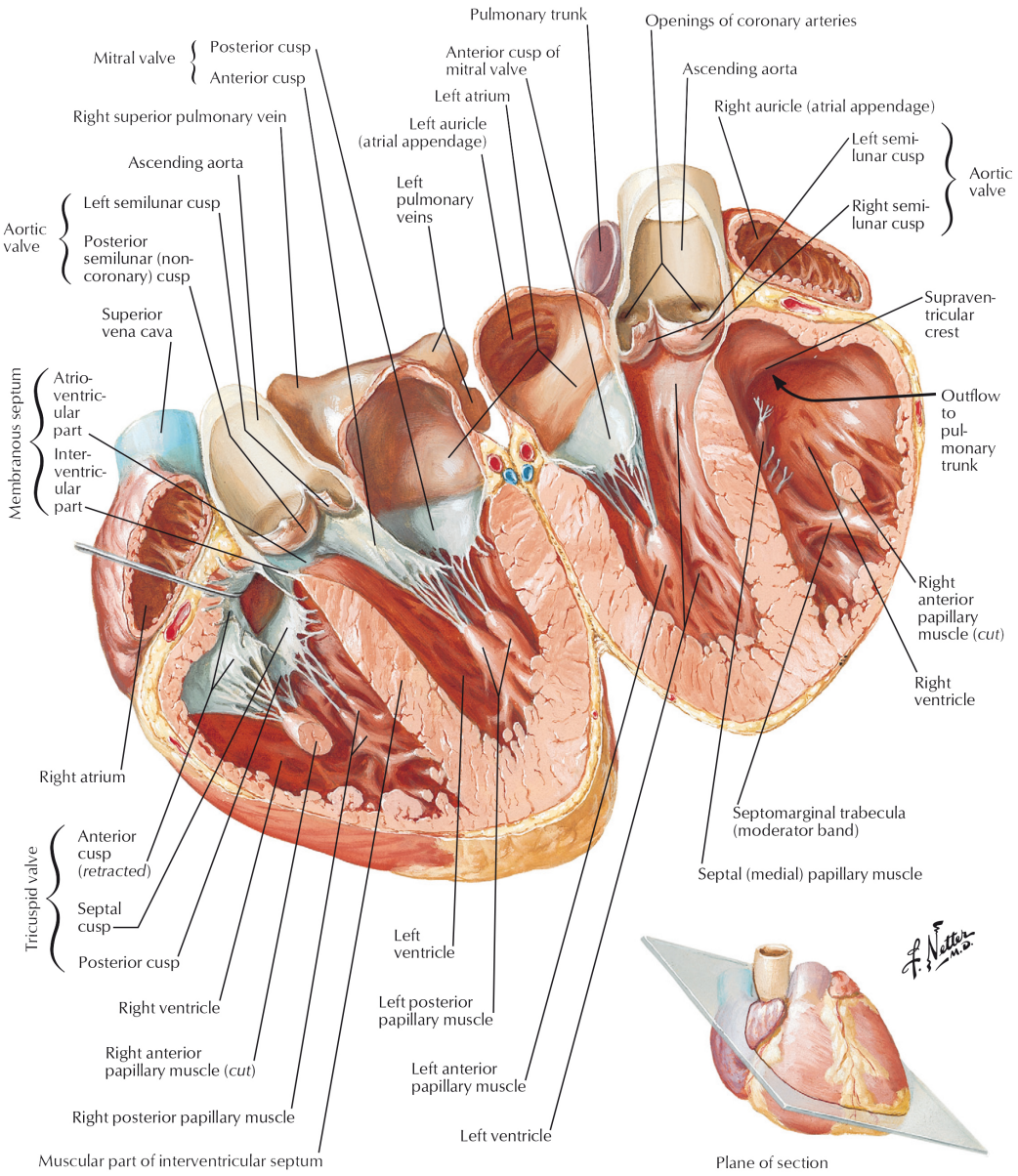

Figure 1.1: *Section of the heart.*[14]

The wall of the heart consists of three layers:

- The external epicardium, a connective tissue with the function of lubricating and protecting the heart;
- The myocardium, the actual cardiac muscular tissue composed of highly specialised cells capable of conducting an electrical signal and contracting to ensure proper heart function;
- The internal endocardium, a sheet of epithelium.[13]

The flow of the blood inside the heart follows only one direction thanks to the presence of four valves, placed on a plane called valvular plane. The atria and the ventricles are divided by the atrioventricular valves, that are, respectively, the tricuspid valve for the right heart and the bicuspid or mitral one for the left heart. Their names are indicative of the number of leaflets present into the valves. Between the right ventricle and the pulmonary artery there is the semi-lunar pulmonary valve, while the left ventricle and the aorta are divided by the semi-lunar aortic valve. Both the semi-lunar valves present three leaflets.

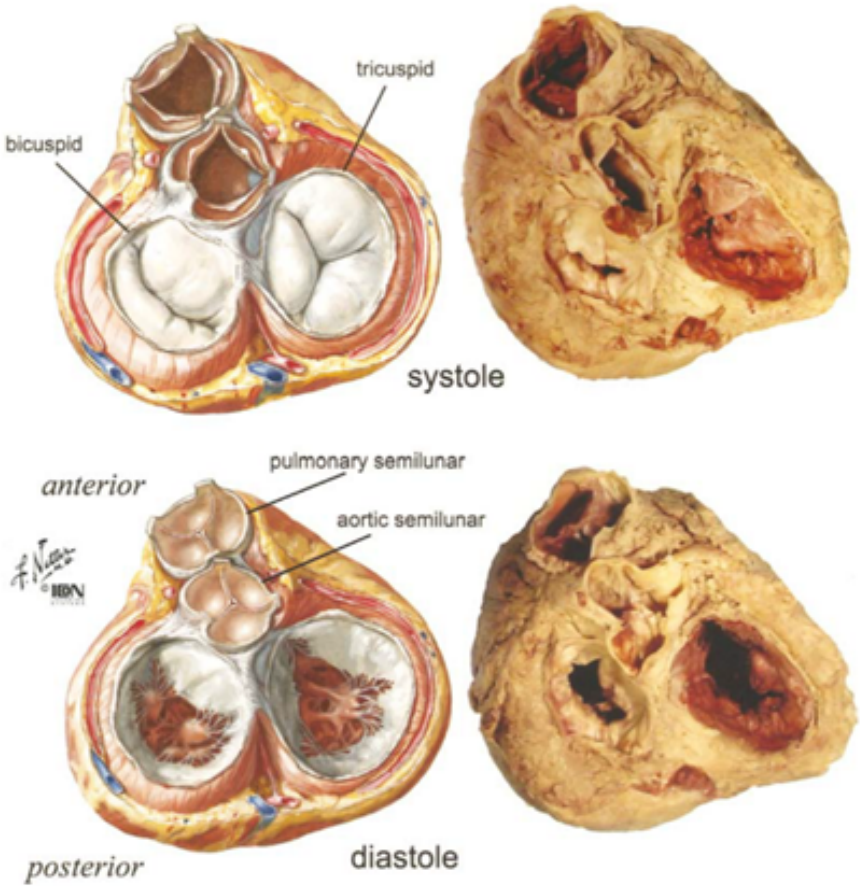

Figure 1.2: *Valves of the heart during systole and diastole.*[13]

The blood flow inside the heart follows only one direction thanks to the presence of four valves, placed on a plane called valvular plane. The atria and the ventricles are divided by the atrioventricular valves, that are the tricuspid valve for the right heart and the bicuspid or mitral one for the left heart. Their names are indicative of the number of leaflets present in the valves. Between the right ventricle and the pulmonary artery, there is the semi-lunar pulmonary valve, while the left ventricle and the aorta are divided by the semi-lunar aortic valve. Both the semi-lunar valves present three leaflets.

1.2. The aortic root

The aortic root is a complex structure that connects the left ventricle with the ascending portion of the aorta, and it includes the sinuses of Valsalva, the valvular leaflets and the fibrous interleaflet triangles. The aortic root is delimitated distally by the sinutubular junction which is where the sinuses interject with the ascending aorta. The proximal edge of the aortic root is defined by a virtual ring that connects the base of the valvar leaflets, known as the basal attachment. This boundary is only virtual because the leaflets describe a semilunar-like profile that, seen in three dimensions, creating a crown-like ring.[15] Those semilunar profiles demarcate the haemodynamic boundary between the ventricle and the aorta: all the structure situated proximally to those attachments are subjected to ventricular pressures, while everything that is placed distal to those attachments is subjected to arterial pressure.[16] This structure is usually used by surgeons in order to suture a valvular prosthesis.[17] The last ring that can be found inside the aortic root is called anatomic ventriculoarterial junction: this is where the ventricular myocardium terminates and leaves space to the wall of the aorta.

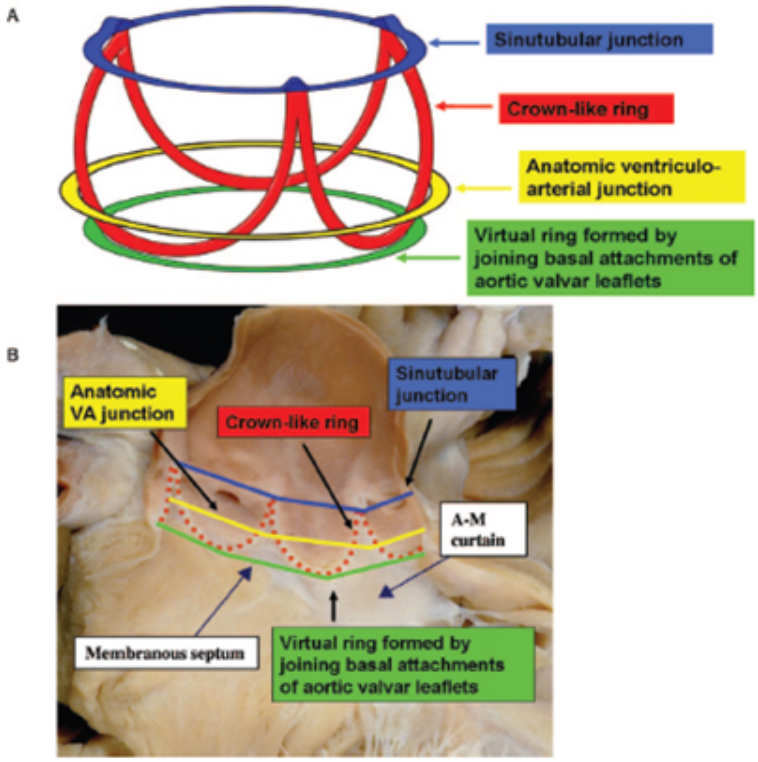

Figure 1.3: *a) Three-dimensional arrangement of the rings in the aortic root; b) The location of the rings in the aortic root with the leaflets of the valve removed.*[15]

The aortic root is characterized by three bulges, called sinuses of Valsalva, running from the basal attachment to the sinutubular junction. Two of the sinuses contain the origins of the coronary arteries and, because of that, are respectively called right and left coronary sinuses. The third one is called posterior or non-coronary sinus because it doesn't give rise to any coronary. When the valve is closed, the sinuses act as reservoirs: the blood is trapped in the sinuses, helping the valve closure during the ventricular diastole and filling the coronary arteries. During the ventricular systole, the leaflets open inside the sinuses and blood can flow with very little or no resistance: the blood vortices inside the sinuses prevent the contact between the leaflets and the walls of the sinuses, ensuring the non-occlusion of coronary arteries.[18] The semilunar attachments of the leaflets inside the aortic root form three portions of the wall called interleaflet fibrous triangles between the leaflets themselves and the basal attachment.

1.3. The aortic valve and its dynamics

The aortic valve is normally composed of three leaflets, called the corresponding sinus of Valsalva. Those leaflets are characterized by a free margin and a margin attached to the aortic root creating a semilunar profile, as we described before. The hingelines of adjacent leaflets meet in the sinutubular junction, forming the commissures, responsible of transferring the load to the aortic wall. The free edges overlap in a region called coaptation region, or lunula. This is originated thanks to a band in the radial plane of the leaflets and is fundamental for the transfer of the load from the centre of the leaflets to the commissures. At the centre of the free edges, there is the node of Arantius which helps the complete closure.[17]

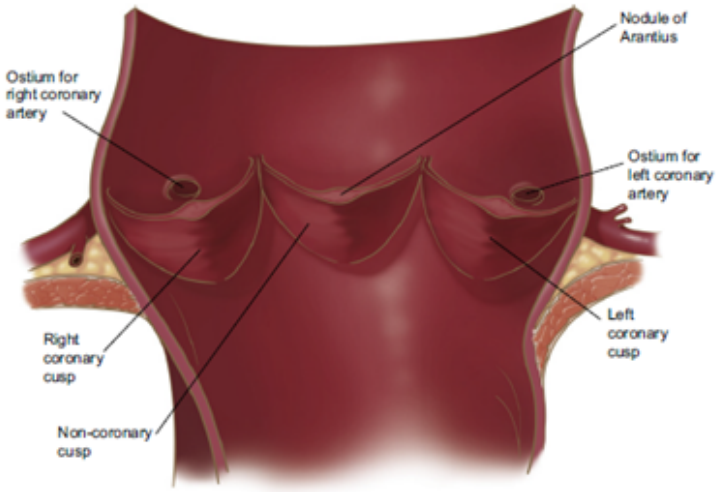

Figure 1.4: *The aortic valve and its components.*[19]

All the leaflets present a smooth surface facing the ventricle, while the aortic side presents some ripples. The thickness of the leaflets grows moving in the direction of their free margin. With regard to the sizes of the leaflets, variations exist among individuals and also in the same individual. It was found that generally the non-coronary leaflet is the one with the largest mean area and weight.[20] The leaflets are composed of three layers:

- The fibrosa, the thickest one consisting of a network of type I collagen fibres aligned in the circumferential direction, parallel to the free margin. This layer is believed to be the one sustaining most of the load. It faces the aortic lumen.
- The spongiosa, a watery connective tissue that contains glycosaminoglycans and proteoglycans that help the deformation and are believed to be responsible for the lubrification between adjacent layers.
- The ventricularis, a network of collagen and elastin that faces the ventricle. The fibres of elastin are aligned radially to reduce the radial strain caused by the blood flow while the valve is open.

As we can see the main components of the ECM are collagen, elastin and proteoglycans. The collagen fibers are responsible for the mechanical strength while the elastin helps the collagen return to its original state. Finally, the proteoglycans take on the function of shock absorbers. The different alignments of the fibers present in the ECM are responsible for the anisotropic and viscoelastic mechanical properties of the valve.

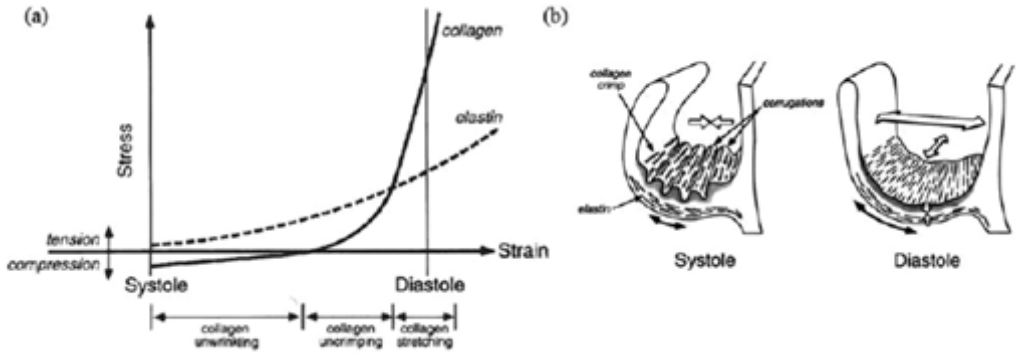

Figure 1.5: *a) Mechanical behaviour of collagen and elastin during the cardiac cycle; b) Representation of the aortic leaflet during systole and diastole.*[17]

The leaflets are avascular, so the nutrients are carried by the surrounding blood. On the country, they are richly innervated. The cellular fraction of the aortic valve is composed of the valvular endocardial cells (VEC) and the valvular interstitial cells (VIC). These cells are fundamental in order to guarantee the complex behaviour of the valve. During

the ventricular systole, the ventricle starts contracting and this leads to an increase in the pressure of the blood contained in this chamber. When the intraventricular pressure becomes greater than the pressure in the aorta (about 80 mmHg) the aortic valve opens, with minimal resistance to the flowing of the blood. In a healthy valve, the opening happens in 20-30 ms. Once the pressure value of 120 mmHg is reached, blood flow begins to decrease due to the end of the ventricle contraction. This decrease is accompanied by a deceleration of the blood and they cause the reversion of the pressure gradient: the valve closes when the pressure in the aortic arch is less than that in the ventricle.[21] The velocity profile of the blood through the aortic valve is laminar and normally flat.[17]

1.4. Valvular Heart Disease

Heart valves can be subject to pathologies that compromise their functioning and, consequently, that of the entire heart, causing significant problems for the individuals concerned. The valves can be affected mainly by two pathologies:

- Valvular insufficiency (or regurgitation, incompetence), occurs when the leaflets can't close completely, resulting in a backward flow referred to as "regurgitant flow";
- Valvular stenosis, occurs when the tissue of the valve leaflets becomes stiffer. This change causes the decrease of the valve opening, thus generating a greater resistance toward the blood flow.[22]

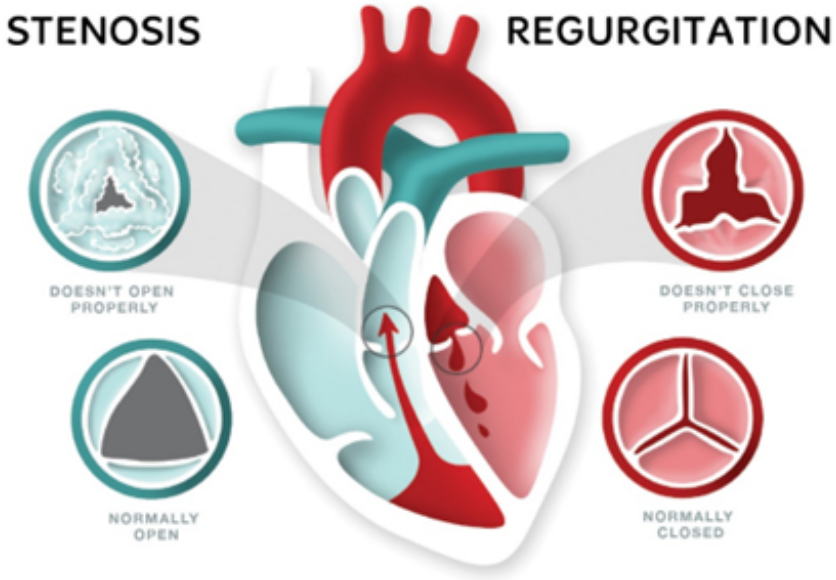

Figure 1.6: *The diseases of the valves.*[23]

1.4.1. Aortic stenosis

Calcific aortic stenosis (AS) is the most common pathology affecting the heart valves in the Western world, thus constituting a major burden on the healthcare system. It is characterized by an obstruction of blood flow through the valve during the ventricular systole, causing an increase in the pressure that the left ventricle must win in order to distribute the blood flow. The leaflet became thicker, fibrous and calcified, resulting in increased valve stiffness, decreased deformability and finally in a progressive narrowing of the valve opening. In order to eject the same volume of blood the left ventricle has to increase its work, leading to its hypertrophy.[1] In the past it was believed that this process was due to "time-dependent wear-and-tear of the leaflets with passive calcium deposition".[24] Nowadays it has been found that AS is an active disease, involving biochemical, biomechanical and genetic factors.

The leading event of this process is believed to be an endothelial damage, like in early atherosclerotic lesions, caused by an increase in the mechanical stress and a decrease in the shear stress. The values of the shear stress are higher on the right and left leaflets because of the coronary flow, while the non-coronary cusp is subjected to lower shear stress: therefore the latter is the most frequently involved leaflet in AS. Regarding the mechanical stress, the higher values can be found on the aortic side of the leaflets, concentrated near their attachments on the aortic root. Those endothelial damages cause an inflammatory response and allow lipids to penetrate the endothelium and to accumulate, further intensifying the inflammation. The inflammatory cells observed in early aortic valve lesions are macrophages and T cells that release proinflammatory and profibrotic cytokines, fundamental for the following steps of the process. At this point, the valve became thicker and fibrotic thanks to the accumulation of fibrotic tissue and to the remodeling of the extracellular matrix. Fibroblast-like cells can be found inside the tissue: a subpopulation of these cells then differentiate into myofibroblasts. The last stage of the process is the calcification. Microscopic areas of calcification are present since the early stages, localizing where there is the lipid deposition and probably caused by cell death and by the release of the apoptotic bodies: those nodules contain hydroxyapatite and are deposited on a matrix made of collagen, osteopontin and other bone matrix proteins. The progression of the calcification is due to a subset of valvular myofibroblasts that are an osteoblast phenotype. The calcifications go through a remodelling process that can lead to active bone formation in about 20% of cases. In the remaining cases, the deposit appears as an amorphous structure without cells.[1] Some studies found two different patterns of calcification, forming in the lunulas and/or radially from the cusp attachment to the center of the valve. Those are the sites where the greatest flexion stresses occur,

suggesting that biomechanical factors may have a role in valve calcification.[25] Finally, the entity of the hypertrophic response is only weakly associated with the severity of the obstruction; instead, it appears to be more correlated to other factors such as advanced age, male sex, obesity and genetic factors.

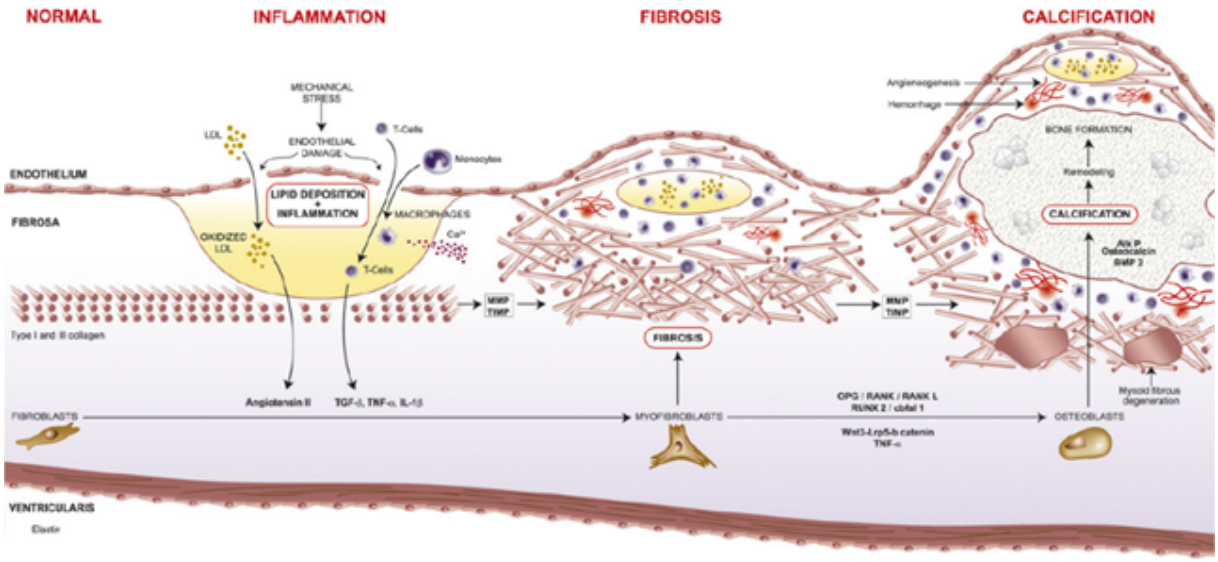

Figure 1.7: *Pathological processes that lead to aortic stenosis.*[1]

1.4.2. Incidence of AS

The incidence of AS was researched in three different studies, two in the USA, with a population of 11.911 and 5.201 individuals, and one in Finland, with a population of 577 individuals. Those researchers have highlighted an incidence near the 2% in individuals with an age between 70-80 years. The prevalence of AS increased strongly with age, reaching 3-9% after the age of 80 years.[26] In particular, in the first USA study, echocardiography was performed on the patients and it was found that the prevalence of moderate or severe AS was age-dependent from 0.02% in subjects aged 18–44 years to 2.8% in patients aged $\geq$ 75 years.[27] A significant increase in these diseases was reported for each increment of 10 years of ageing. This trend is similar in other developed countries: in these areas, the increase in life expectancy has led and will continue to lead to a growth in the incidence of this disease. According to recent projections from The OxVALVE population study in the United Kingdom, the number of elderly people with moderate or severe valvular heart disease, including AS, will be more than doubled by 2056.[28] The global prevalence of AS is expected to increase given the projected increase in the world's population, which is expected to surpass 10 billion by 2100 with Asia and Africa being the most populous regions.[27]

1.4.3. Assessment of the degree of AS

The standard diagnostic method used to evaluate AS is echocardiography, with the aim of assessing the anatomy and the residual movement of the leaflets and the extension of calcifications.[29] The severity of this disease can be assessed by measuring three main parameters:

- Antegrade velocity, or peak jet velocity: it's the maximum velocity measured during the systole across the narrowed aortic valve.
- Mean transaortic gradient: this is the mean pressure gradient between the left ventricle and the aorta during the entire systole. This parameter is found by averaging the instantaneous gradients over the ejection period. The transaortic pressure gradients (ΔP) can be found using the simplified Bernoulli equation:

  $$\Delta P = 4v^2$$

  Where v is the velocity measured.
- Aortic valve area (AVA) by continuity equation: this index is calculated based on the concept that the stroke volume ejected by the left ventricle all passes through the stenotic valve orifice. Thanks to this, the following is obtained:

  $$SV_{\text{av}} = SV_{\text{lvot}}$$

  The volume flow through any crossectional area (CSA) is equal to the CSA times flow velocity over the ejection period so we can rewrite the past equation as:

  $$AVA \cdot VTI_{\text{av}} = CSA_{\text{lvot}} \cdot VTL_{\text{lvot}}$$

  The AVA can be found as:

  $$AVA = \frac{CSA_{\text{lvot}} \cdot VTL_{\text{lvot}}}{VTI_{\text{av}}}$$

General thresholds have been set by the ACC/AHA (American College of Cardiology/ American Heart Association) and ESC (European Society of Cardiology) for categorizing AS severity as mild, moderate, or severe. In some cases, clinical decision-making should consider other parameters.[30]

	Aortic sclerosis	*Mild*	*Moderate*	*Severe*
Aortic jet velocity (m/s)	≤ 2.5	2.6-2.9	3.0-4.0	> 4.0
Mean gradient (mmHg)	-	<20 (<30)	20-40 (30 - 50)	> 40 (> 50)
AVA (cm^2)	-	> 1.5	1.0-1.5	< 1.0

Table 1.1: *Threshold values proposed by ESC and ACC/AHA.*

It is also important to evaluate the progression of the disease by subjecting the patient to serial echocardiography, with the timing of examination depending on the severity of AS and on the clinical status of the individual in question. In addition to echocardiography, other diagnostic techniques such as CT and PET are also used. CT can quantify the mass, the density, and the volume of macroscopic valvular calcification, while positron emission tomography (PET) informs about specific biological processes, such as inflammation and calcification.[31]

2 | TAVI

2.1. First operations of heart valves

For severe aortic stenosis, the percent survival can reach 90% at sixty years, before the onset of severe symptoms. In this period there is an increasing obstruction and myocardial overload. Then, when severe symptom occurs, the average survival is about two years.[32] The first solution was aortic valve replacement (AVR), and there is no medical therapy that has shown a similar efficacy. The first successful open heart valve replacement took place in 1960, and since that time this kind of operation saw a rapid increase inside the surgery rooms. However, there are some problems related to this technique. The main problem is that one-third of the patients are not indicated for surgical aortic valve replacement (SAVR): in fact, according to Iung et al. (2005)[33], surgery in the first years of the century was denied in 33% of patients, due older age or left ventricular dysfunction. This can lead to an operative death risk during the operation as high as 10%, and there is another 10% of risk when the patient suffers from chronic renal disease.

2.2. The introduction of TAVI

To solve these problems, a new operation had been implemented: the transcatheter aortic valve implantation (TAVI), a less invasive method to replace heart valves than the open-heart surgery. In this way also high-risk patients can be treated. The aim is to reach the heart with an antegrade catheter with a valve over it, inserted inside the body from a low invasiveness spot (like the femoral artery for example). The valve needs to be placed without sutures, must be biocompatible, with a good hemocompatibility (so it must not increase risk of thrombosis or infection) and durability.[34] The first operation of transaortic valvular implant or replacement was a percutaneous heart valve, made in 2002 in a 57-year-old man with severe calcified bicuspid and other diseases, not related to the heart, like a lung cancer. The post-intervention follow up was good, and the patient could also do some off-bed activities thanks to the clinical improvement. He passed away 17 weeks after the operation, but no episode of heart failure occurred in this time. It is

important to remember that the PHV function was satisfactory on the echocardiography made at 1, 4, 7 and 9 weeks after implantation.[35].

2.3. Patients selection criteria

As seen before for the SAVR, patient selections have a very important role also in the success of TAVI. Usually, the evaluation of the risks of an operation is based on cardiac surgical risk algorithms and anatomical selection criteria.[36] The latter is based on the study of multimodality images, obtained using a combination of angiography, echocardiography and multi-slice computed tomography. A clinical evaluation should still be preferred to the analysis of the results provided by the algorithm. Nowadays there is no algorithm for the TAVI procedure like the ones for surgical patients, but there are some baseline variables that must be counted inside the evaluation, like low body mass, functional status, left ventricular dysfunction, low gradient aortic stenosis, and many more. Referring to the anatomical patient selection criteria, the most interesting aspects are referred to the arterial vasculature and aortic valvar complex. Thanks to this information, it's possible to identify the best access ways and the potential complications of the procedure. To worsen the situation there is the use of large bore catheters and imperfect vascular closure devices, which leads to vascular complications between 2% and 30% of patients undergoing TAVI. The possible evaluation techniques are peripheral contrast angiography and multi-slice computed tomography (MSCT). The former is practical, and cheap, and the quantity of radiation exposure is lower than MSCT, which instead provides a better resolution of the vessels.[37]
In 2021 a committee of members from the American College of Cardiology and the American Heart Association[38] wrote a guideline for the management of patients with valvular heart disease. Those guidelines can be reassumed in ten points:

1. There should be a classification (stages A, B, C, D) of disease stages in patients with VHD.
2. The examination should be correlated with result of tests like ECG, chest x-ray, TTE.
3. There should be a shared decision-making process about the possibility of adopting an anticoagulative therapy for patients with VHD and atrial fibrillation.
4. The evaluation should be made by a multidisciplinary team.
5. The intervention should be based on symptoms or a severe reduction in the systolic function, while an early treatment should be taken in consideration only after the

result of specific tests.

6. The decision about the intervention should be taken considering the lifetime risks, choosing the best valve and the best approach.
7. In case of an intervention for valvular regurgitation a physician must obtain relief of symptoms and prevention of the long-term consequences of left ventricular volume overload. Note that the threshold for intervention now is lower because of lower procedural risks and more durable treatment options.
8. A mitral transcatheter edge-to-edge repair is of benefit to patients who are at high risk for surgery.
9. Patients presenting with severe symptomatic isolated tricuspid regurgitation may benefit from surgical intervention to reduce symptoms and recurrent hospitalizations.
10. TAVI is reasonable in selected patients with bioprosthetic leaflet degeneration or paravalvular leak and absence of active infection.

2.4. Transfemoral approach

There is more than one access for the TAVI that allows the surgeon to reach the heart. The transfemoral approach is the usual and most common choice because it is the least invasive. The physician creates a percutaneously access through the femoral artery and then a wire is advanced in a retrograde fashion across the aortic valve to the left ventricle. The delivery system and the transcatheter valve are positioned over the wire. Is important to check the condition of the peripheral vessels. The first-generation valve delivery system required a 22 Ft sheath and, due to the tortuosity inside the peripheral vessels due to vascular diseases, so those patients required a more invasive approach, to avoid the femoral artery. Nowadays the dimension of the sheath is only 14 Fr, so the transfemoral approach is possible for more patients.[39] An important parameter to evaluate whether the patients may undergo this operation is the sheath-to-femoral artery ratio (or SFAR), the ratio between the sheath outer diameter and the femoral artery minimal lumen diameter (both values are measured in millimetres).[40] This index is a predictor defined by Valve Academic Research Consortium (VARC), evaluated with contrast angiography. Values higher than 1.05 are an indicator of major complications and 30-day mortality. The threshold can change with (1.00) or without (1.10) calcium. Peripheral vascular diseases are not an absolute contraindication for TAVI, but since the peripheral vessels represent access inside the human body, it's mandatory to guarantee the right catheter movement inside.

Some attempt to advance to reach the heart, implant the valve and repair the complications on the way out by percutaneous transluminal angioplasty or stent implantation. Alternatively, peripheral vascular interventions can be performed before the TAVI.[39]

2.4.1. Other transcatheter approaches

The other possible approaches are described in the following table.[39]

Approaches	**Operation needed**	**Advantages**	**Disadvantages**
Transapical	Anterior thoracotomy via the left fifth intercostal space	Can be useful in case of peripheral vascular disease	Performed under general anaesthesia; Post operative pain; Respiratory insufficiency; Myocardial injury; Acute lung injury
Direct Aortic	Partial sternotomy	Useful in case of peripheral vascular disease or pulmonary disease because they may not tolerate a thoracotomy and in patients with prior bypass grafts	Aortic dissection and injury of other thoracic vascular structures
Transsubclavian	Less-invasive incision in the deltopectoral groove	Avoid a thoracotomy and the risk for aortic injury is less than in the direct aortic approach	Not recommended in patients with patent mammary grafts (blood flow through the mammary graft can be compromised)
Transcarotid	Incision in the carotid	Useful in patients that are not candidate for a transcatheter or thoracotomy; done under local anaesthesia	No disadvantages
Suprasternal	Access in the innominate artery	No need of a thoracotomy. Associated with earlier ambulation and shorter hospital length of stay	Needed of a neck extension, so there is neck immobility
Transcaval	Access through the inferior vena cava	Useful in patients who have unfavourable groin anatomy or vessel inaccessibility	No disadvantages

Table 2.1: *Other possible approaches apart from transfermoral approach.*[39]

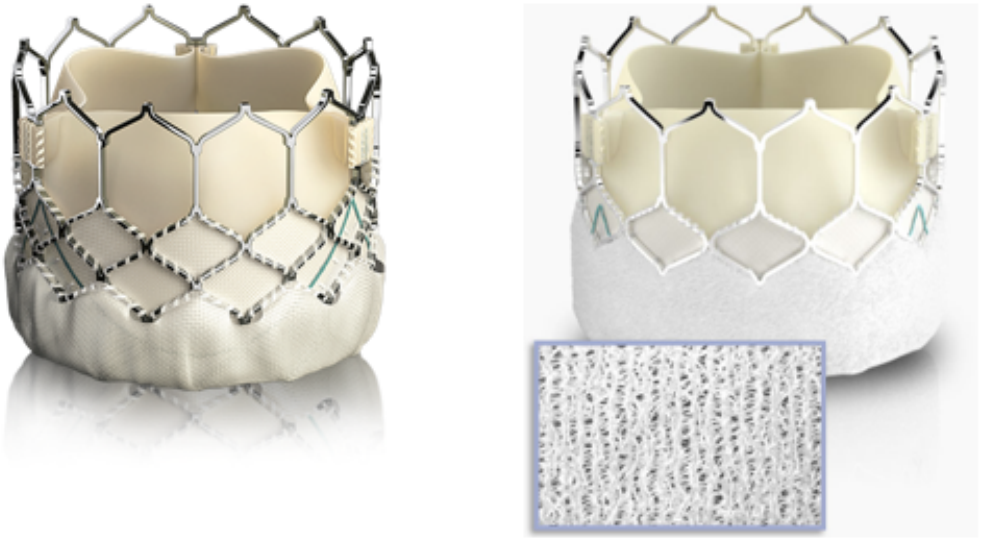

Figure 2.1: *On the left Edwards Sapien 3, on the right Edwards Sapien 3 Ultra THV system.*[42]

2.5. The type of valves

Transcatheter heart valves can be divided by mechanism of the valve frame expansion and leaflets positions. There are four categories: balloon-expandable valves, self-expanding valves, mechanically-expandable valves, and valves for aortic regurgitation.[41]

2.5.1. Balloon-Expanding Devices

The Balloon-Expanding (BE) valves were the first implemented. Valve opening is allowed by a fast balloon expansion during rapid ventricular pacing. This may not be tolerated in diseased patients, for example the ones with a reduced left ventricular ejection fraction or impaired renal function). Those valves are intra-annular, are not repositionable and have a lower profile with respect to the other kind of valves. Thanks to the balloon-release system there is an increased steerability than self-expanding or mechanically-expanding valves, which may help the implant in patients with an aortic angulation greater than 60°, a condition called "horizontal aorta". The first generation of balloon-expanding valves saw the Edwards Sapien and Sapien XT. Nowadays the devices approved by the FDA are the Edwards Sapien 3 and Sapien 3 Ultra THV System. They are made by a cage in cobalt-chromium, while for the valve tissue is used bovine pericardium leaflet. The Edwards Sapien 3 Ultra THV System features a textured fabric made of polyethylene terephthalate (PET) skirt[42] , as we can see in figure 2.1. They can be used in case of severe aortic stenosis or complications related to a biological implanted valve (like insufficient, leakages

or both). The last approval by FDA stans the possibility to use those prostheses also in case of mitral valve's failure in patients in whom a prosthetic ring was already implanted to help the valve to keep its form.Those valves may be used just in patients that face a high risk of death or complications if undergoing open heart surgery. It's important to not use this valve in patients with heart inflammation, where the mitral ring is damaged or that cannot tolerate anti-coagulation drugs.

2.5.2. Self-Expanding Devices

For Self-Expanding (SE) valves there is a wider range of devices than the balloon-expanding ones. In this case the valve is supra-annular, which means lower gradients, lower rate of prosthesis-patient mismatch (PPM) and higher EOA (that is the equivalent orifice area). The EOA is an important index expressed in cm^2 that corresponds to the area of a circular orifice that causes pressure drops equal to those of the valve prosthesis considered. An adequate EOA is important to improve clinical outcomes and lower the PPM (so the valve will have the right dimensions and won't be too small compared to the orifice of the patient). In this case, a rapid ventricular pacing is not requested, and the valves are repositionable and/or retrievable. Of course, this can happen only in exchange for lower steerability.
There are two main productors: Medtronic, with the Medtronic Corevalve, and Boston Scientific, with the ACURATE neo.
The former was the first self-expanding THV. After the Corevalve, Medtronic produced the Evolut R, then the Evolut PRO and PRO+. All these devices (as the ones produced by the Boston Scientific) have CE and FDA approval. Medtronic's CoreValve was the first generation of self-expandable valves. There were multiple studies that assured the lower rate of death of TAVR then SAVR[43], the decrease of major vascular complications and major bleeding[44]. Although, CoreValve wasn't a perfect device. It was relatively bulky, and the catheter had large diameters, which could increase the rate of intraprocedural complications. Its effectiveness relied on operator expertise. There was needed for smaller profile delivery systems which ensure higher safety and easier manoeuvrability. The problems were related to vascular complications, paravalvular leaks, strokes and so on. The next generation of devices, the Evolut R, tried to solve some of them: the valve was tailored in a manner to reduce the height of the prosthesis, while the height of the skirt was the same, but its length was higher, to reduce the paravalvular leak. Also, the delivery system was implemented, allowing a more accurate positioning and complete re-capturability. Studies that followed Evolut R had promising outcomes, however, there have been concerns over the higher incidence of PVL in TAVR with respect to SAVR.

To face this problem, Medtronic developed its latest device, called Evolut PRO. This valve consists of an external pericardial tissue wrap which ensures a reduction in valve regurgitation, maintaining the advantages of the previous generations. This was possible because the external wrap allows an increased surface contact with the native anatomy with the added tissue volume. Doing this the gap between the native anatomy and the prosthesis is reduced.[45].

Figure 2.2: *From left to right: CoreValve, Evolut R, Evolut PRO.*[45]

Boston Scientific's ACURATE neo valve was designed to reduce the post-TAVI complications, such as PVL, PPM or PPI, all associated with long-term mortality. On this device, there are three stabilization arches, that allow the axial self-alignment of the valve within the native annulus, an upper crown (maybe the most important difference from the Evolut line) which consents the supra-annular anchoring that guarantees a minimal protrusion inside the left ventricular outflow tract. The lower crown allows the supra-annular anchoring that guarantees a minimal protrusion inside the left ventricular outflow tract. The implant procedure is very simple: the valve is comprised of a self-expanding nitinol frame.Deployment is made by a top-down and two-step operation, that provides haemodynamic stability during the procedure and allows for stable and predictable release. The radial force exerted by the valve frame is low, and this is a positive factor, in fact it reduces the risk of annular rupture and mechanical injury, especially during implantation.[46] ACURATE neo has demonstrated favorable clinical outcomes with low rates of mortality and PPI, but then was discovered that there was a high incidence of PVL, so an evolution of the device was necessary.[47] ACURATE neo2 keeps key features of the previous valve (supra-annular positioning and the simplified implant procedure), but there is an innovative design, aimed to alleviate some complications of the operation. The skirt is

60% larger, and the delivery catheter has been upgraded with a new tip design, able to reach a wider range of anatomies. There is also a radiopaque marker, which increases the accuracy of the positioning of ACURATE neo2 valve.

Figure 2.3: *On the left Acurate neo, on the right Acurate neo2.*[47]

SE valves' stent are made of Shape Memories Alloys (SMA). Those materials are characterized by two unique behaviors: shape memory effect and pseudo-elastic effect; both can be activated by thermic or mechanic variations. The former is the ability to maintain a deformed shape until a temperature variation restored the original shape, while the latter is the recovery of the original shape after large deformations (previously induced by a mechanic load). Those alloys are made by a particular crystallographic structure that allows recovery of the original shape even after deformation and an applied force. SMAs are made of two solid phases: an austenitic one (stable at high temperatures and with high symmetry) and martensitic one (stable at low temperatures and with low symmetry). There are two possible configurations of martensitic phase: a multivariant one (stress-free, where displacements with respect to the near structures are minimized and there is no macroscopic deformation) and a single-variant one (which instead is stress-induced, there is an alignment alongside the main direction, with a macroscopic deformation). Transformation between two phases is a stress-temperature-induced athermal diffusionless thermoelastic martensitic transformation (TMT).[48]

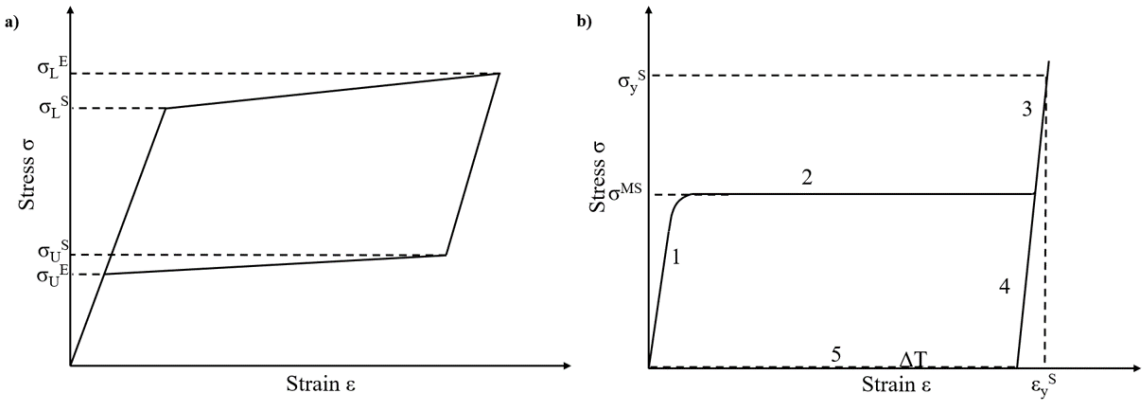

Figure 2.4: *a) Pseudoelastic effect. (1): elastic deformation of austenite; (2): Austenite to single-variant; (3): elastic deformation of SV; (4): elastic strain recovery; (5): SV to austenite. (ε_y^s = single-variant martensite yield strain, σ_y^s = single-variant martensite yield stress. b) Shape memory effect. (1): elastic deformation of multivariant martensite; (2): multivariant to single-variant; (3): elastic deformation of SV; (4): elastic strain recovery; (5): transformation strain recovery (induced by thermal loading ΔT, that increases the temperature to A_f).*[48]

When the temperature is higher than A_f and the stress reaches a value equal to σ^{AS} there is the transformation from the austenitic phase to the martensitic one (the single-variant phase). However, the martensitic phase isn't stable at those temperatures, so when the stress is removed, reaching a value equal to σ^{SA}, there is a variation from the single-variant martensitic phase to the austenitic. When a material is deformed at a temperature lower than a certain value called M_f there is a transformation between the multivariant martensite (a stress-free form) to the single-variant martensite (induced by stress). This happens when stress reaches a threshold value, called σ^{MS}. Then, after a elastic deformation and recovery, there is the transformation induced by thermal loading ΔT, that increases the temperature to A_f , allowing the return to multivariant form. The most common alloy in the SMA's production is the superelastic nickel-titanium (Ni-Ti), or nitinol. Its characteristic of interest is the capacity of maintaining a deformed shape until a temperature variation causes a return to the original shape. It is important for its biocompatibility, fatigue resistances, physiological compatibility (in fact, it is very similar to biologic tissue response). Also, there is excellent magnetic resonance and computer tomography compatibility, which is very useful during follow-up. The term superelasticity is referred to the ability to undergo large elastic deformation. The difference between pseudoelasticity is that the latter shows nonlinear unloading behaviours, while the former exhibit an inflection point.[49]

2.5.3. Mechanical-Expanding Valves

In this typology the expansion is mediated by a mechanical controlled system, and the valves are retrievable, repositionable and intra annular. There is no need for rapid ventricular pacing. This kind of valve includes the LOTUS line, produced by Boston Scientific, but they were recalled due to issues with the delivery system.

2.5.4. Valves for aortic regurgitation

This is a type of valve made for patients with aortic regurgitation. The only valve with a CE certification is the Transapical JenaValve [39][50]. It has an anchor mechanism that allows fixation onto the valve leaflets, allowing the implant also in patients with that disease. Its implantation is safe and effective in patients at high risk for surgery.[51]

2.6. Aim of the study

The aim of this study is to develop a structural computational model consisting of the Acurate neo2 device and the patient-specific anatomies of six patients who underwent TAVI surgery, i.e. aorta, natural valve and calcifications, using the finite element (FE) approach. The simulations developed should trace as closely as possible the actual positioning of the valve within the anatomies, reproducing and comparing it with available angiographies obtained during the six patient operations.
From the results of these simulations, the main quantities of interest will then be highlighted, in order to better understand the procedure, the device and its interaction with six different anatomies.
The role of computational simulations in the biomedical field, and more specifically applied to the TAVI intervention, will be thoroughly investigated in the following chapter.

3 | State of the art

In recent years, computational simulations have become increasingly important within the biomedical field; they are based on the development of complex models of the anatomical site of interest and their resolution by means of numerical calculation software. Their purposes can be diverse: mainly they are used to help surgeons in pre-operative planning and to understand the associated biomechanics, but they can also be developed to optimise and assist the design process of a new device.
The advantages of these *in silico* models include:

- once developed, they allow different implantation scenarios to be simulated, thus representing a very versatile instrument;
- these models make it possible to study very complex problems, that would otherwise be difficult to evaluate except by means of invasive methods or animal experiments;
- the result can be analysed with extremely high spatial and temporal resolution;
- the parameters that can be evaluated are significantly more than the ones that can be studied within an experimental setup;
- the input parameters can be isolated. [2]

All these aspects represent advantages compared to experimental tests. These do not allow precise control of the variables of interest, nor do they make their manipulation so easy. Furthermore, it is not possible to study a large variety of situations without conducting a large number of tests, which entails very high costs and time, as well as, in some cases, high exploitation of animals. However, computational methods are still less used due to the difficulty in accurately and precisely reproducing a biological environment, its mechanical properties and boundary conditions. This limitation results in the need to rely on simplifications, which are inevitably reflected in the results obtained. Therefore, it becomes necessary to validate the models developed against real studies of the phenomenon. To this end, the FDA has formulated some procedures in order to evaluate the credibility of computational modelling in the medical field. Regardless, *in silico* models could speed up the introduction of new devices and procedures, reducing at the same time

in vivo experimentation.

The development of an *in silico* model involves several aspects. In the context of TAVR, the process starts with the development of all the geometries associated with the surgical procedure, then it proceeds with the modelling of the biomechanical tissue response, boundary and loading conditions and then with the start of the numerical calculation. Once the simulation is complete, various types of information can be obtained, depending on the type of analysis conducted. Usually, the first analysis conducted is the structural one, which involves the analysis of mechanical quantities such as stresses and deformations during the crimping and deployment phase of the procedure, using the finite element method (FEM). This type of analysis is what will be addressed in this thesis. The FEM method is based on the discretization of the domain into sub-volumes called finite elements. The equations that dominate the problem are then solved only in few specific points, called nodes and defined by the elements themselves. The set of elements that make up the domain is called mesh. This method allows to find the displacements associated with each node under certain load and boundary conditions and to then derive the deformations and finally the stresses. The equations ruling the problem can be solved numerically by implicit or explicit approaches. In the implicit approach, the displacement are updated based on their solution in the previous time step. In the explicit approach, the equilibrium is imposed, but it is only approximated based on the previous time step. The implicit approach is usually preferred because the approximation is more accurate. Moreover, explicit approximation requires smaller time steps in order to achieve stable convergence. Instead, the explicit approach is favored in cases that include fast and large deformations that can benefit from small time steps.[52]

After FEM, computational fluid dynamics (CFD) analysis can be conducted in order to evaluate parameters associated with the fluid domain of the simulation, i.e. the haemodynamic associated with the post-TAVR configuration. The advantages of this sequential approach are the easy implementation and the limited computational time required. The great disadvantage is the assumption that CFD requires rigid structures.[53]

An alternative to this sequential method is the fluid-structure one (fluid-structure interaction, FSI). In this approach the fluid model is coupled with the structural one, thus making it possible to reproduce more accurately the problem. The setup of FSI is clearly more complex than the one for the CFD and FEM but it's the most effective method in order to assess all the aspect involved in TAVR.[54]

Before analysing the FSI models in the literature, it is necessary to go over the main aspects of these *in silico* models. The first one is the modelling of the geometry. A complete model should include all the components of a TAVR, i.e. the patient domain with the aortic root, the native valve and the calcifications, the transcatheter aortic valve

and the blood domain. Usually, some simplifications can be assumed in order to reduce the complexity and computational time, but they should be done carefully because they may compromise the accuracy. In particular, the patient's domain can be idealised or patient-specific. The latter is based on the segmentation and reconstruction of the aortic geometry from CT or MRI. This method enables the study of very specific conditions but it has some limitations, such as a strong dependence on the image quality and limited reproducibility due to manual steps.[55]

Two other important assumption of a model are the geometry discretization adopted and the materials' properties. The type of elements used defines the degrees of freedom and the integration points. For what concerns the materials' properties, the native tissues and the pericardium of the device are characterized by anisotropic non-linear behaviours that should be considered in the simulations. However, simplifications can be adopted, depending on the aim of the study. Regarding the stent, all the works present in literature use a shape memory behaviour to describe nickel-titanium (NiTi), and an isotropic hardening model for cobalt-chromium.[53] The blood is usually assumed to be an incompressible Newtonian fluid, in region of high shear rates.

Another important element that influences the numerical results is the choice of the boundary conditions (BCs). For patient-specific modelling, the BCs used are obtained from clinical test, such as echocardiography and phase-contrast MRI. Cardiac output, flowrates, flow profiles, pressure measurements and displacements (e.g. leaflet motion and wall deformation) are used in literature. Usually, inlet BCs are flow rates, while pressure is used for outlet BCs. When clinical measurements aren't available, idealised BCs are used.

In TAVR simulations different contacts are present: between the leaflets, between the leaflets and the stent, as well as between the stent and the surroundings. Appropriate contact modelling should be chosen. Typically, among the leaflets, a self-contact is used, although it can cause some issues with body-fitted methods that can lead to unrealistic results. The leaflets are then usually connected with the stent using a tied-type/bonded contact. When the deployment procedure is incorporated, a frictional contact may be applied between the stent and the tissue, allowing the analysis of the contact forces between the native annulus and the stent.

Lastly, turbulence modelling is needed in order to reproduce an accurate situation. With prosthetic heart valves, the blood flow can't be assumed laminar and turbulence effects strongly the flow field. Several methods exist for turbulence modelling, such as direct numerical simulation (DNS), large eddy simulation (LES) and Reynold-averaged Navier-Stokes (RANS).[55]

A model built taking all these aspects into account can be used to estimate several quan-

tities. In literature, in silico models are used in order to assess paravalvular leaks, the need for permanent pacemaker implantation, fluid-dynamic alteration, valve thrombosis, leaflet durability and to study TAVR procedure applied in different pathologies, such as bicuspid aortic valve (BAV), mitral regurgitant, and in patients with previously implanted bioprosthetic valves (valve-in-valve procedure).[53] Although our work will only be based on structural simulations, in the following sub-chapters some FSI models found in the literature will be analysed as they appear to be the most complete and suitable for describing the procedure and the associated haemodynamic. In particular, the works will be divided based on the use of idealised or patient-specific geometries.

3.1. Models with idealised geometries

The use of an idealised geometry is usually associated with the aim of studying numerical methodologies, technical aspects and general clinic questions by simplifying some really complex anatomical structures.
Liu et al.[3] developed a computational model with the aim of studying the influence of different valve flap design on the mechanical properties and flow field of TAVR using a FSI approach. Three different leaflet designs for the same stent were studied in an ideal aortic root design. Abaqus (SIMULIA, Johnston, RI, United States) was first used to simulate the implant of the valve with its crimping and deployment phases. The material of the stent was a nickel-titanium alloy, while the leaflet and the skirt were modelled as linear elastic materials. For the crimping phase, a crimping tool was used. The contact between the inner surface of the rigid cylinder and the outer surface of the stent was defined as face-to face, with a friction coefficient equal to 0.1. After that, the device was released and held in the aortic valve site by the crimping tool. The face-to face contact between the prosthetic valve and the native one was defined as a penalty function contact, and the friction coefficient was set as 0.2. All the sutures present in the device were approximated as a bound contact. After the structural analysis, the FSI simulation was carried out in LS-DYNA (ANSYS, Canonsburg, PA, United States). An "operator-split" Lagrangian-Eulerian method was used. This approach transmits the influence of the moving structure to the fluid through structural forces, and the advection algorithm is used to couple the two domains. The inner wall of the aorta is simplified and considered as the wall of the fluid domain. For the boundary conditions, pressures under the pulsation cycle load found in a previous study were used. Blood was considered a Newtonian incompressible fluid and turbulence was neglected, assuming the flow to be laminar. Regarding the mesh generation, the types of elements used to discretize the two domains were not reported. Using this model it was found that different leaflet shapes have a great impact on the

procedure and its outcomes.

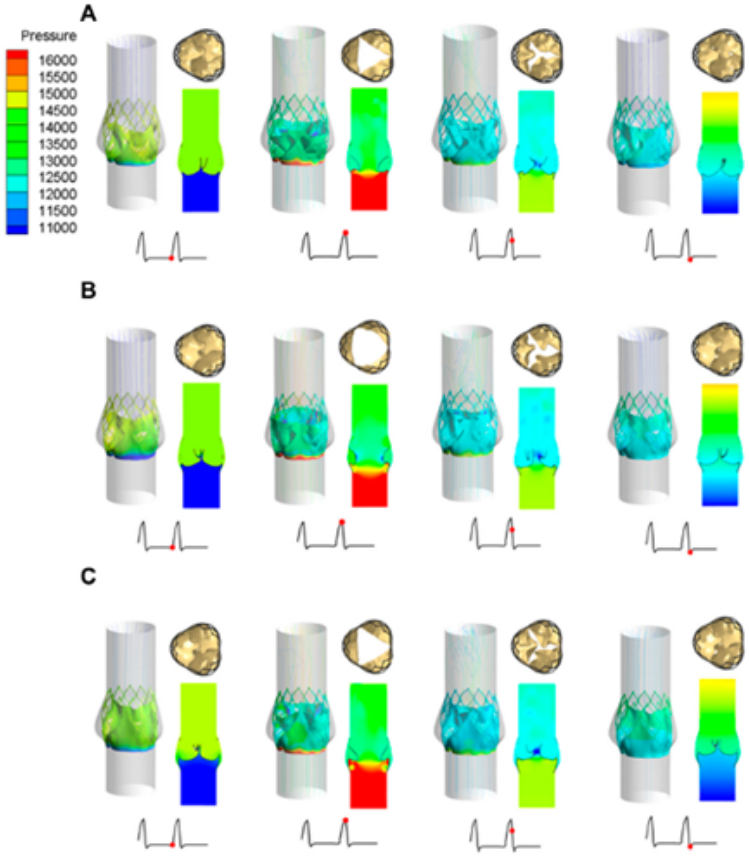

Figure 3.1: *Leaflet states and pressure distribution at four different stages, in the three different leaflets models ((A) valve stent model A, (B) valve stent model B, (C) valve stent model C)).*[3]

Wald et al.[4] developed a simplified 2D model in order to assess the haemodynamic in healthy, AS and TAVI conditions. The simulations were carried out with the commercial package ADINA (ADINA R&D, Inc. v. 9.0.0). The geometries created included the aortic root, the leaflets and the coronary arteries. The physiological native valve and the aortic root were reconstructed based on a 3D experimental model. An arbitrary Langrangian-Eulerian (ALE) method was selected for the coupling between the solid and the fluid domain. The solid mesh used 4-node quadrilateral plane strain elements, while the fluid one used a combination of 4-node quadrilateral and 3-node triangle plane elements, with some refinements near the boundaries. For the material modelling, blood was assumed to be Newtonian, incompressible and homogenous. The leaflets were modelled as linear elastic. Five cases were studied: one healthy, two stenotic (mild and severe), with a uniform calcification along the leaflets, and two types of TAVI models (short and long).

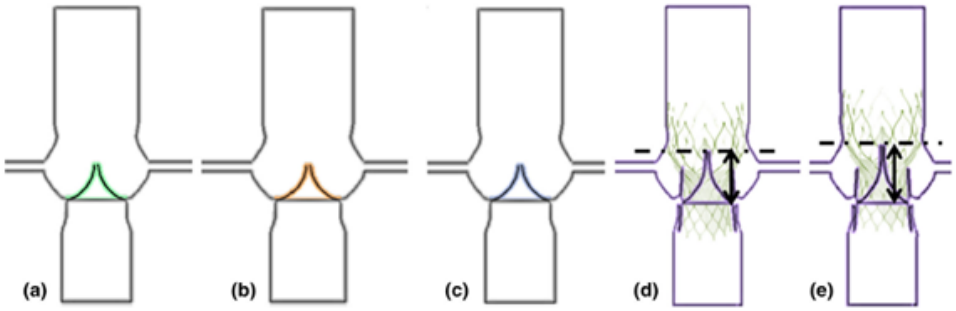

Figure 3.2: *Geometric models of the five cases: a) healthy case, b) mild stenosis, c) severe stenosis, d) short TAVI and e) long TAVI.*[4]

The geometry of the TAVI case was based on commercially used TAVI devices. In all five cases identical idealised boundary conditions were applied. A contact algorithm between the two valve leaflets based on a frictionless and elastic contact model was used. The main limitations of those models were the 2D geometry and the idealised boundary conditions, but also the choice of linear elastic properties for the leaflets could represent a problem, especially in the stenotic cases. Finally, the laminar flow assumed may negatively influence the results. The aortic flow may undergo a transition between laminar and turbulent flow, but this is difficult to model.

3.2. Models with patient-specific geometries

Patient-specific modelling has been adopted in the later years because of its prospect to study patient outcomes and therapies. This approach is obviously more labor-demanding and requires more time, compared to the idealized ones. The great advantage is the possibility to reproduce a more realistic representation of the clinical situation.
In order to assess PVL, geometric and effective orifice areas, the mechanics of the prosthetic leaflets and the fluid stresses for different implantation depths, Gosh et al.[5] developed an FSI model. The anatomy was based on SIMULIA Living Heart Human Model (LHHM), which is a validated 3D model that was modelized as an anisotropic hyperelastic material and that can reproduce patient-specific geometries.The patient-specific calcifications were introduced on the native aortic valve as a homogeneous linear elastic material. The stent of the prosthetic valve was modelled as superelastic nitinol, while the leaflets were defined as isotropic hyperelastic material. For what concerns the blood, a Newtonian fluid model was adopted.

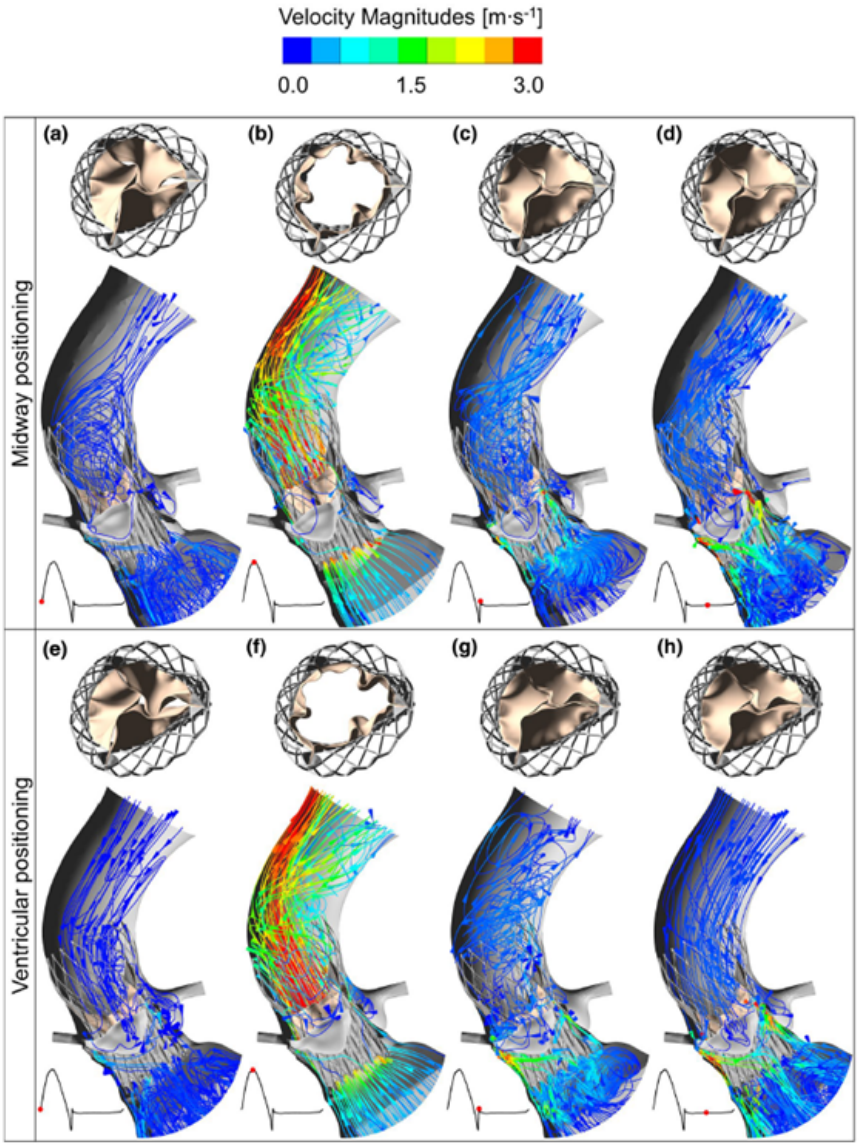

Figure 3.3: *Flow velocity streamlines at four different moments of the cardiac cycle in midway and ventricular positioning.*[5]

A partitioned technique was used in order to solve the fluid and the structural domain; in particular, a body-fitted sub-grid geometry resolution (SGGR) method was chosen. LHHM components and stents were idealized as stationary structures. The BCs allied were time-dependent pressure waveforms at the ventricular and aortic side, while time-dependent flow was imposed at the coronary outlet. In this study, given the transient nature of turbulence in the presence of a prosthetic valve, a turbulence model was adopted. About the mesh, the LHHM native aortic valve and the calcifications were discretized with four-node tetrahedral elements, while the TAVR device was discretized with eight-node reduced integration hexahedral elements. The analysis conducted with this model was

used in order to find optimal TAVR valve implantation depths. The FSI simulation can be improved by modelling deformable anatomy structures. Another improvement can be done by including the prosthetic leaflets prestress due to crimping.
Luraghi et al.[6] developed a patient-specific FSI simulation in order to investigate how the clinical data affects the numerical results of *in silico* models of the AS pathological condition.

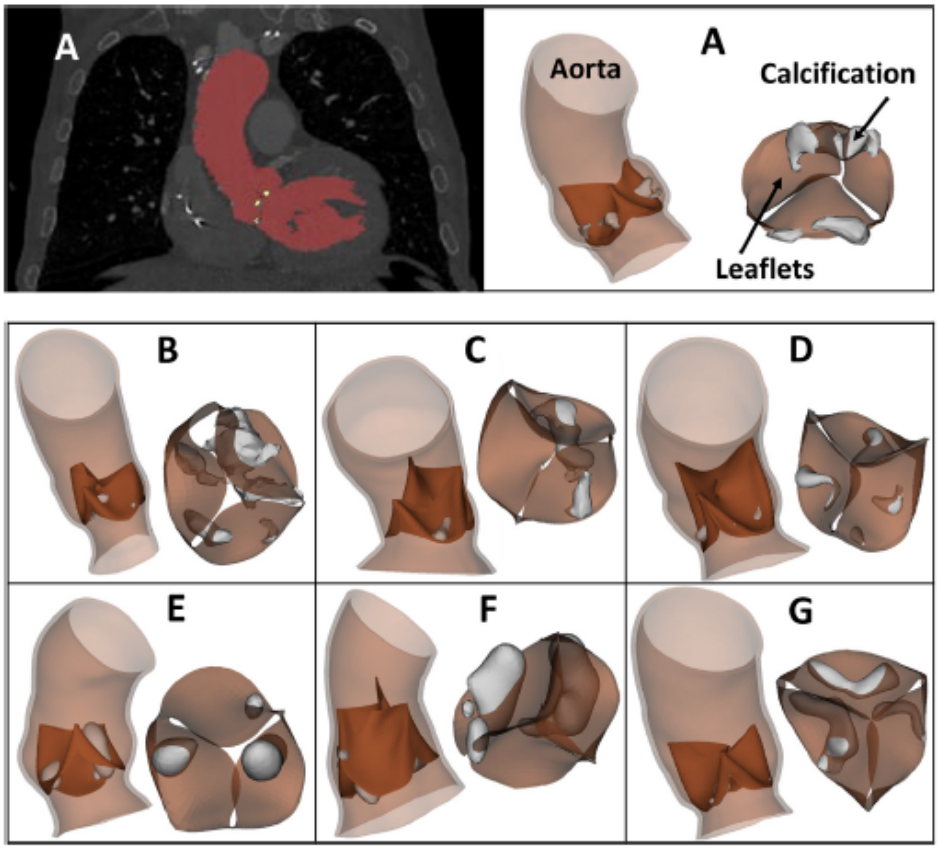

Figure 3.4: *A) Example of segmented CT image and reconstructed geometries of aorta, native valve and calcification for the first patient. From B to G) geometries of all the other patients.*[6]

The CT scans of the patients' aortic vessels were processed with Mimics (Materialise, Leuven, Belgium) and then discretized with hexahedral tri-linear fully integrated solid elements. The fluid domain was discretized with hexahedral elements. The valves were discretized using quadrilateral bi-linear shell elements with one-point integration and viscosity hourglass control, while for the calcifications tetrahedral elements were used. The aortic tissue was assumed to be anisotropic and hyperelastic, while the native valves and calcifications were modelled as linear elastic. For blood, a Newtonian fluid model was used. As for the BCs, only one patient had available pressure curves; for the other a physiological idealised waveform was scaled in order to be consistent with the patients'

maximum and minimum pressure values. Both ends of the aorta were fixed. Finally, for what concerns the contacts, node-to-surface tied ones were defined between the commissural edges of the native valves and the internal surface of the aorta, while surface-to-surface tied contacts were chosen between the calcifications and the leaflets. In order to solve the FSI model, the "operator split" Lagrangian-Eulerian method was used in LS-DYNA 971 R10.0 (LSTC, Livermore, CA. USA). The main limitations of this work are the not patient-specific tissue material properties and the use of hyperelastic models for the valve leaflets and elastoplastic models for the calcifications. In addition, the native valve was reconstructed from reference points of the patient-specific aorta because it was not possible to segment it. However, the developed model can be used to simulate the implantation of the TAVR and could help clinicians.
In another study, Luraghi et al.[7] used this model introducing also the TAVR device. The stent was discretized with hexahedral linear elements with reduced integration and hourglass control, while the leaflets were discretized with quadrilateral linear shell elements with one point integration and viscosity hourglass control. Triangular membrane elements with viscosity hourglass control were used to discretize the skirt of the prosthesis. For the mechanical properties, the stent was assumed to be pseudo-elastic NiTi, while the leaflet and the skirt were modelled as linear elastic. The stent and the pericardium were connected with a node-to-node contact and a penalty self-contact was defined between the three leaflets. The simulations consisted of three steps:

1. Insertion of the crimped device;
2. Transcatheter aortic valve implantation;
3. Two cardiac cycles after the implantation.

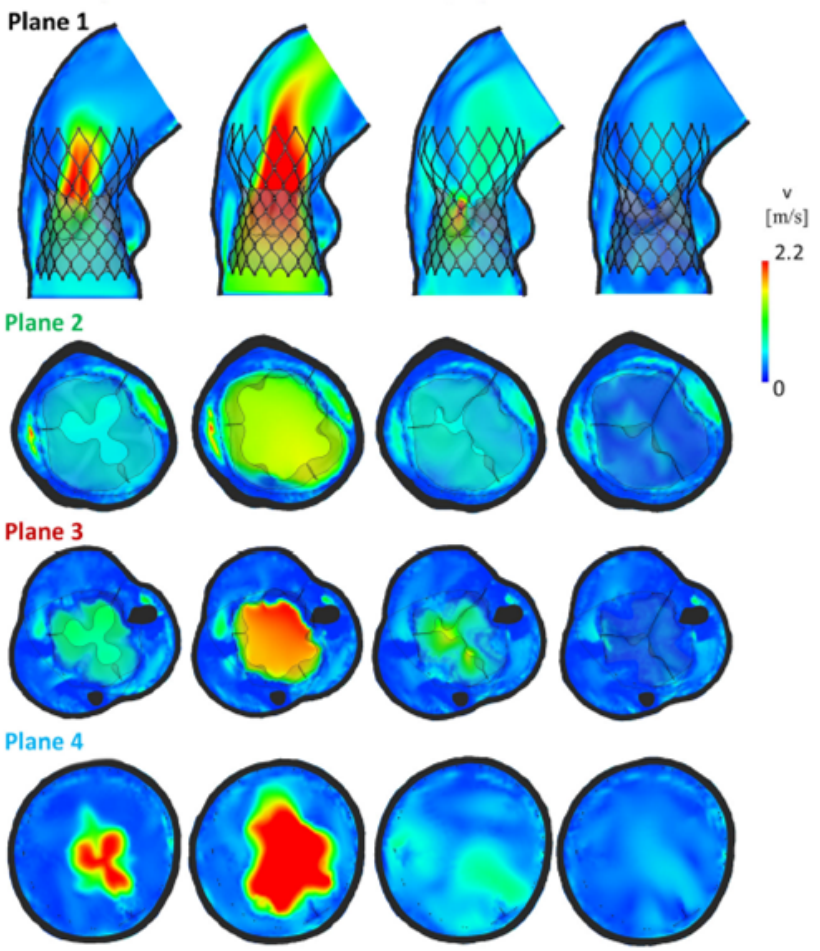

Figure 3.5: *Velocity magnitude of the blood domain on four planes.*[7]

Some aspects can be improved. For example, the pre-stress field on the aorta should be included and the pathological aortic root's material properties of the patient domain should be used. In order to better understand clinical outcomes, the inclusion of the coronary arteries could be useful. Turbulence model was not considered in this work. Finally, this model entails very high computational costs.

Another FSI simulation is implemented to investigate the relationship between PVL and the severity of leaflet calcification in a patient-specific aorta model by Basri et al.[8] A 3D patient-specific aorta was created and assumed to be linear elastic. The flow was modelled as turbulent, incompressible and Newtonian. The mass flow rate and pressure are considered as the respective inlet and outlet with the condition of pulsatile blood flow. The interaction between fluid and solid domains is coupled in a two-way approach by an immersed boundary method.

Two FSI simulations were developed by Kandail et al.[9] in order to study the impact of annular vs supra-annular positioning of a TAVR prosthesis. Patient-specific geometries

for the aortic root, ascending aorta and coronary arteries were reconstructed based on post-operative CT scans. FSI simulations were carried out using the SGGR method. The stent and pericardium elements of the device were meshed using linear hexahedral elements and quadratic tetrahedral elements, respectively. Only the pericardium parts were modelled as a compliant body, while the stent and the aortic wall were considered rigid. The leaflets and the skirt were hypothesised to be linearly elastic and stitched to the metallic frame with tie constraints. The flow was assumed to be laminar and blood was considered to be incompressible and Newtonian. Time-dependent flow waveforms were imposed at the inlet and at the coronary outlets, while a pressure waveform was used at the aortic outlet of the ascending aorta.

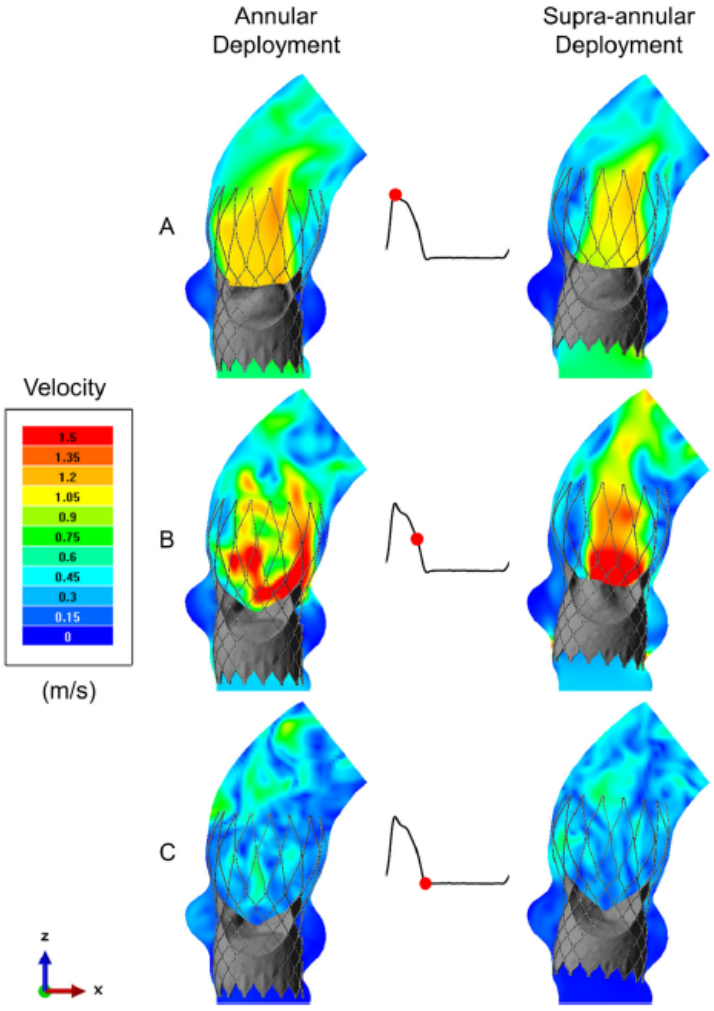

Figure 3.6: *Velocity contours at annular (left column) and supra-annular depths (right column) during three different instants (A, B, C) of the cardiac cycle.*[9]

Diseased native valve and calcifications were not included in the model. The rigid wall assumption of the aorta is one of the main limitations of this study, in addition to the

absence of residual stresses in the valve leaflets after deployment.
Li et al.[10] presented an FSI model to compare the difference in outcomes between the balloon-expandable valve and the self-expandable valve. The anatomical site was patient-specific and based on clinical image data. The native leaflets and calcification were meshed with tetrahedral elements, while the aorta was meshed into wedge grids and assumed to be linear elastic. The stent was instead discretized with hexahedral elements. The balloon-expandable stent was modelled as elastic-plastic, while the self-expandable one as hyperelastic. Both the cuff and balloon were linear elastic material. The leaflets of the prosthetic valve were discretised with shell elements and the constitutive model used was the isotropic incompressible hyperelastic one. All the solid elements were treated as rigid bodies, in order to reduce the computational cost and time required. The blood was assumed to be weakly compressible Newtonian fluid. For the BCs, left ventricular pressure and aortic pressure were applied at the inlet and outlet of the model, respectively, by using waveforms from the literature. The immersed boundary method was adopted to solve the fluid-structure interaction.

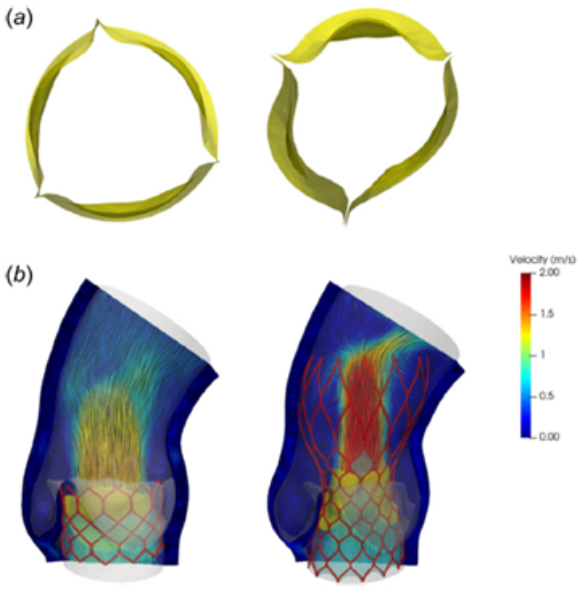

Figure 3.7: *a) Full valve opening of balloon-expandable valve on the left, and self-expandable valve on the right; b) systolic flow distribution and streamlines in the case of balloon-expandable valve (left) and self-expandable valve (right).*[10]

FSI models were also used by Pasta et al.[11] to simulate TAVR in stenotic bicuspid patients, in particular in order to assess the PVL. Patient-specific aortic root and calcifications from CT images were reconstructed. With ICEM meshing software (Ansys v.18, ANSYS, Inc.), the aortic root surface and the native leaflet were discretized with struc-

tured quadrilateral shell elements with reduced integration. Calcifications were meshed by a combination of hexahedral and tetrahedral solid elements. Structured hexahedral solid elements with reduced integration were used to discretize the stent, while the sealing skirt was discretized with structured quadrilateral shell elements. The aortic wall and native leaflets were idealised as hyperelastic and isotropic materials. Calcifications were considered linear elastic, while plasticity and isotropic hardening were adopted for the metallic frame. The skirt of the prosthesis was modelled as an elasto-plastic material, while the prosthetic leaflets were considered linear-elastic. Physiological pressure waveforms were used as BCs. The FSI interaction was solved with the SPH method.
Finally, Caballero et al.[12] developed a patient-specific left heart model with severe AS and significant mitral regurgitation, analyse the influence of implantation depth in this specific pathological condition and investigate the possible outcomes. The device implanted was a balloon-expandable one. A fully coupled FSI numerical approach using the SPH method was chosen. Time-dependent pressure BCs were applied in the pulmonary veins and at the aortic outlet. Cardiac wall motion was imposed as a nodal displacement BCs. The main limitations were given by the not available patient-specific tissue properties and by the high computational cost.

4 | 3D CAD Model

SolidWorks 2022 (Dassault Systèmes SolidWorks Corporation, Waltham, MA, USA) is a three-dimensional design and drafting software that allows designers to create sketches, models, drawings, and experiments. It was created in 1993 by Jon Hirschtick, a MIT student, released in 1995 and acquired by Dessault Systèmes (3DS) in 1997, a European society property of Dassault Group. SolidWorks is a CAD system. The acronymous has two possible meanings: computer-aided drafting (aimed to create mainly bi-dimensional models) and computer-aided design (used to obtain three-dimensional models). In the latter case the final object can also be used for static or dynamic analysis, under the name of computer-aided engineering (CAE).
In this study a three-dimensional model of Acurate neo2 valve has been developed using SolidWorks. This valve is composed of a metallic stent, a skirt and three leaflets, that mimic the natural aortic valve. The structure of the stent can be divided into three zones: a lower cage, a middle one (which represents the main characteristic of this valve, because of its orientation, that is orthogonal with respect to the others) and an upper one.

Figure 4.1: *Acurate neo2*[47]

There are three sizes of this valve on the market, named small, medium, and large. Their

dimensions can be seen in the figure below. Size medium has been reproduced in Solid-Works, while sizes small and large have been scaled in LS-DYNA (ANSYS, Canonsburg, PA, USA).

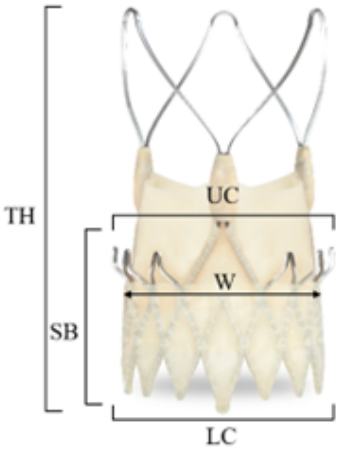

	S (23 mm)	M (25 mm)	L (27 mm)
Waist (W)	23	25	27
Upper Crown (UC)	28	30	32
Lower Crown (LC)	26	28	30
Stent Body (SB)	18	18.5	19
Total Height (TH)	48	49	51

Figure 4.2: *Acurate neo2 table*[56]

4.1. Measurement

To obtain all the dimension, ImageJ has been used, a digital image processing program developed by National Institute of Health in United States. To measure the size of the valve a photograph has been taken of it near to graph paper (as reported in figure 4.3.a). Then a scale was set using the dedicated function of ImageJ, called "set scale" (figure 4.3.b).

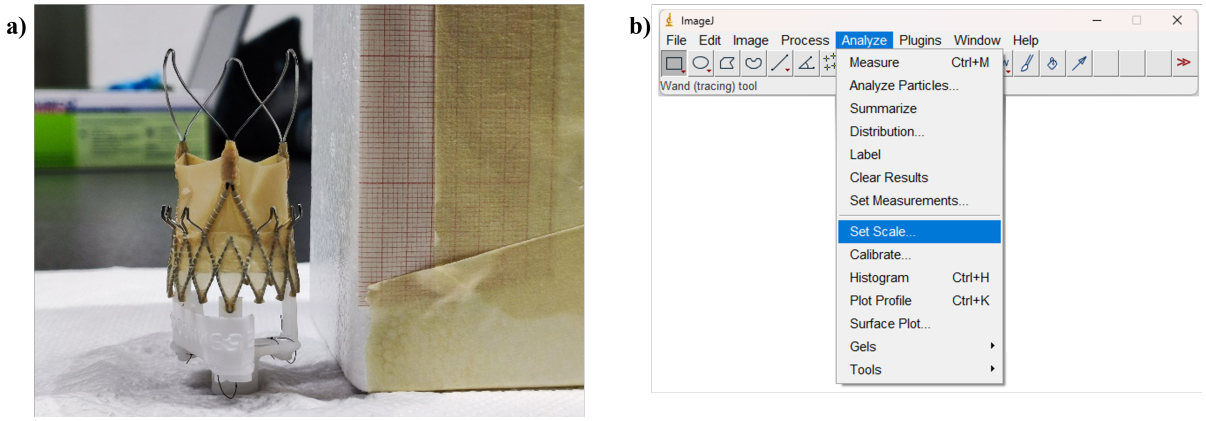

Figure 4.3: *a) Photography used for the measurement. b) Command "Set Scale" in ImageJ.*

To measure the thickness of the leaflets a caliber has been used. The stent's thickness is

equal to 0.7 mm, while the pericardium's is equal to 20 µm.

4.2. Bidimensional design of the stent

The bidimensional design is made through the sketch section in SolidWorks. The aim is to realize a repeatable unit, that will be extruded, wrapped around a cylinder, copied two more times, and merged to obtain a configuration like the real one.

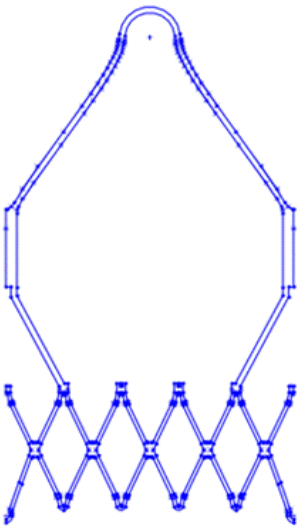

Figure 4.4: *Base unit in the bi-dimensional design.*

In figure 4.5 the structure of the lower cage is shown. It can be divided into four main zones, from A to D. Those will be duplicated by symmetry around line E.

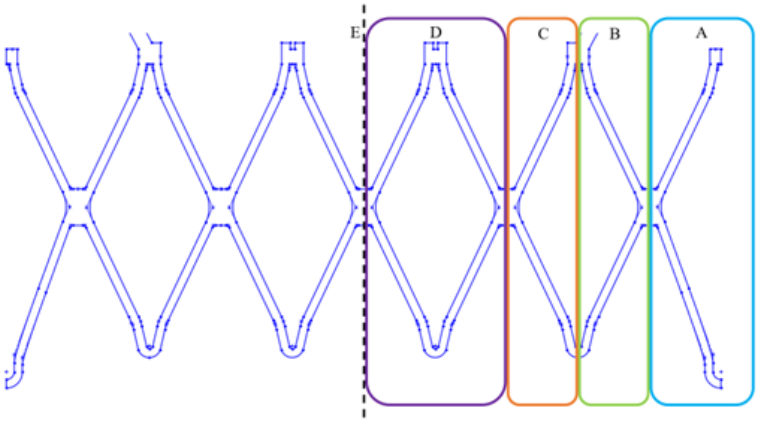

Figure 4.5: *Lower cage division into 4 different cell (or section) types: A, B, C and D. E is the simmetry line.*

Inside section A, the lower part is created with a circumference, while the curves with the command “style spline”, noted in the figure below. This cell is bigger than the near ones.

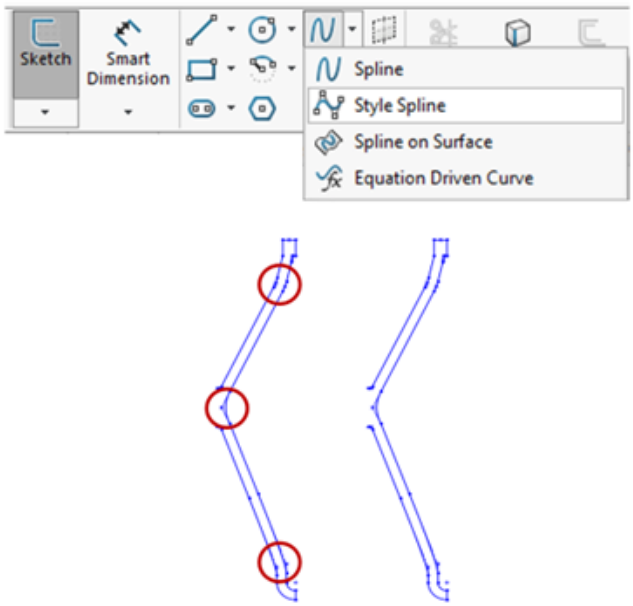

Figure 4.6: *Example of application of the “Style Spline” command in cell A.*

Cell B has been created in the same way, but it is shorter than the former.

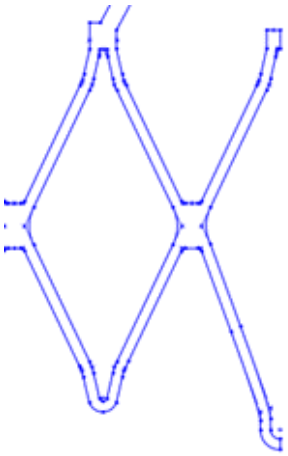

Figure 4.7: *Cells A, B and C*

The top of this cell also shows the presence of part of the upper crown, so this unit won’t be symmetric with the one in section C.

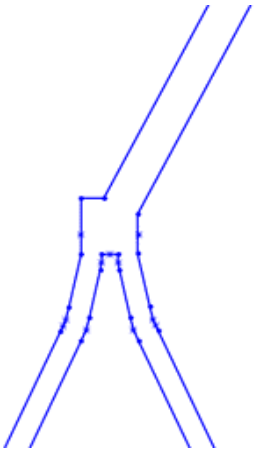

Figure 4.8: *Upper part of section B and C*

Unit D is made of two equal parts. The superior part is needed to link the lower crown with the middle one.

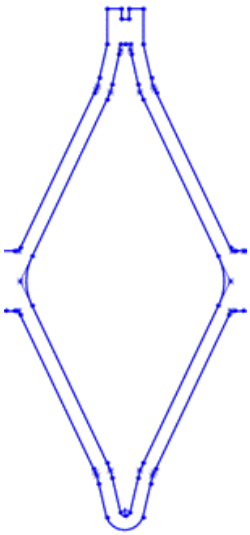

Figure 4.9: *Section D*

The upper crown starts from section B of the lower crown and is followed by a structure that works as a link zone with the cell next to it. The top is mainly made with the style spline command, to obtain a structure like the real one, and a circumference. This design is then extruded.

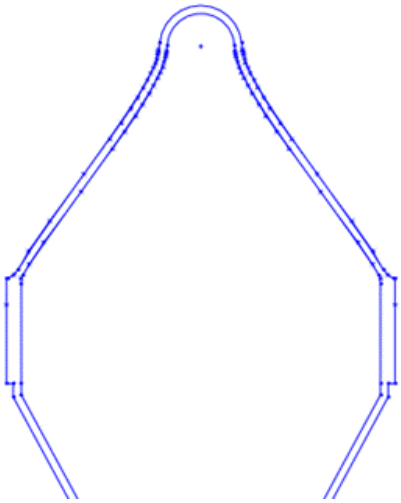

Figure 4.10: *One cell of the upper cage.*

After the creation of the first of the three units of the bi-dimensional design, a cylinder (around whom the stent can be placed) has been created. Then the stent has been placed with the feature "wrap".

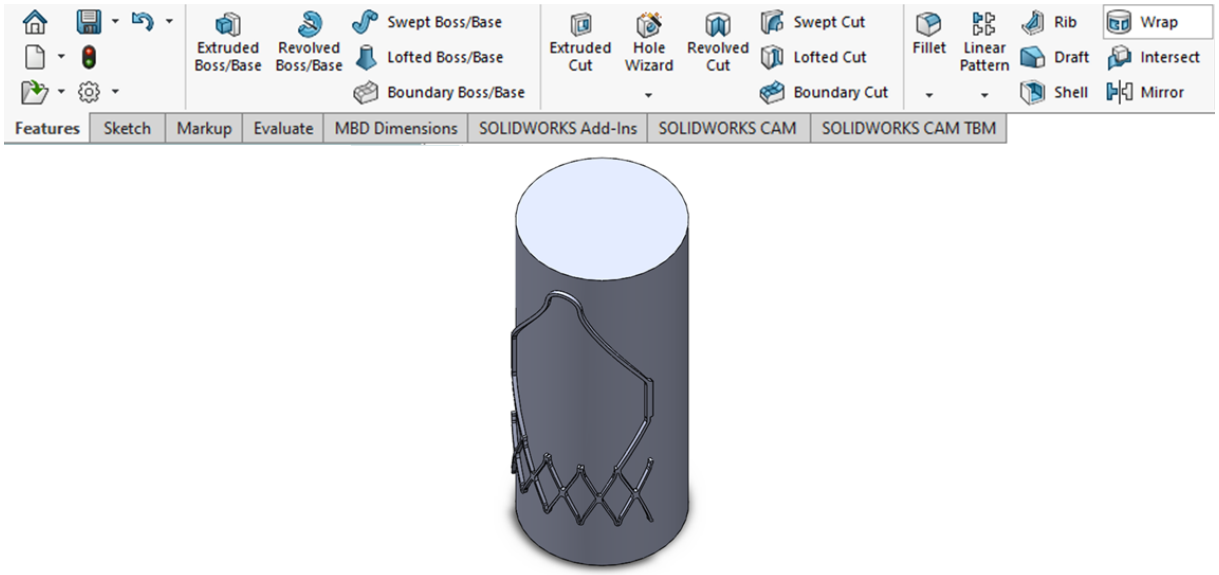

Figure 4.11: *Example of application of the "wrap" command on the bi-dimensional unit extruded and wrapped around the cylinder.*

After deleting the cylinder, the unit has been multiplied other two times with the feature "circular pattern".

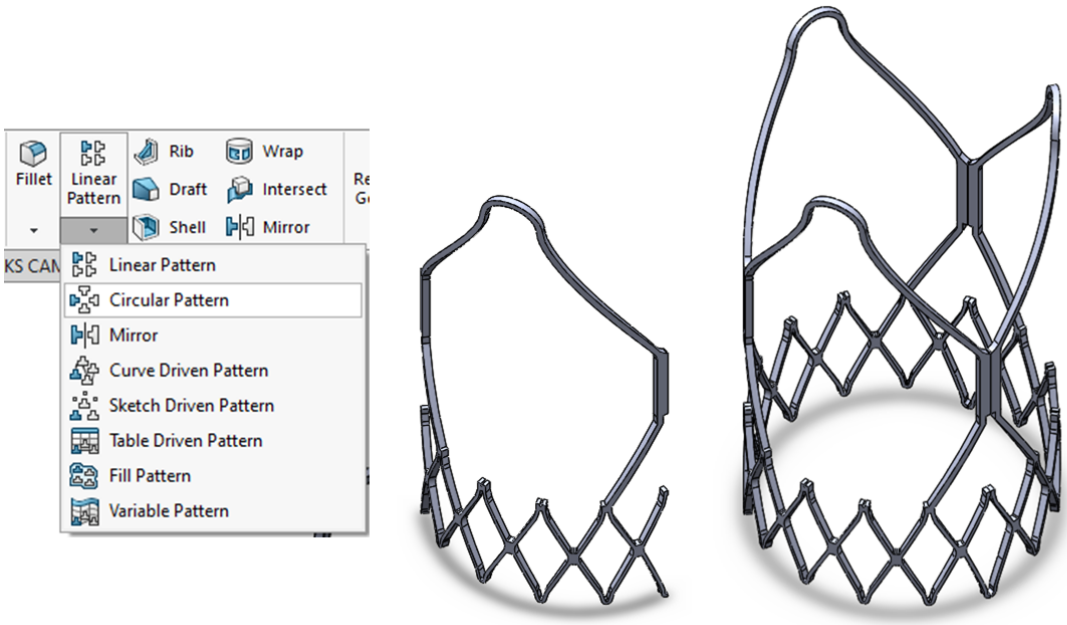

Figure 4.12: *Example of application of the "Circular Pattern".*

With the function "deform" was than possible to recreate the profile of the device, with its smaller middle diameter and the enlargement of the lower and upper part.

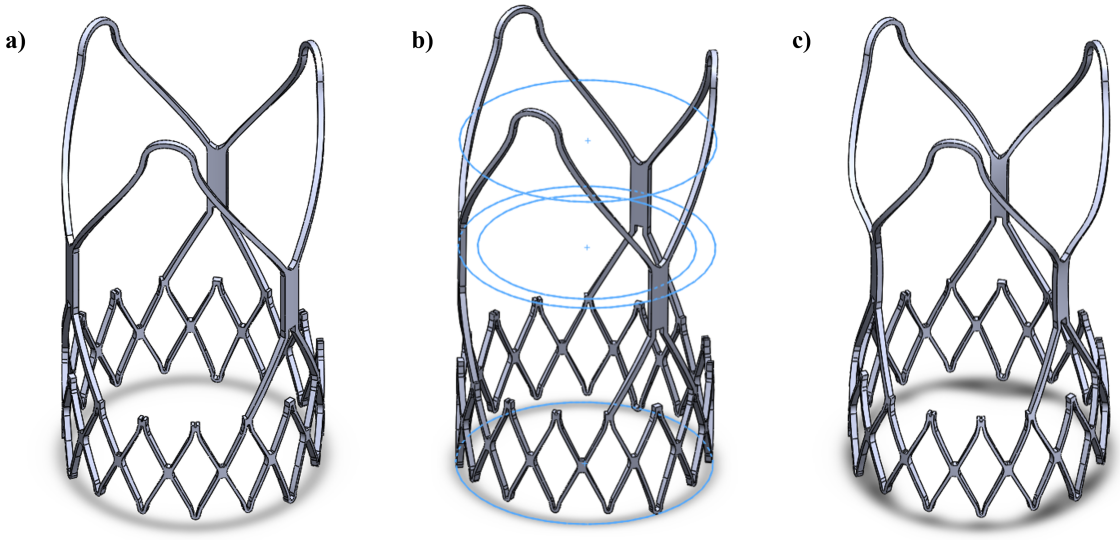

Figure 4.13: *a) Non-deformed stent. b) Circumferences for the deformation. c) Deformed Stent.*

The middle cage presents orthogonal cells with respect to the upper and lower zone. This part has been created with a 3D sketch of a line that represents the guideline for the

sweep command, used to extrude the connection surfaces between the two cages.

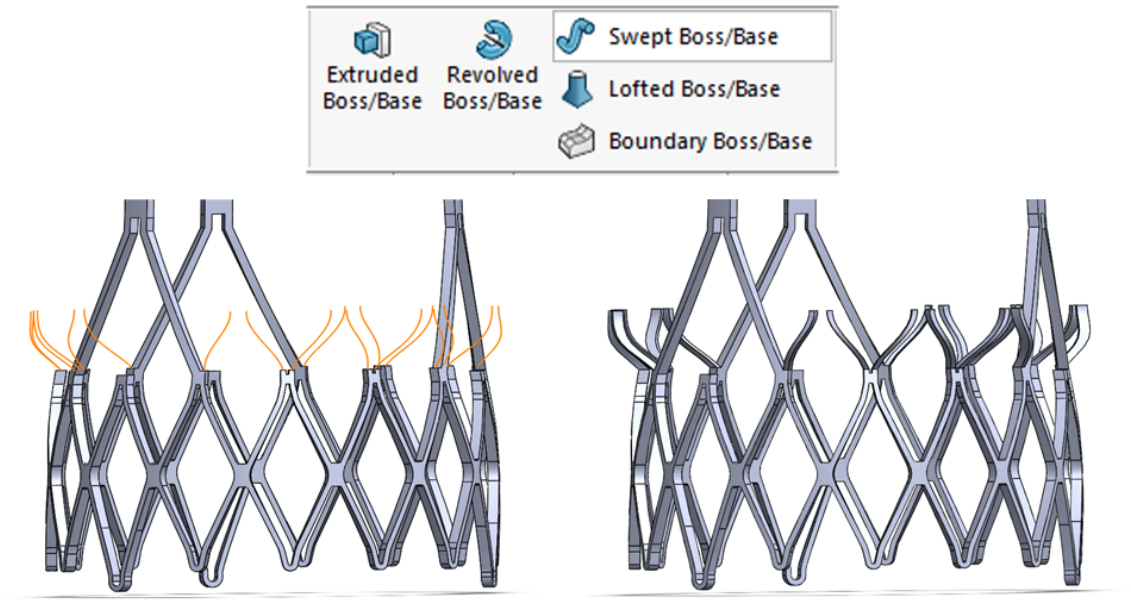

Figure 4.14: *Example of application of the "Swept" command. a) Guidelines for the middle cage, orthogonal to the others. b) Extrusion of the cells that make the middle cage.*

A half circumference has been created to close these cells with a 3D-sketch, starting and ending at the centre of the top and then, again, a sweep.

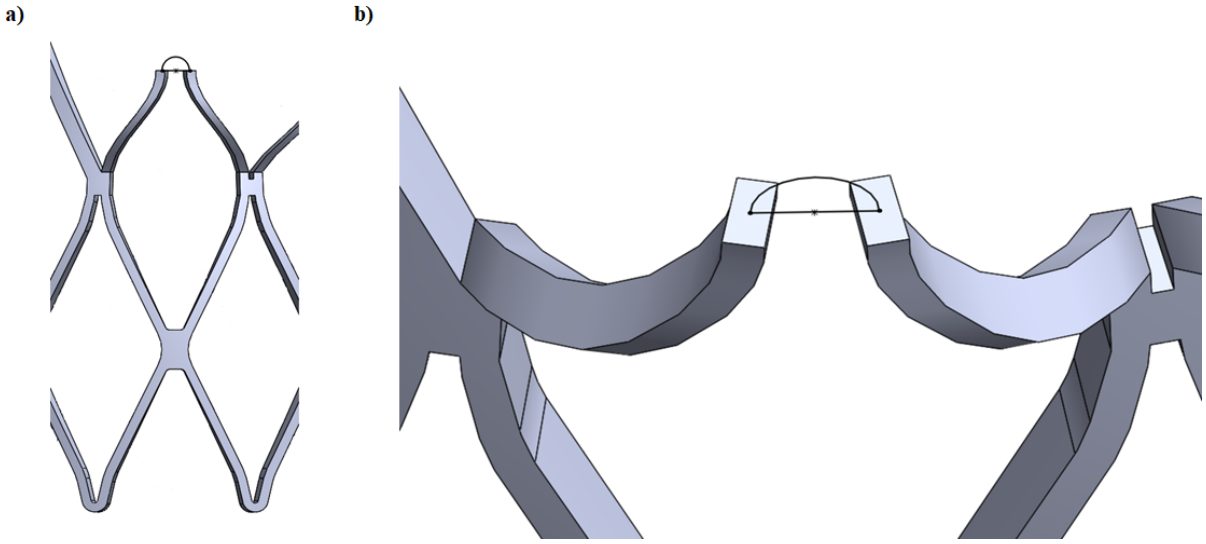

Figure 4.15: *Example of guidelines for the link between two halves of a cell in the middle cage.*

In the figure 4.16 the final configuration of the lower and middle cages is reported.

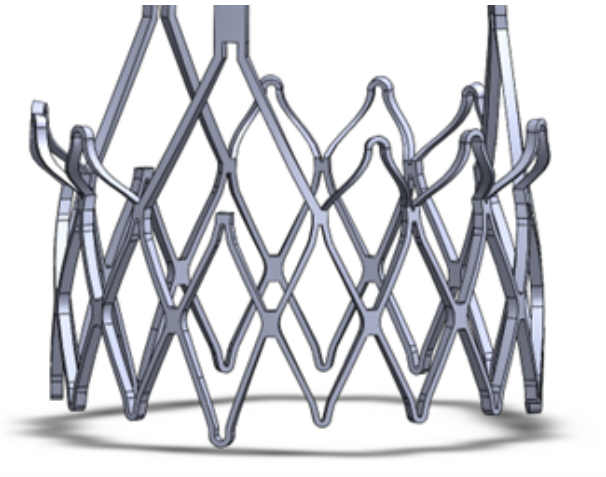

Figure 4.16: *Lower and middle cage.*

4.3. Skirt and leaflets

The skirt has been created as a surface, using the command "filled surface" inside the surface's toolbar. The edges are the boundaries of the internal contours of the three types of cells. As is possible to see in the figure below, in 4.18.a there is an example of a part of the skirt inside the lower cage, in 4.18.b the middle zone and in 4.18.c the upper crown. The latter must be cut to obtain the leaflets of the prosthetic valve, as shown in 4.18.d.

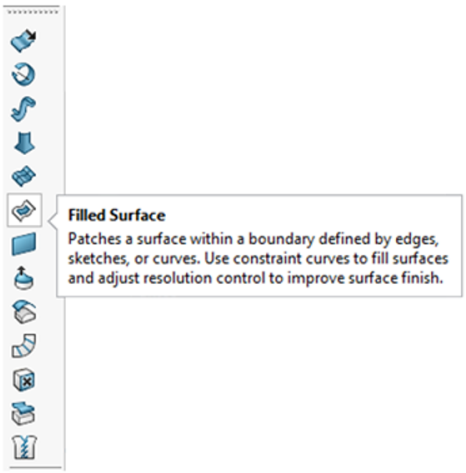

Figure 4.17: *Filled surface command inside the surface's toolbar.*

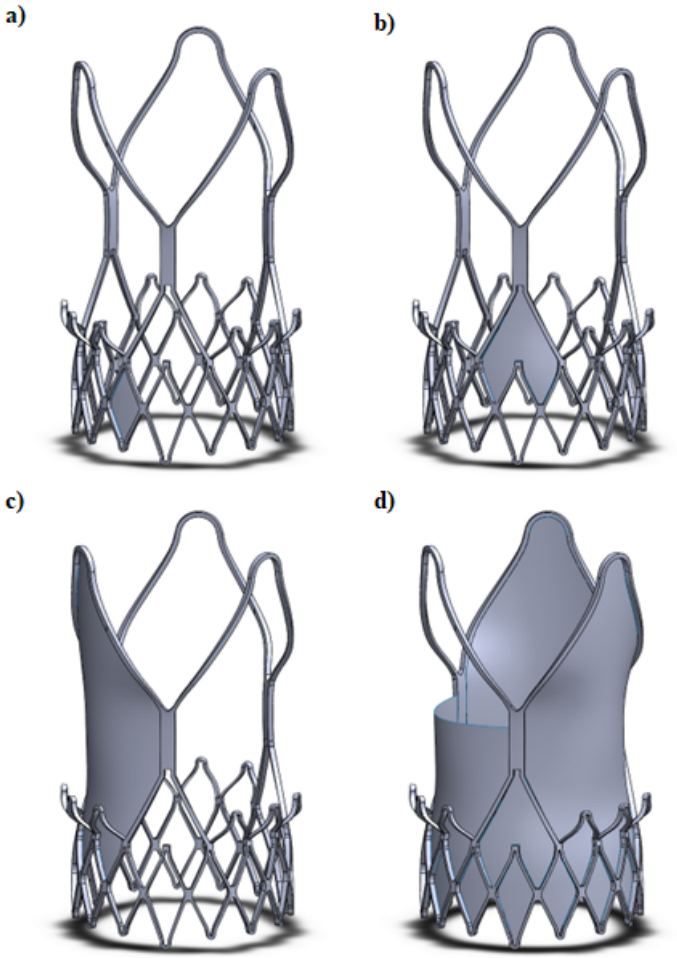

Figure 4.18: *a) Repetitive unit of the skirt in the lower part of the stent; b) Repetitive unit of the skirt in the middle of the stent; c) Creation of the leaflets, before removal of the excess part; d) Comparison between a finished leaflets and two non-finished ones.*

The cut is created with the command "trim surface", which allows to cut a surface alongside a line created before in a sketch (Figure 4.20.a) and then to choose which of each half has to keep (Figure 4.20.b). In this way, the form of the leaflets is very similar to the real one.

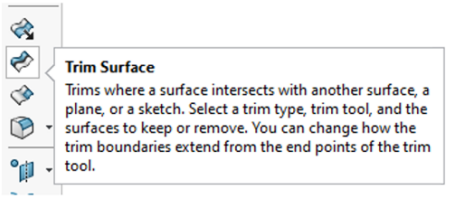

Figure 4.19: *Trim surface command inside the surface's toolbar*

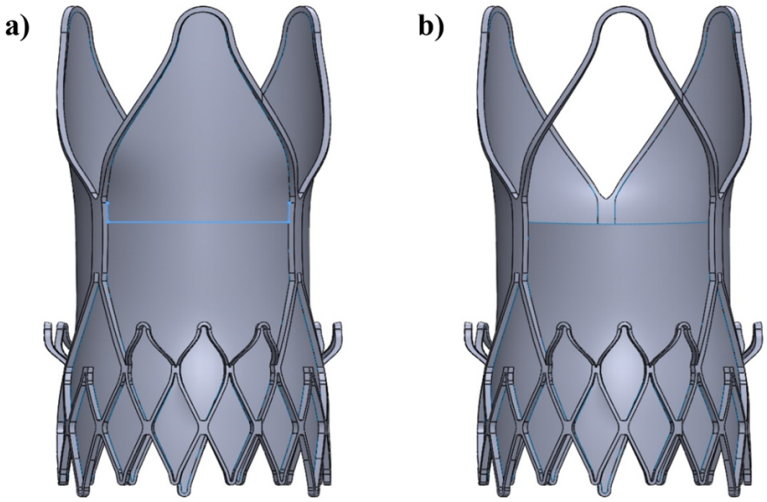

Figure 4.20: *a) Device with three unfinished leaflets; b) Comparison between a finished leaflets and two unfinished ones.*

The result can be seen in figure 4.21 below.

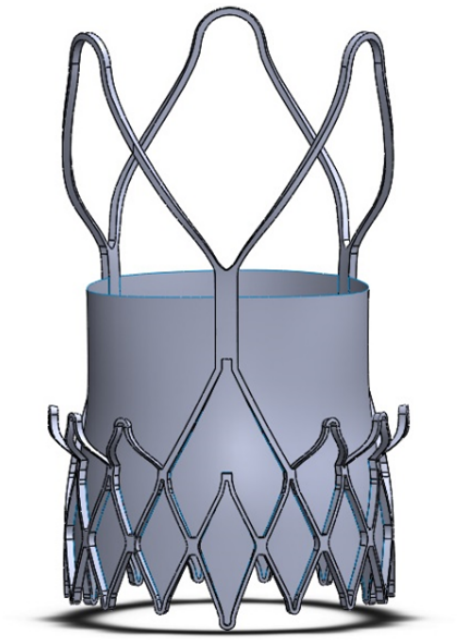

Figure 4.21: *An ultimated CAD model of an Acurate neo2 valve.*

5 | Components of the simulations

5.1. Stent discretization

Once obtained, the full stent structure has been discretized in elements using ANSA Pre Processor v22.1.2 (BETA CAE Systems,Switzerland), a computer-aided engineering (CAE) tool. It is developed by BETA CAE system and allows the creation of a link between a CAD geometry and a finite element mesh. The choice was to use hexahedral elements, due to the lower number of elements created (increasing the efficiency) and higher precision. The final mesh resulted in a total of 103908 elements. The formulation was then chosen in LS-DYNA as hexahedrons with reduced integration and Puso hourglass control. The mash has been created starting with the command "faces cut" inside "topo", to divide the stent (Figure 5.1).

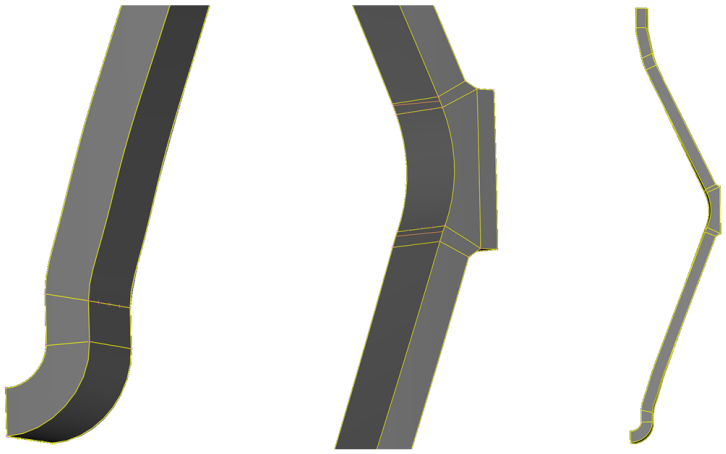

Figure 5.1: *Examples of application of command "plane cut" in the lower part of the stent.*

Every part was meshed with the command "4 sided" under "mesh generation" in "mesh". The element's size is equal to 0.12 mm. Three-dimensional mesh was made with an extrusion (using the command "extrude" in "structured mesh" under "volume mesh") of the bi-dimensional layer created before, with four elements in the thickness.

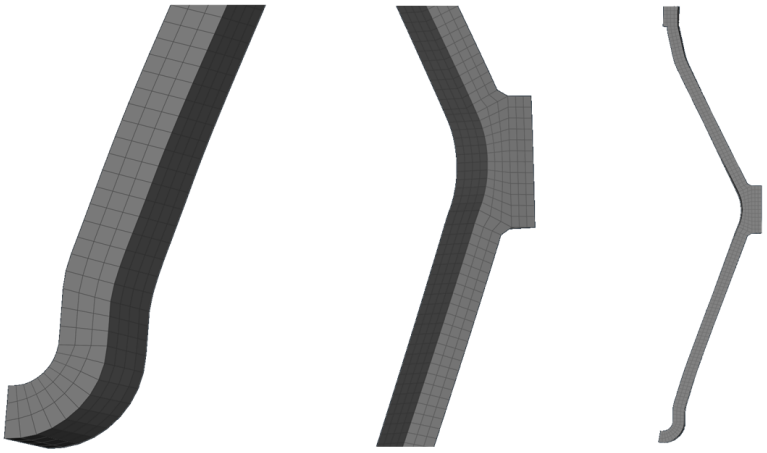

Figure 5.2: *Example of discretization in the lower part of the stent.*

In figure 5.2 there is the lower crown's three-dimensional mesh, obtained following the steps illustrated before. After completing the mesh of every unit, they have been duplicated with the command "copy". In Figure 5.3 the lower part of the stent is represented.

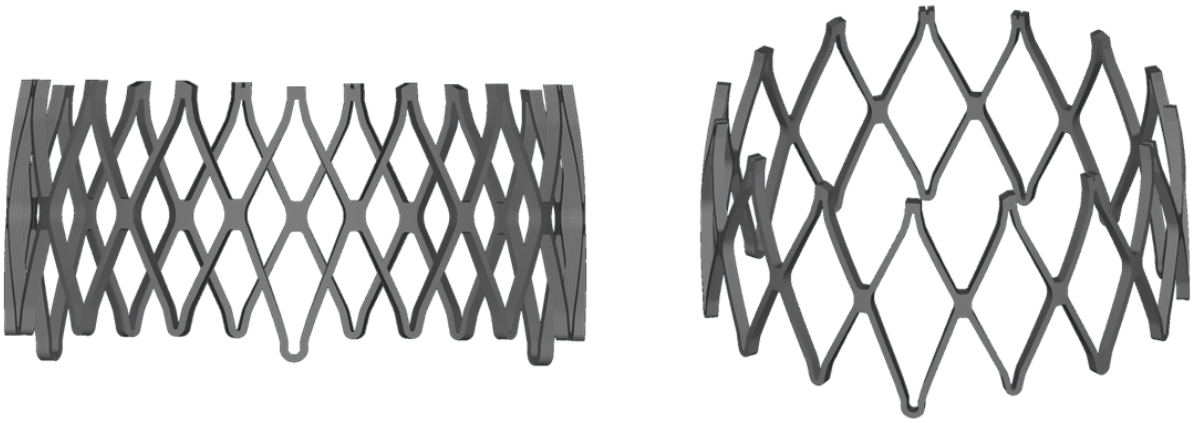

Figure 5.3: *Lower part of the stent discretized.*

The middle crown has been realised in the same way, starting with a discretized shell, and then extruded to obtain a full discretization. In figure 5.4 is reported one of three units of these cells.

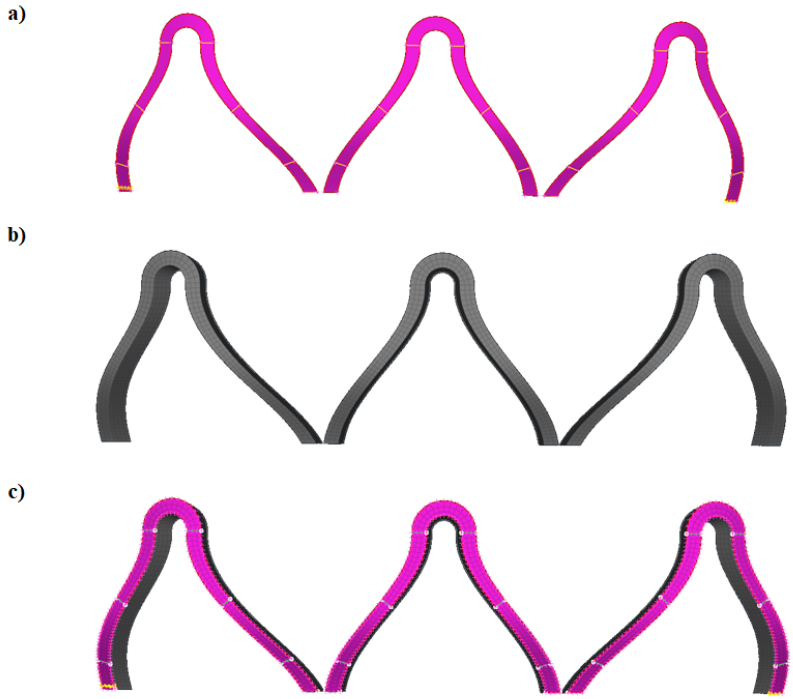

Figure 5.4: *a) Middle cage's shell; b) discretization of the middle part of the stent; c) Combination of elements and shell.*

The same procedure is applied also to the linking parts. An example is shown in figure 5.5.

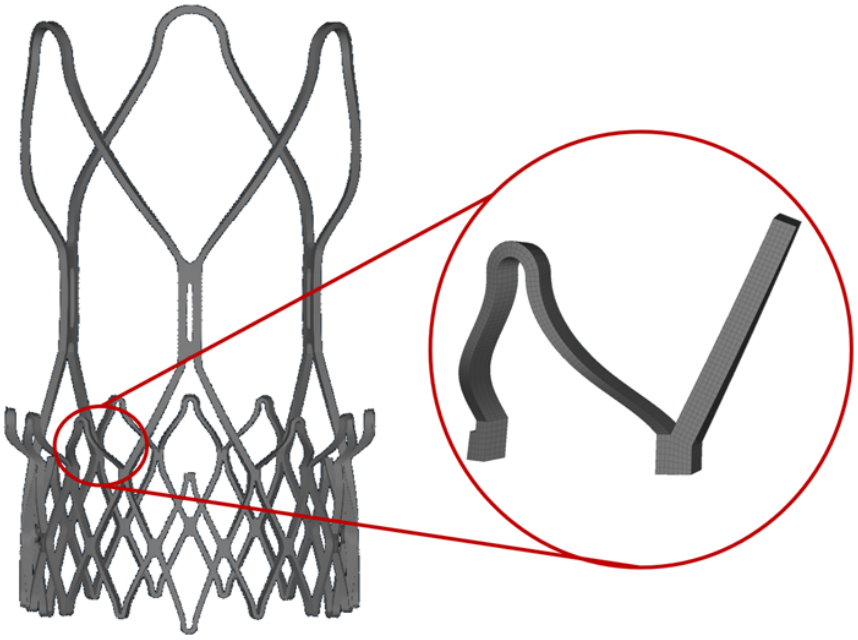

Figure 5.5: *Zoom on the connection between middle and upper part*

The connection between the middle cage and the upper one has a problem related to the fact that this part is covered by the pericardium and sutures. To better understand the shape of this junction, the device was studied using angiographies from six real patients, made available to us in order to correctly reproduce the implantation of the valves.

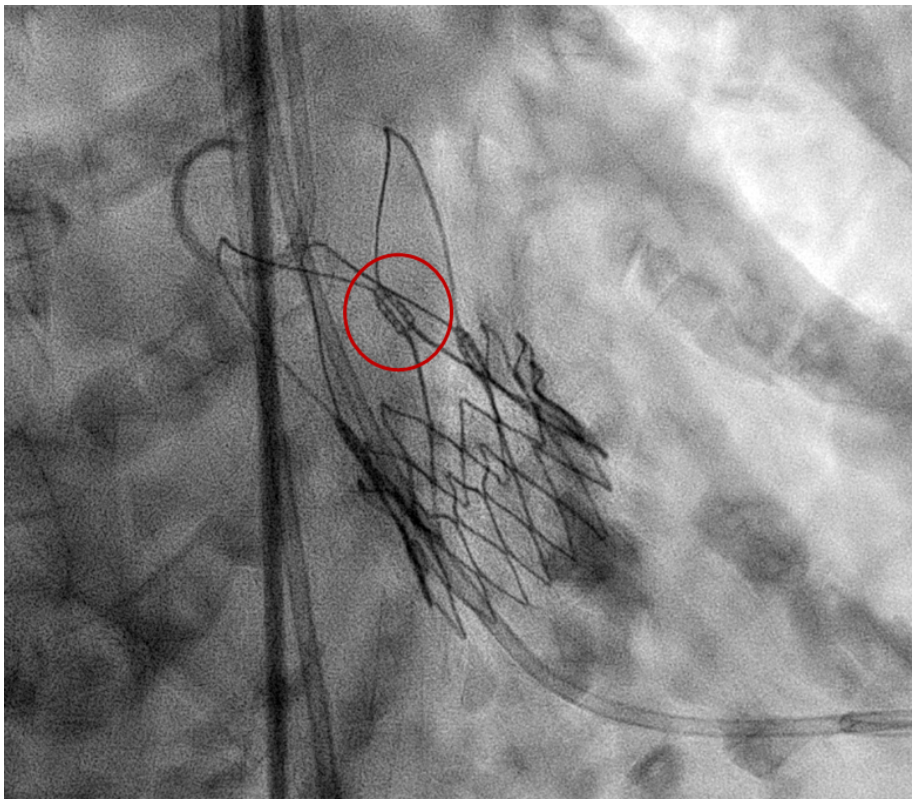

Figure 5.6: *Device seen through an angiography.*

For this reason the conjunction has been changed to try to reproduce the real geometry, switching from the configuration (Figure 5.8a) developed in SolidWorks to a new one with an hole inside of it (Figure. 5.8b). To make a comparison, a zoom on the conjunction of the device is shown in figure 5.7.

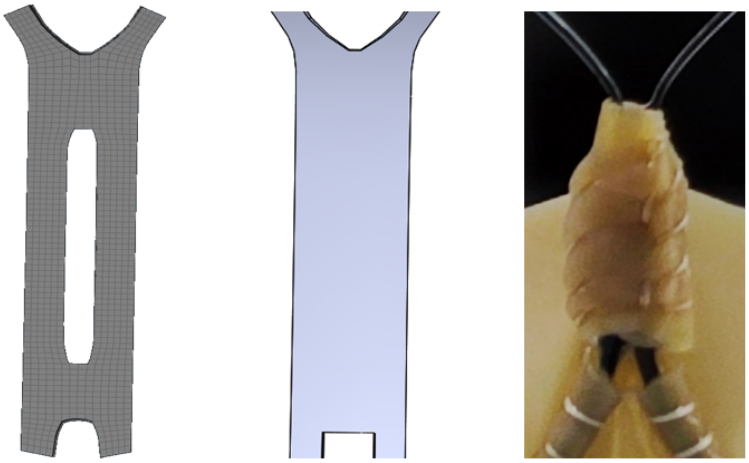

Figure 5.7: *a) Final version of the connectors in the upper zone; b) Older version created in SolidWorks; c) Photography of the connectors, covered by the leaflets.*

The upper crown has been created in the same way as the lower and the middle.

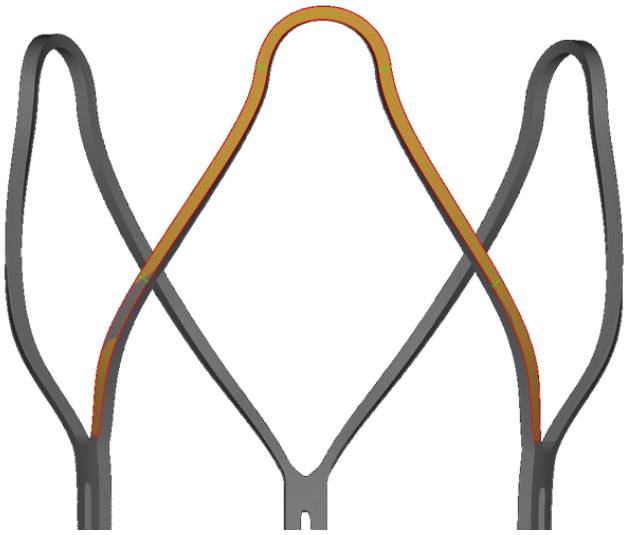

Figure 5.8: *Shell and discretization of the upper cage.*

5.2. Leaflets and skirt

The skirt is made with a triangular mesh of 16335 elements, with a dimension that is three times the one of the stent's elements. The nodes of the triangles must correspond to the nodes of the stent, to merge them. The element formulation chosen is the Belytschko-Tsay membrane one.

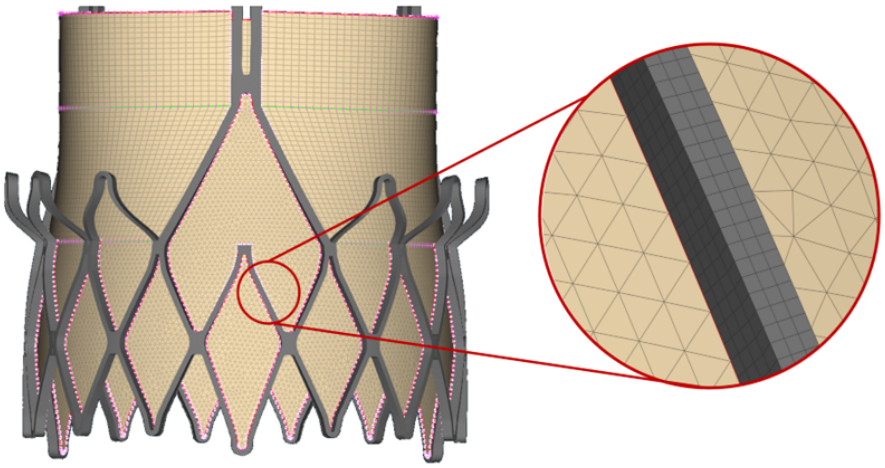

Figure 5.9: *Zoom on the merge between the stent and the skirt.*

The leaflets instead are discretized with 6486 fully integrated rectangular shell elements. The sewing sutures were not modeled, which is why the stent and the pericardium parts were fixed together with a node-to-node connection. In figure 5.10 is possible to see the complete discretization of the prosthesis.

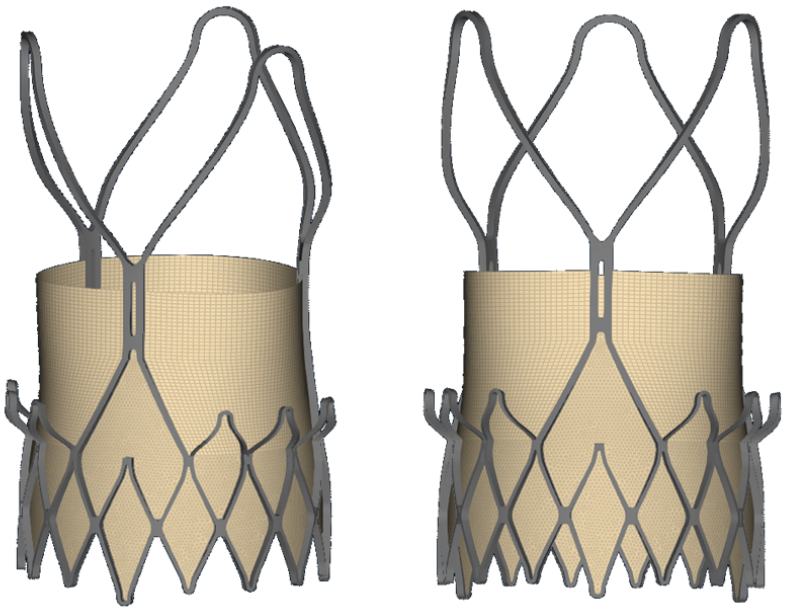

Figure 5.10: *Ultimate version of the discretized Accurate neo2 valve.*

5.3. Materials

The stent structure was considered as Nitinol, with the following characteristics obtained according to Morganti et Al.[57] This material is defined among those present in the software used for the simulations, LS-DYNA.

Parameter	*Value*
Austenite's Young's modulus (E^a)	51.7 MPa
Poisson's ratio (μ)	0.3
Start of transformation loading (σ_L^S)	600 MPa
End of transformation loading (σ_L^E)	670 MPa
Start of transformation unloading (σ_U^S)	288 MPa
End of transformation unloading (σ_U^E)	254 MPa
Recoverable strain (ϵ_{max}^R)	0.0426
Difference response in tension and compression (α)	0.19

Table 5.1: *Mechanical properties of Nitinol.*[57]

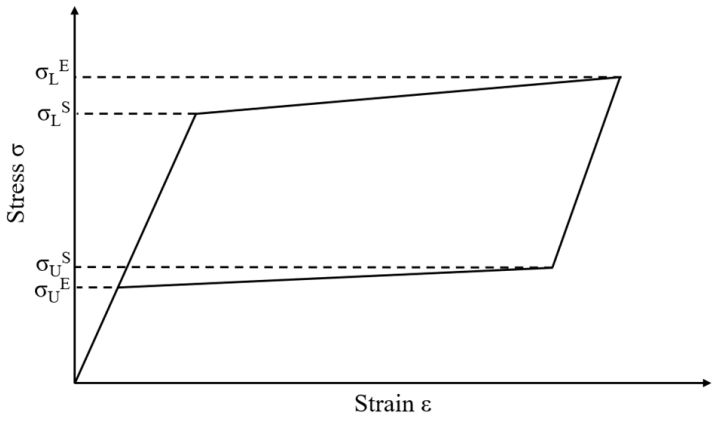

Figure 5.11: *Graphic of Nitinol behaviour.*

The pericardium, i.e. skirt and leaflets, were modelled as linear elastic, with a Young's modulus E equal to 3.20 MPa, Poisson ratio μ equal to 0.30 and density ρ equal to 1100.00 $\frac{kg}{m^3}$.[58]

5.4. Aorta

As far as the anatomical site geometry used in the simulations is concerned, it is patient-specific in each of its components, i.e. aorta, natural valve and calcifications. In particu-

lar, the aortas of six patients were segmented from contrast-enhanced CT images before surgery and device implantation: the models derived included the proximal outflow tract of the left ventricle, the sinuses of Valsalva, the native aortic valve, the coronaries and the initial tract of the ascending aorta. The segmented geometries were then processed with ANSA software. Before meshing, however, it was necessary to smooth out the starting geometries in order to obtain an optimal and as homogeneous discretization as possible. Following this operation, the shell mesh of the aorta was created, using triangles with an average size of 0.8 mm. Three tetra layers were then obtained starting from this shell with the help of the ANSA Batch Mesh. This is a tool which performs automatic mesh generation on geometries through customizable meshing sessions. Different meshing parameters were used for the aorta and the coronaries, joined by a third transition zone, which was necessary to connect the different layers (Figure 5.12).
The next table shows the different thicknesses obtained for the three zones.

	Thickness [mm]
Aorta	2.1
Transitions	1.4
Coronaries	0.7

Table 5.2: *Thickness of the three layers obtained with the batch mesh tool in the three zones of the geometry.*

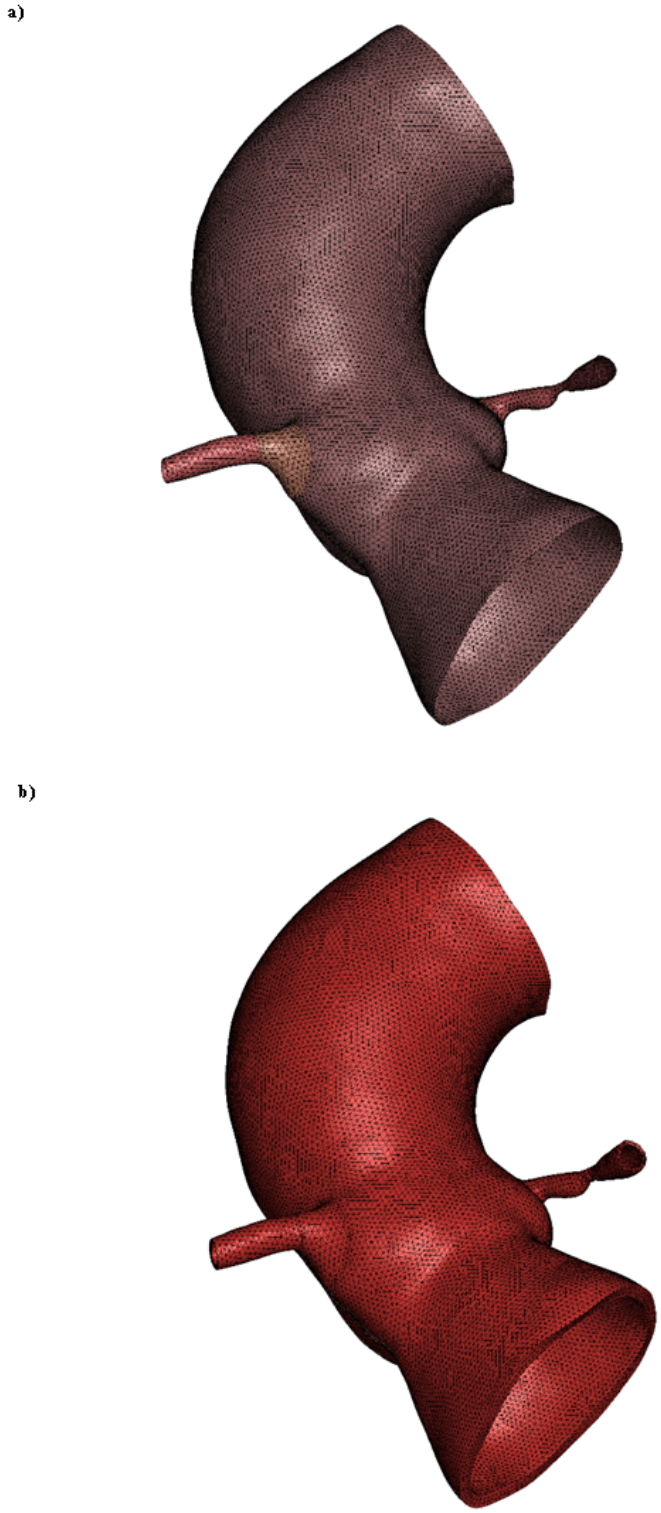

Figure 5.12: *a) Aorta shell with the three different zones highlighted; b) Final volume mesh obtained through the batch mesh tool.*

The formulation of the elements was then chosen in LS-DYNA as tetrahedron with one integration point. The numbers of volumetric elements for the six different patients are shown in the table 5.3.

Patient	*Number of solid elements*
1	322191
2	253998
3	220910
4	225720
5	306716
6	315144

Table 5.3: *Number of solid elements for the discretization of the six patients' aortas.*

With regard to the material, it was modelled as isotropic, incompressible, nonlinear hyperelastic, starting from a study conducted by Azadani et al.[59] From the stress-strain profile obtained by this research group, the values of the coefficients used in the simulations were chosen and applied to the Yeoh hyperelastic model, as it follows:

$$W = C_{10}(I_1 - 3) + C_{20}(I_1 - 3)^2 + C_{30}(I_1 - 3)^3$$

where I_1 is the first invariant of the Left Cauchy-Green tensor and C_{10}, C_{20} and C_{30} are material model coefficients indicative of the mechanical properties. The value of the coefficients are shown in table 5.4.

Coefficient	*Value [MPa]*
C_{10}	0.0417
C_{20}	0.1186
C_{30}	0.4550

Table 5.4: *Values of the coefficient for the material of the aorta.*

The density ρ was set at 1060.00 $\frac{kg}{m^3}$ and Poisson ratio μ was equal to 0.48.
The contacts involving the aorta are those with the calcium, the pericardium part of the device, i.e. skirt and leaflets, and the stent defined with an Automatic Surface-to-Surface contact, only the last of which with a friction coefficient.

5.5. Native valve

The native valves couldn't be derived from the images obtained through CT. Therefore, in order to construct aortic valves with geometry as close as possible to that of the patients' real valves, these were generated following reference points identified by the shape of the sinuses. Three curves were constructed in ANSA to delimit the three leaflets and three surfaces were constructed to fill these contours (Figure 5.13). The nodes of the elements lying on these three curves were made to coincide with those of the mesh of the aorta.

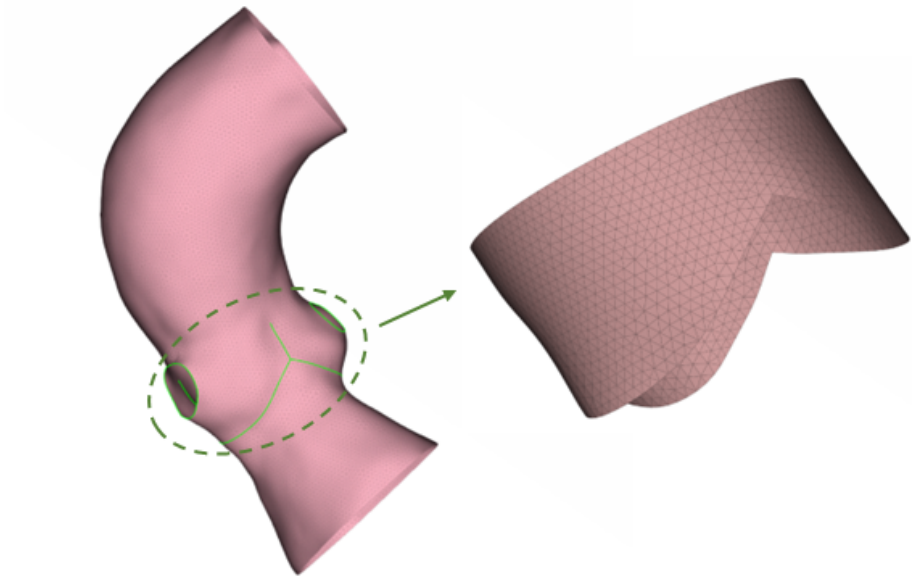

Figure 5.13: *The native valve obtained by joining some reference points on the sinuses.*

The valves were discretized with triangular elements following the Belytschko-Tsay membrane's formulation, with an average dimension of 0.8 mm. The native valves and the aortas were fixed together with a node-to-node connection. The number of elements of the six natural valves are reported in the table 5.5.

Patient	*Number of shell elements*
1	3236
2	2599
3	3494
4	3870
5	3659
6	3822

Table 5.5: *Number of shell elements for the discretization of the six patients' native valves.*

As for the material, the native valves were assumed to be linear elastic, with a really low Young's modulus E, equal to 0.10 MPa, in order not to further complicate the simulation. This assumption is reasonable because the interaction between the device and the native valve is always easily won by the metallic stent in reality. The density ρ was set at 1100.00 $\frac{kg}{m^3}$ and Poisson ratio μ was equal to 0.30.[58]
In order to obtain a more realistic geometry of the native valves (Figure 5.14), those obtained in ANSA were subjected to an initial simple computational simulation in LS-DYNA consisting of applying pressure to the leaflets, while the commissural edges were instead deprived of all degrees of freedom.

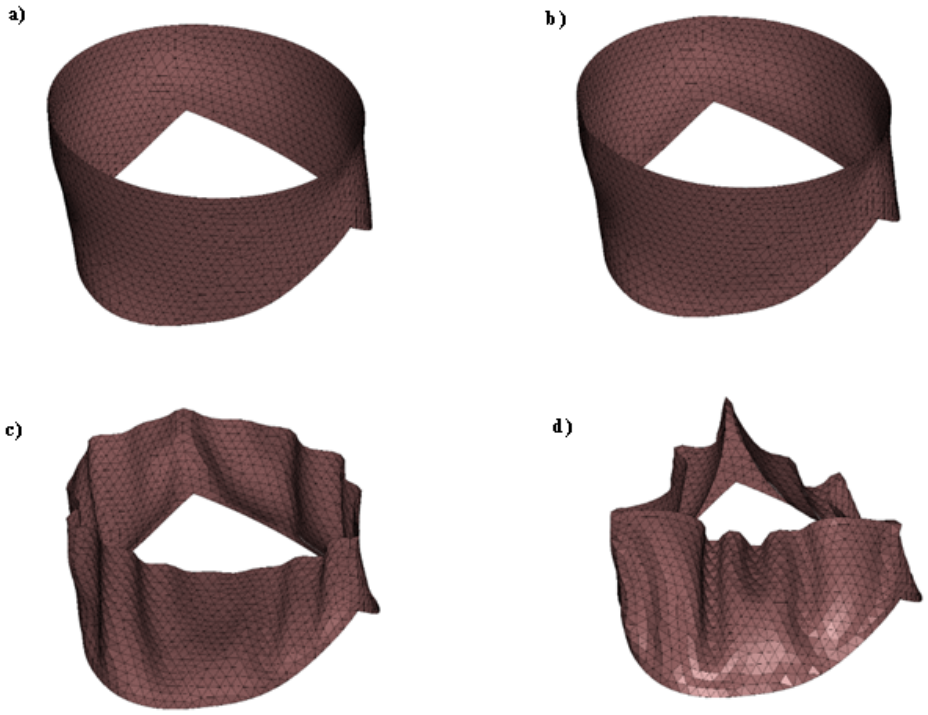

Figure 5.14: *Four instants of the initial simulation on one of the patients' native valves: a) t = 1, b) t = 3, c) t = 6, d) t = 10. The configuration d) is an example of the final configuration for the native aortic valve used in the implant simulation.*

The contacts involving the native valve are the ones with the two catheters needed for the implant, the stent and the pericardium skirt of the device. For all of these, an Automatic Surface to Surface type of contact was chosen, with no friction coefficient. The contact between the natural valve and calcifications has been neglected in order to not complicate an already demanding simulation. This approximation is reasonable since the calcium is an element that presents fairly limited displacements, besides being pushed towards the wall of the aorta like the natural valve.

5.6. Calcifications

The geometry of the calcific deposits was also derived in the same way as the aorta, starting from the CT images of each patient. The segmented calcifications were then smoothed in ANSA and meshed with solid tetrahedral elements (Figure 5.15), which can follow better the complex and irregular geometry of the deposits with respect to hexahedral elements. In particular, the formulation chosen was the same chosen for the aorta, i.e. tetrahedron with one integration point.

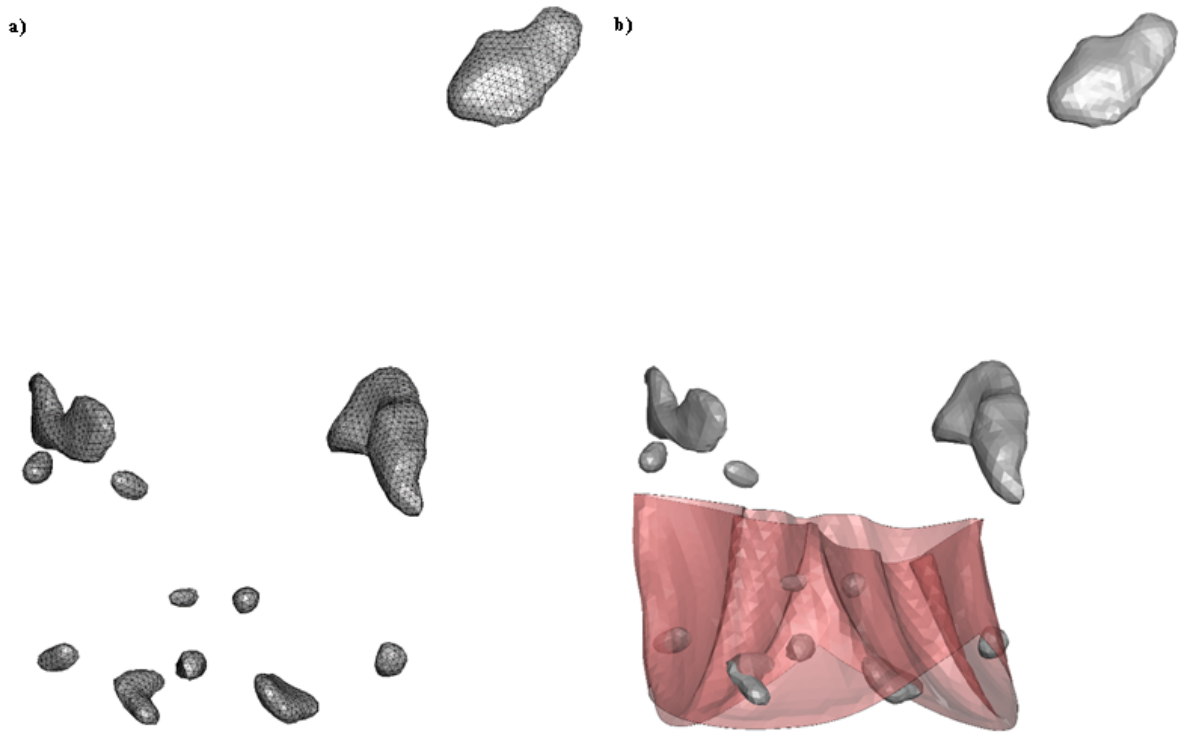

Figure 5.15: *a) Example of the volume mesh for the calcifications of one patient; b) Calcifications and native valve of a patient.*

Patient	*Number of solid elements*
1	13632
2	18274
3	51554
4	2700
5	2014
6	13141

Table 5.6: *Number of solid elements for the discretization of the six patients' calcifications.*

The material was modelled as linear elastic, with a density $\rho = 2000.00 \frac{kg}{m^3}$, Young's modulus E = 12.60 MPa, and Poisson ratio $\mu = 0.45$, according to Holzapfel et al.[60]
With regard to contacts, they are defined as Automatic Surface-to-Surface (as for the native valve and the aorta) with the two catheters, the aorta with the device, i.e. with the stent, the skirt, and the leaflets. None of these contacts is characterised by a friction coefficient.
The final anatomies obtained for the six patients are shown in figure 5.16.

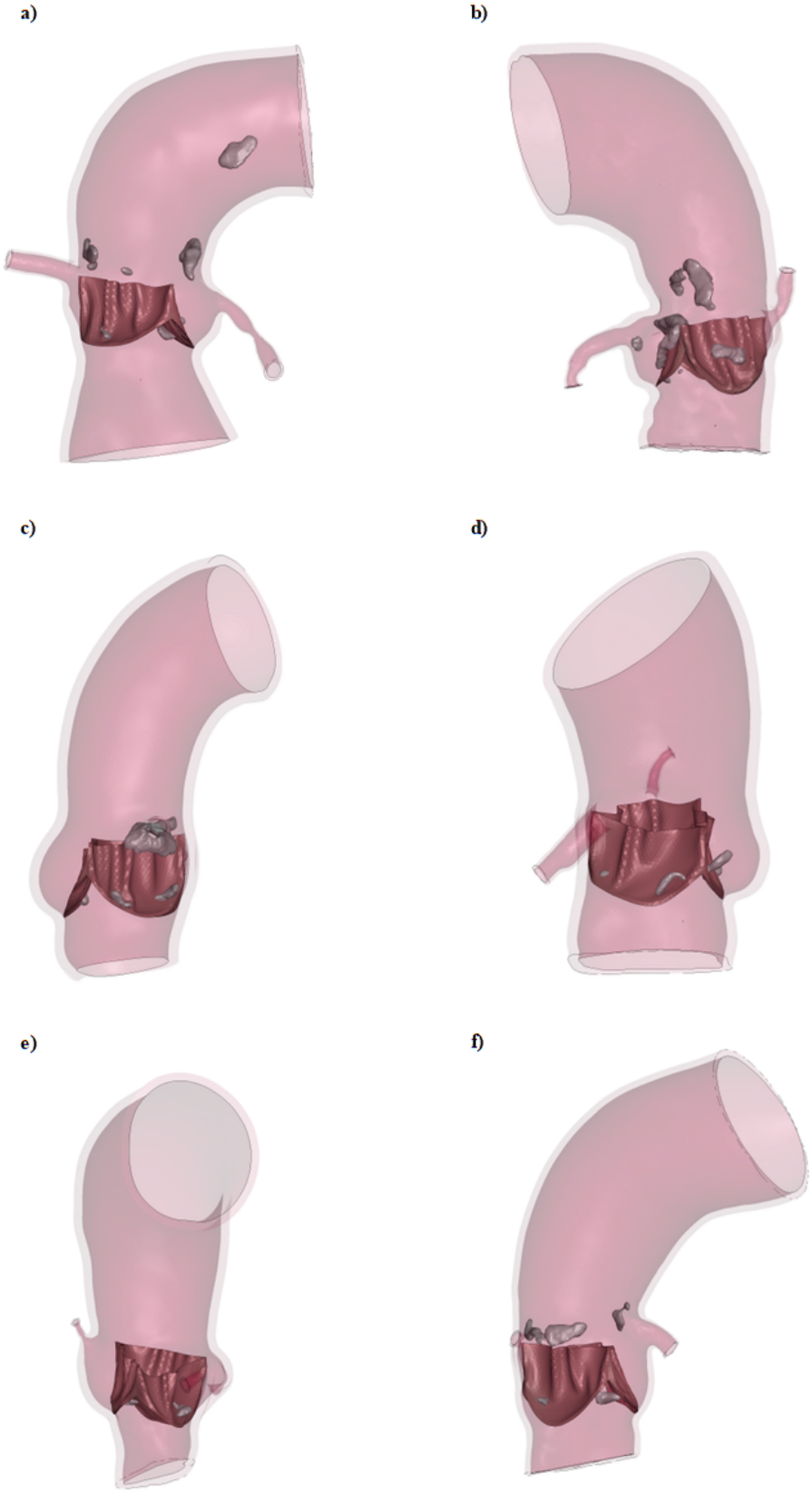

Figure 5.16: *From a) to f): models of the anatomy of the six patients.*

6 | Simulations and results

6.1. Simulations

During the real surgery, the valve is crimped on a catheter that reaches the aortic valve (Figure 6.1.a), and then the deployment phase begins. The upper part of the catheter begins to release the prosthesis (Figure 6.1.b), and the upper crown will expand (Figure 6.1.c). The aortic valve is not yet totally open. The deployment of the lower part begins (Figure 6.1.d), which releases the middle and the lower cages (Figure 6.1.e). Now the aortic valve is kept open. The catheter will be than retracted and taken outside the body from the same place of insertion.

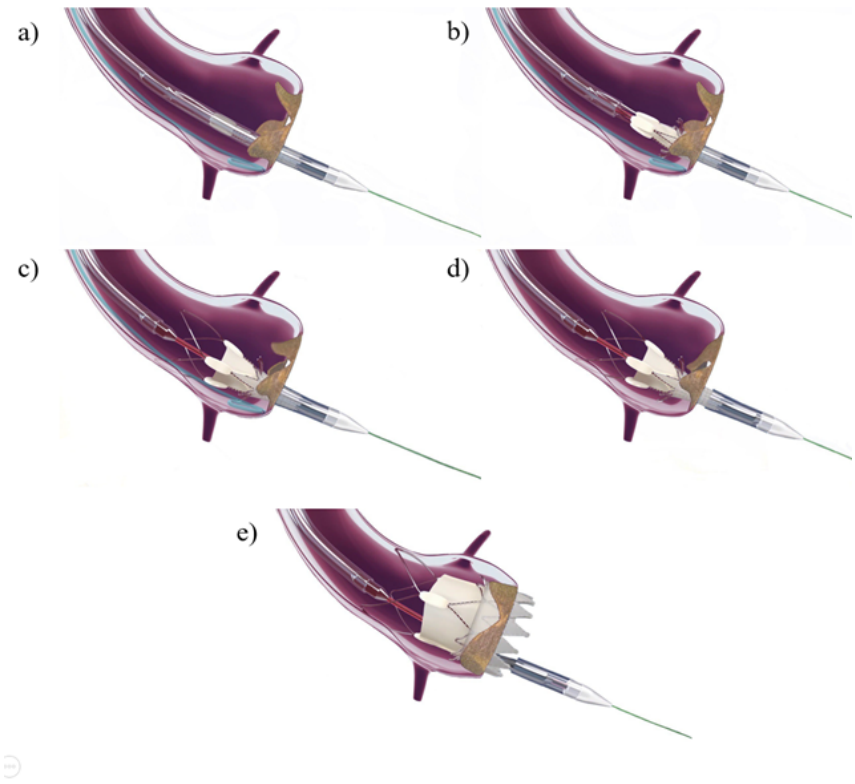

Figure 6.1: *Implant process of the Acurate neo2 valve.*

To reproduce accurately the real implant of the device, the simulations can be divided in

two phases:

1. Crimping phase;
2. Deployment phase inside the aortic root.

Implant simulations take place within six patient-specific aortic anatomies (natural valve, calcifications, and aorta), obtained from CT images of six patients who underwent implantation of this device. In order to do so, anatomies were imported and the right stent size was optimally placed for every patient. As a rule, the correct orientation of the anatomies was obtained when the most distal points of the natural valve leaflets were aligned with the catheters needed for the deployment of the Acurate neo2 valve (Figure 6.2).

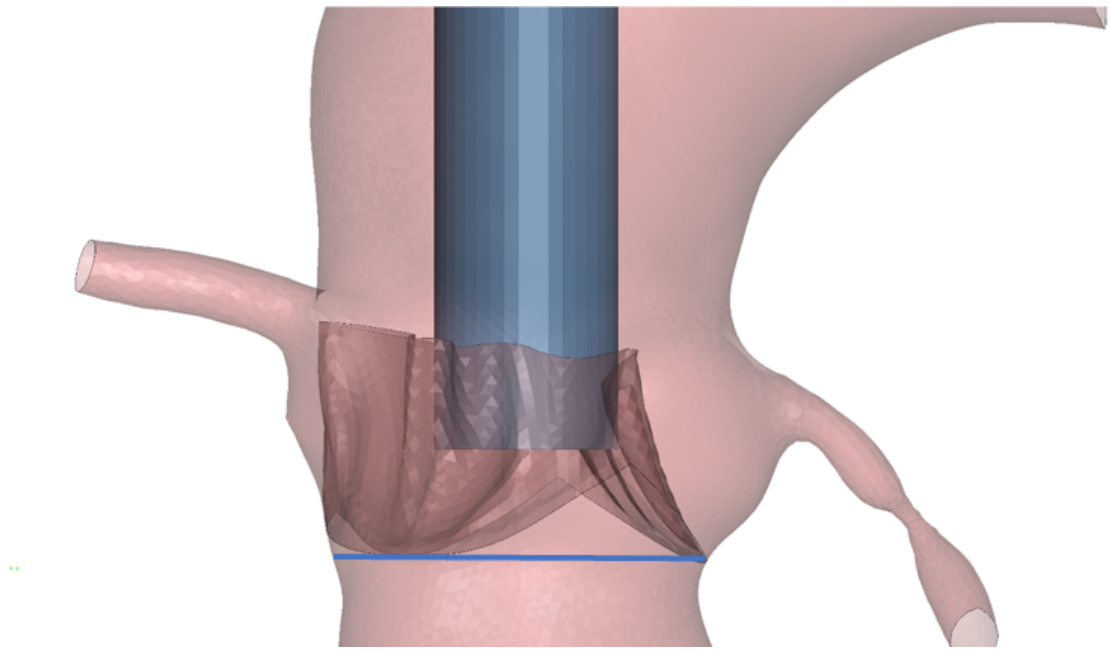

Figure 6.2: *Example of the correct anatomy orientation.*

As for the implantation depth, it was possible to reproduce it as accurately as possible thanks to the availability of the angiographies of the six patients, obtained during implantation. As can be seen in figure 6.3, the angiographies revealed the structure of the stent and its position with respect to the Valsalva sinuses.

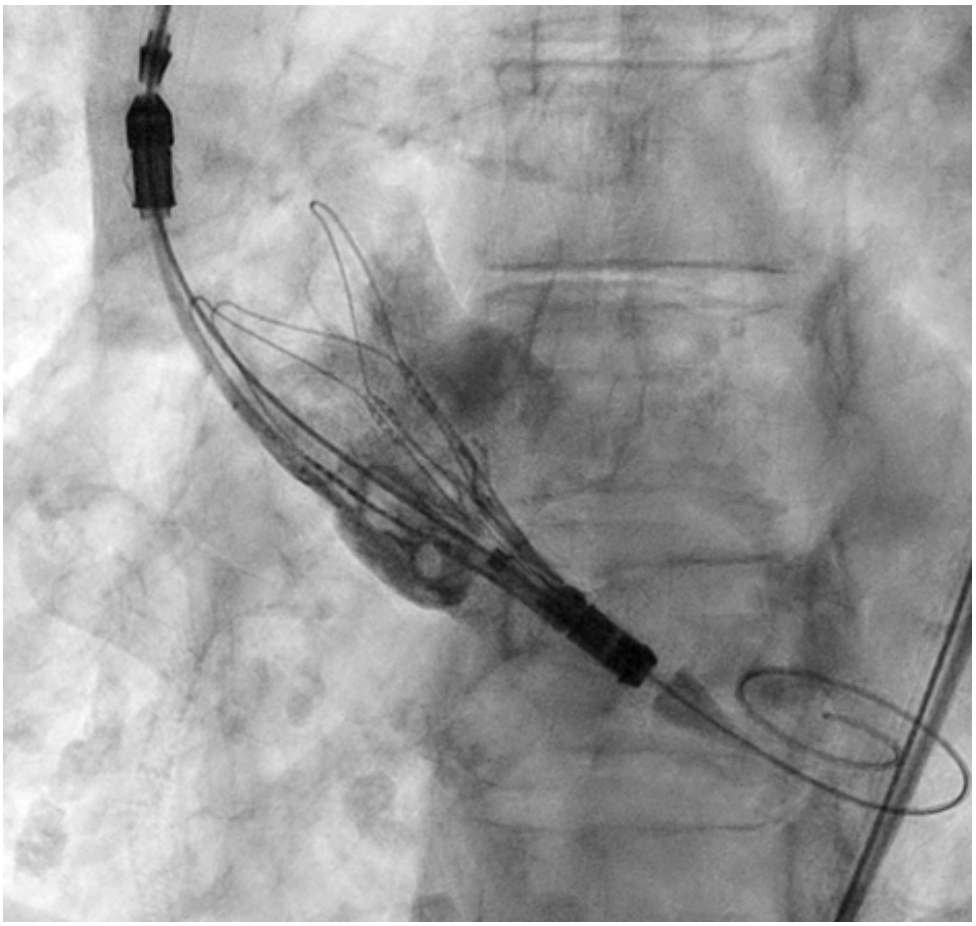

Figure 6.3: *Image taken from an angiography in which the Valsalva sinuses and the stent during its release can be seen.*

6.2. Crimping

The crimping process of the Accurate neo2 valve happens through several steps in which the valve is mounted on two catheters by progressively reducing its diameter. To represent this process, 12 rigid concentric planes were created, placed outside the entire device (Figure 6.4.a). A prescribed motion boundary condition was imposed on these planes (Figure 6.4.b): each plane describes a radial displacement of 11.75 mm, to meet the valve and push it to close until it reaches the diameter of the catheters, which is approximately 12 mm. This first phase lasts 350 ms. At this stage, the contacts between the stent and the other components (calcifications, natural valve, aorta) are not activated.

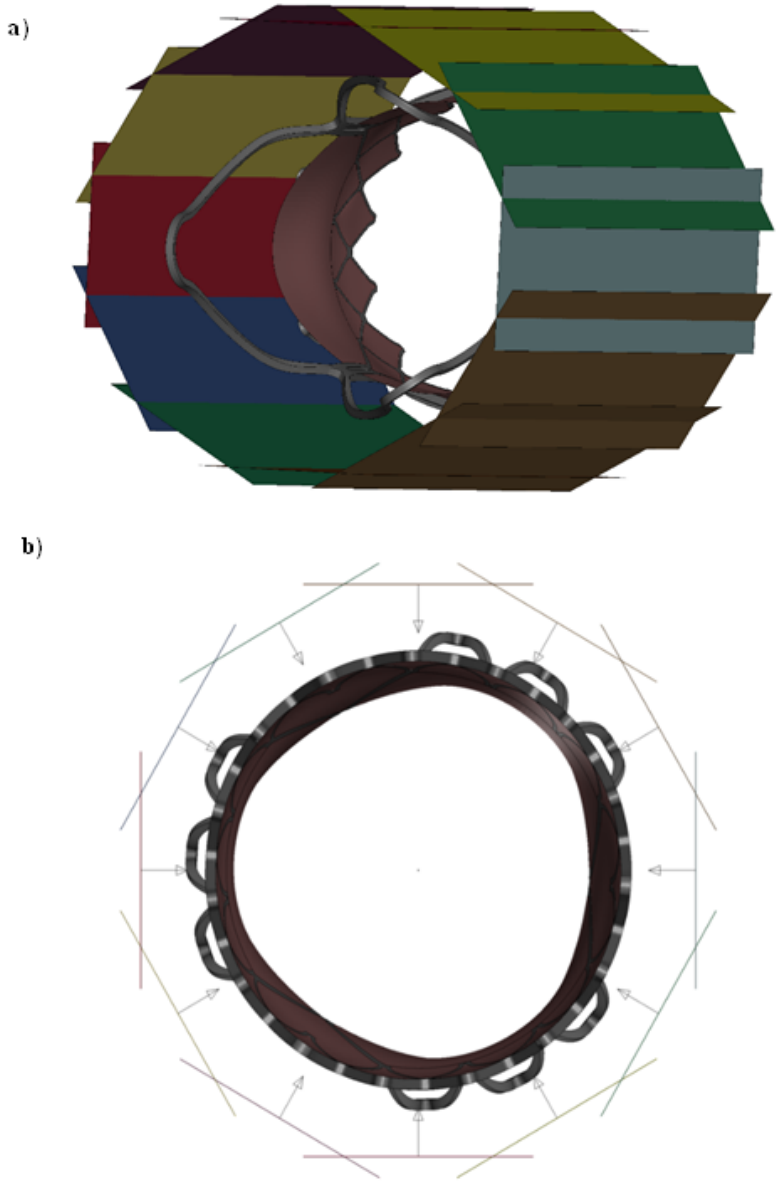

Figure 6.4: *a) Side view of the twelve planes used for crimping. b) Prescribed motion imposed on the planes.*

The planes were discretized with 130 shell elements following the Belytschko-Tsay formulation and the material was modelled as rigid. During these 350 ms, two types of contacts are active. The first is an Automatic Surface-to-Surface contact imposed between the planes and the stent; the second is an Automatic Single-Surface contact imposed on the stent to avoid interpenetration due to the small diameter it must reach. In figure 6.5, different phases of the crimping process are shown.

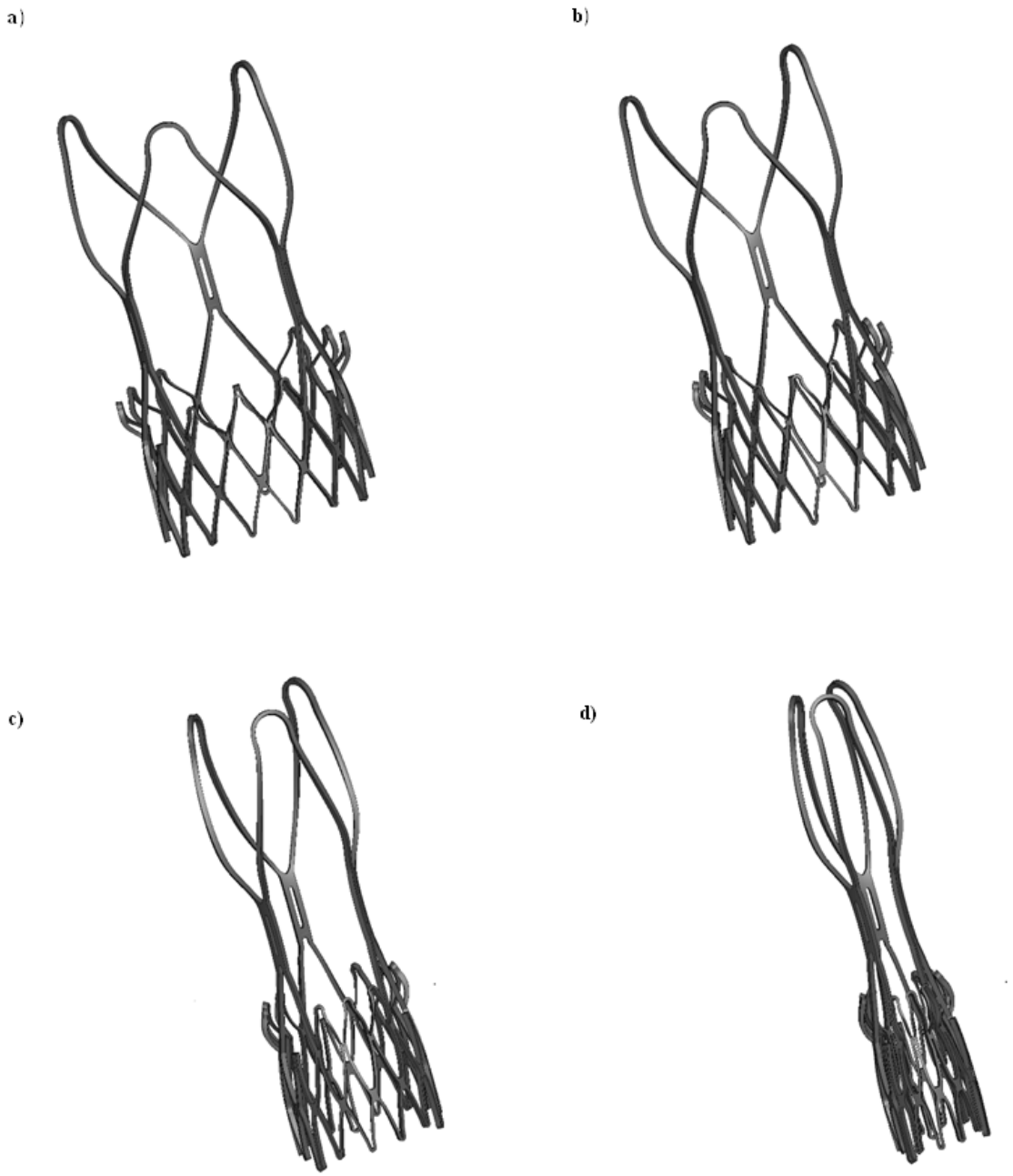

Figure 6.5: *Various instants of the crimping phase: a) t = 0, b) t = 150 ms, c) t = 250 ms, d) t = 350 ms (end of the crimping phase).*

6.3. Deployment inside patient-specific aortic roots

After the crimping phase, the release of the device into the patient-specific anatomies begins. This phase takes place from t = 350 ms to t = 800 ms, which coincides with the

end of the simulation, thus lasting 450 ms.
In order to reproduce the deployment of the Acurate neo2 valve, two cylinders constituting the two release catheters of the device were modelled. A motion boundary condition was imposed on these simulation elements. The first catheter to move is the upper one, which moves upwards; this movement start at t = 350 ms and ends at t = 650 ms. The movement of the second catheter, i.e. the lower one, is instead imposed downwards and begins at this instant and ends at t = 750 ms.

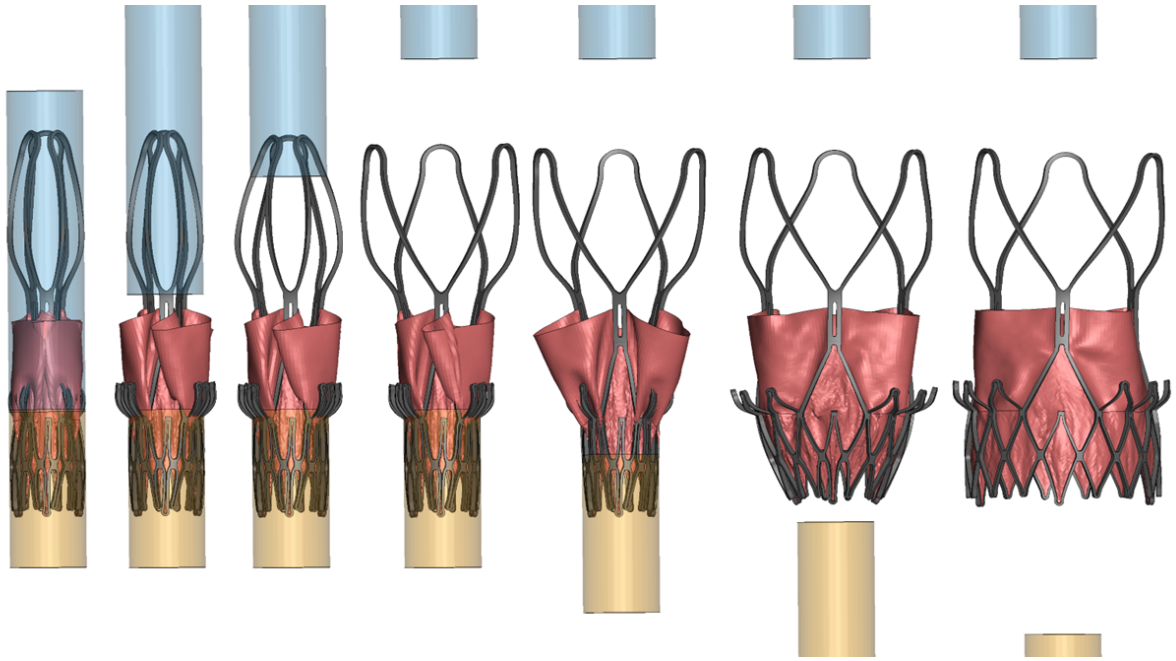

Figure 6.6: *Evolution of the deployment.*

The upper catheter was discretized with 2457 quadrilateral elements, while the lower one consists of 1209 quadrilateral elements, all following the Belytschko-Tsay formulation. With regard to the material, catheters were modelled as rigid bodies. Both catheters are involved in the contact with the device, i.e. with the stent, skirt and leaflets, so as not to allow interpenetration between these elements and thus correctly reproducing the role of the catheters in containing the crimped device. In addition to these, two other contacts are activated, namely those with the calcifications and the natural valve. Indeed, the fundamental methodological difference between the crimping case and this second phase is that in the latter, all contacts involving the patient's anatomy are activated.
In addition to the contacts involving the catheters, many others, which are listed below, are necessary in order to faithfully replicate the implantation of this device.

- Stent – aorta: this is the only contact characterised by a friction coefficient of 0.2, as it is the most important to ensure the correct positioning of the prosthetic valve,

without overcomplicating the simulation;

- Stent – natural valve;
- Stent – calcifications;
- Aorta – pericardium skirt;
- Aorta – calcifications;
- Aorta – leaflets;
- Calcifications – leaflets;
- Calcifications – pericardium skirt;
- Natural valve – pericardium skirt

All these contacts are of the Automatic Surface-to-Surface type.
To avoid its translation during the valve release, the aorta model has been locked in the three directions of movement on the two aortic free edges and on the two coronary free edges, as shown in figure 6.7.

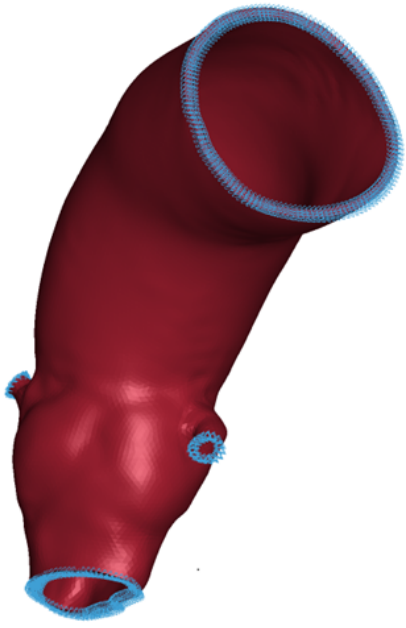

Figure 6.7: *Aortic model edges locked in the three directions.*

An example of the final configuration obtained from these simulations is reported in figure 6.8. The results will be addressed in more detail in the next chapter.

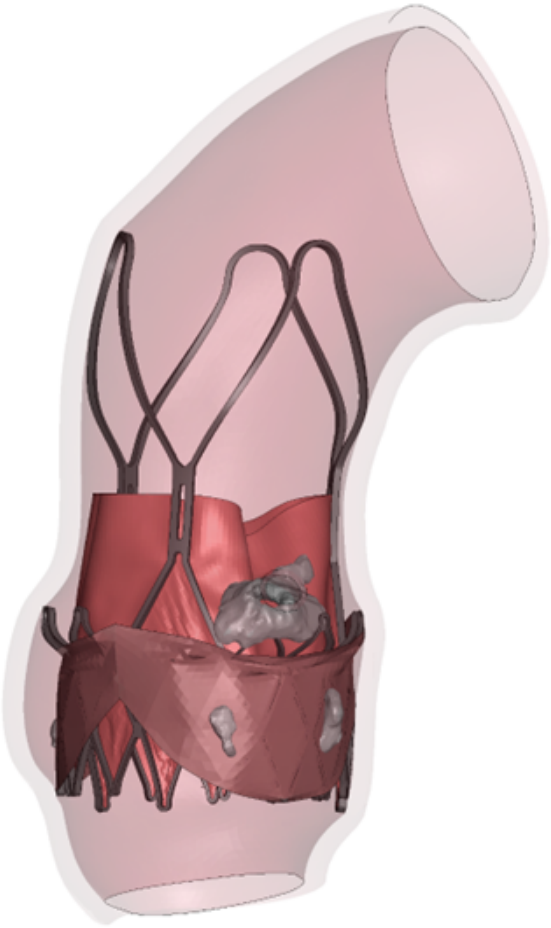

Figure 6.8: *Final configuration obtained for one of the patients.*

6.4. Results

Simulations made in LS-DYNA (shown in the following figures) allow to obtain the deployed configuration of the prosthesis inside the patients' aortic roots. These configurations were then superimposed on the patients' angiographies to confirm from a qualitative point of view not only the correctness of the replication of the patient's anatomy, but also the correct positioning of the device in the post-deployment configuration.

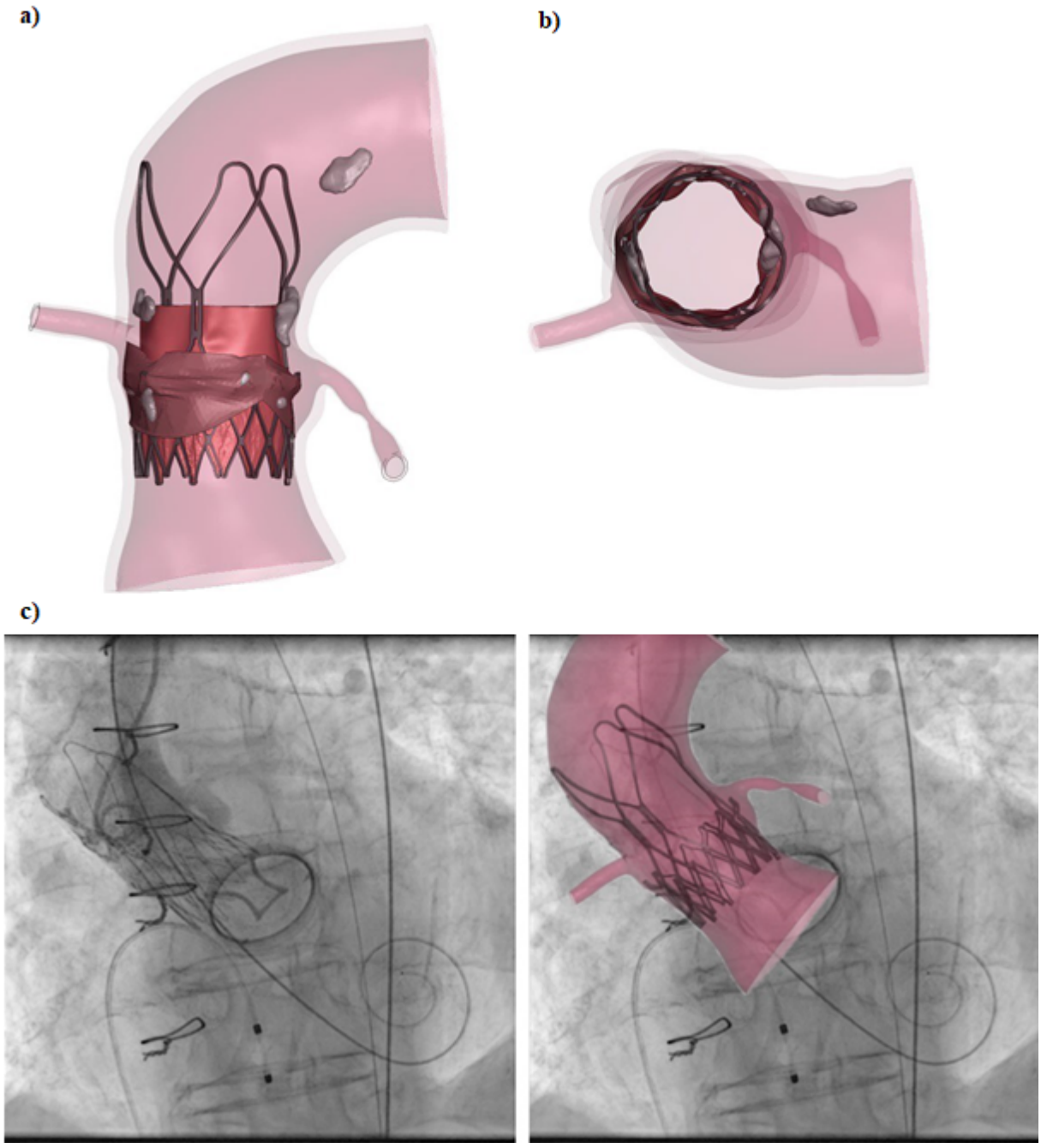

Figure 6.9: *a) Patient one, side view; b) Patient one, top view; c) Comparison between patient one's angiography and the same after superimposing the modelled aorta with the device.*

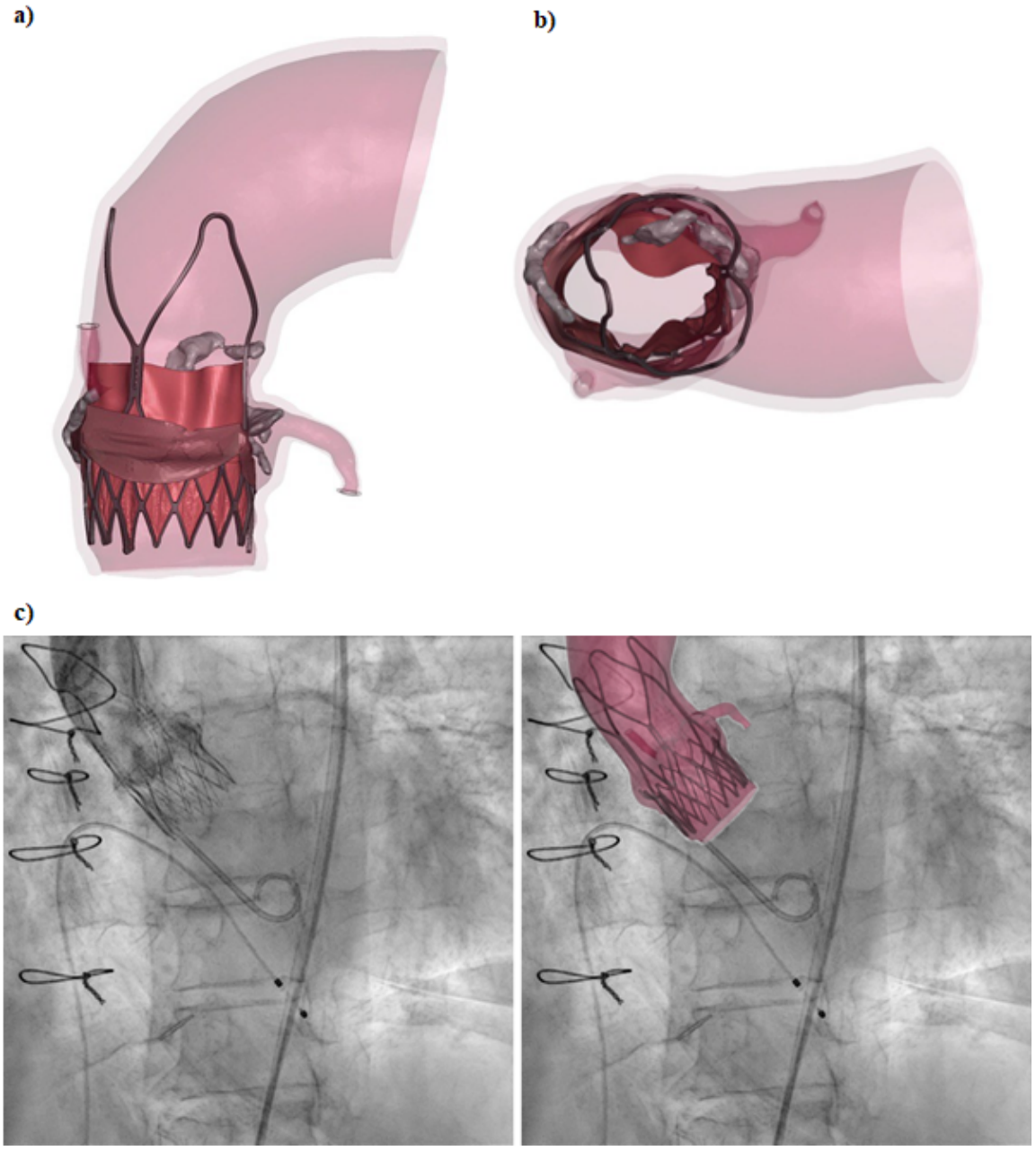

Figure 6.10: *a) Patient two, side view; b) Patient two, top view; c) Comparison between patient two's angiography and the same after superimposing the modelled aorta with the device.*

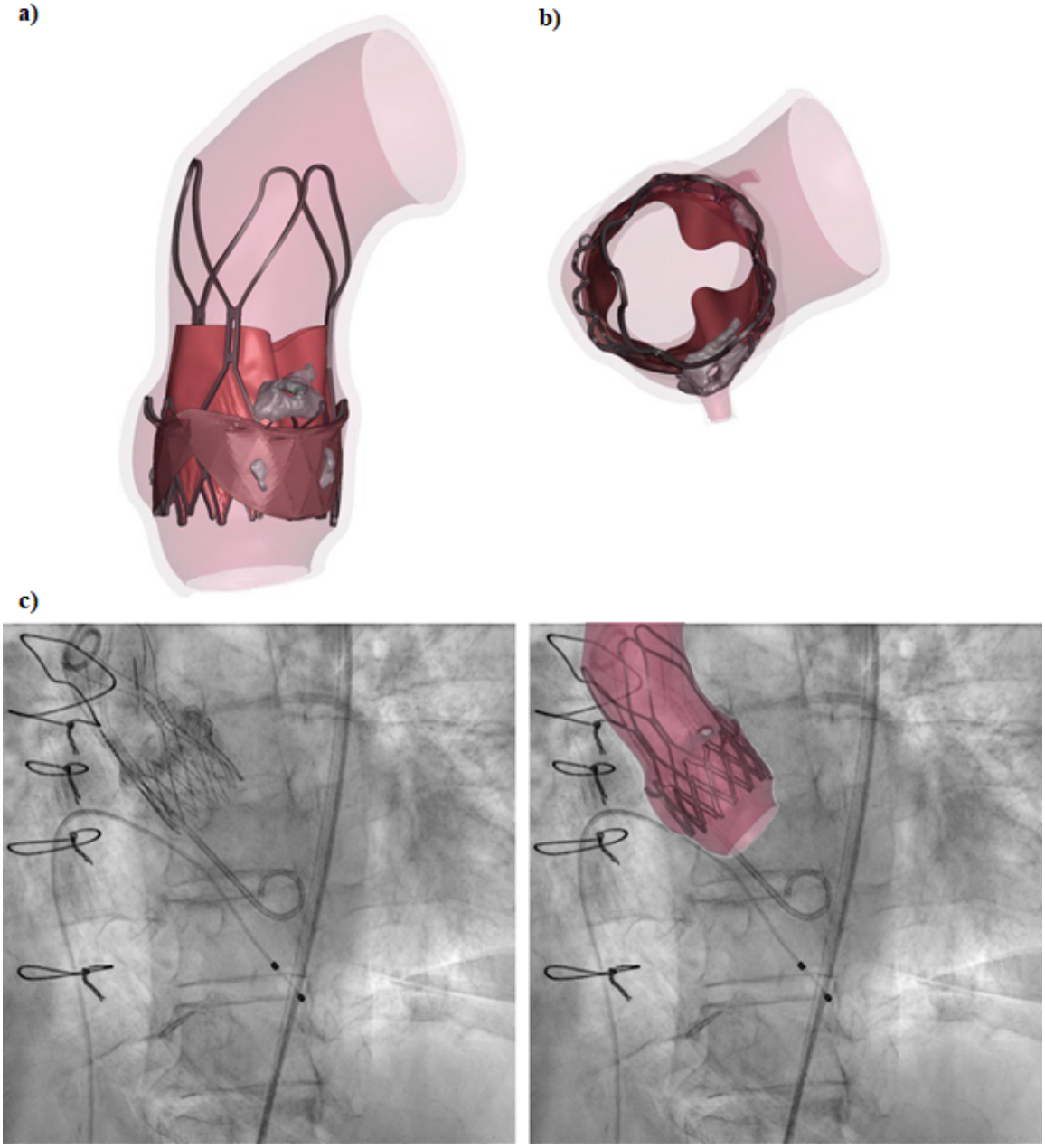

Figure 6.11: *a) Patient three, side view; b) Patient three, top view; c) Comparison between patient three's angiography and the same after superimposing the modelled aorta with the device.*

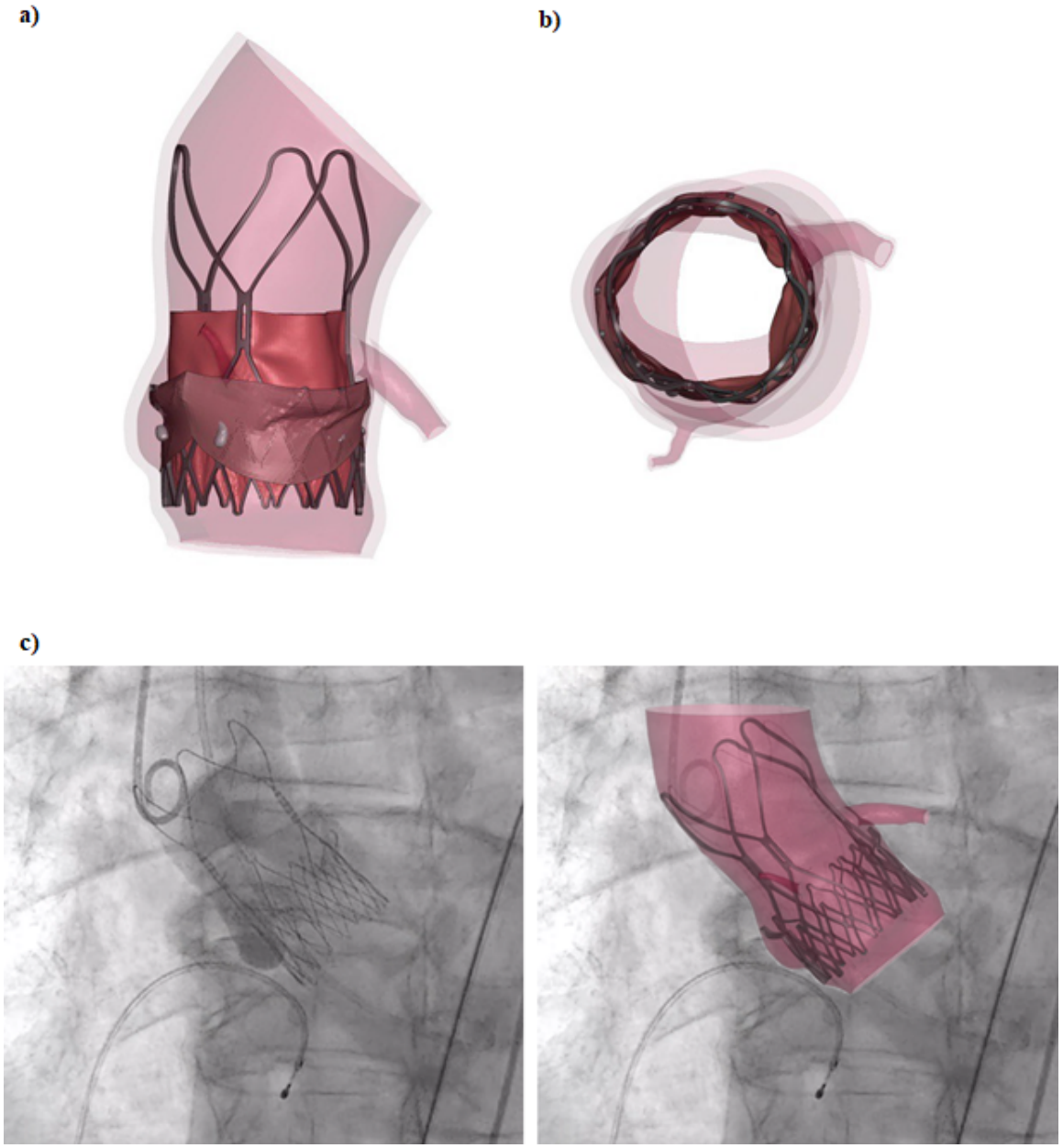

Figure 6.12: *a) Patient four, side view; b) Patient four, top view; c) Comparison between patient four's angiography and the same after superimposing the modelled aorta with the device.*

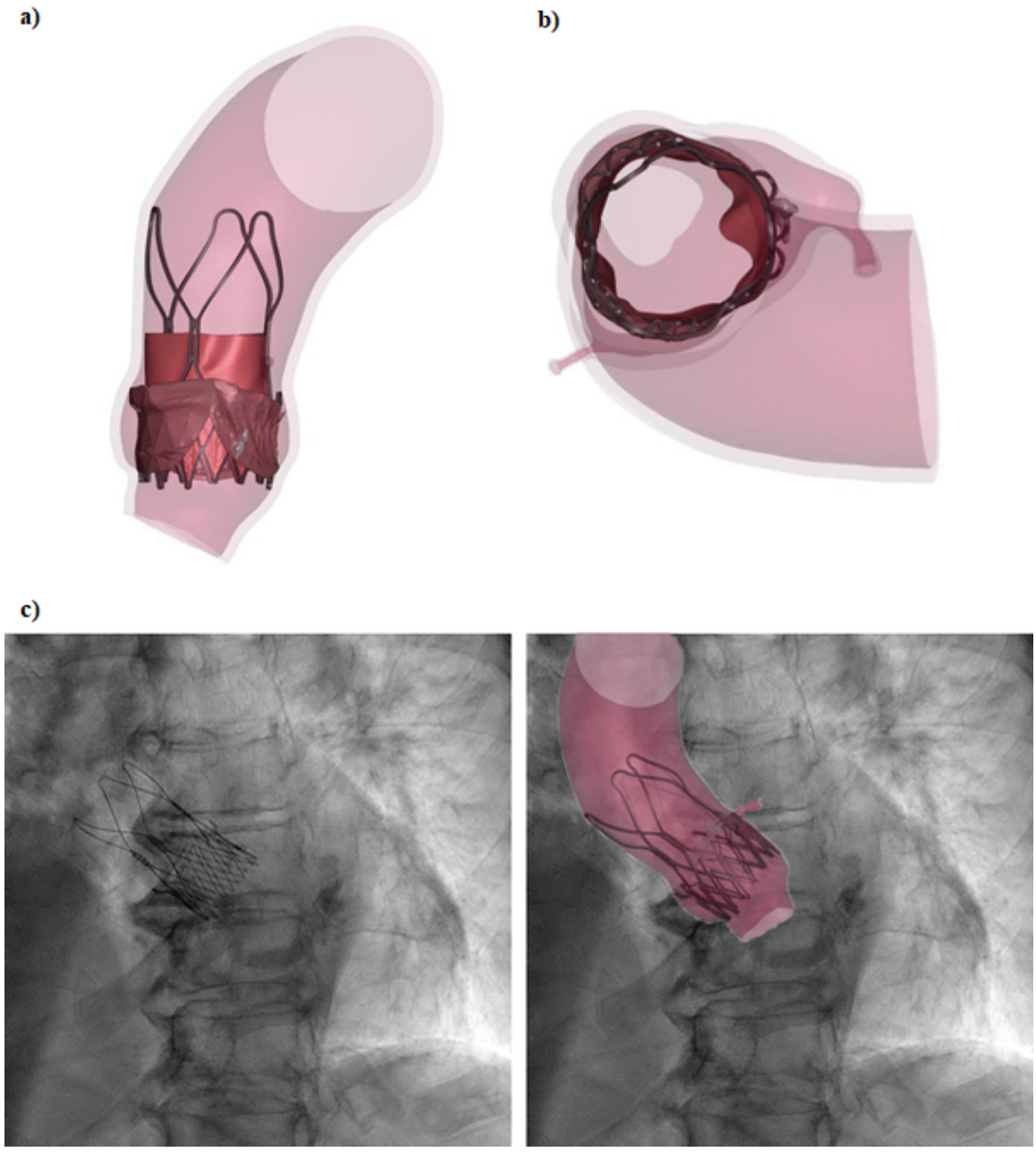

Figure 6.13: *a) Patient five, side view; b) Patient five, top view; c) Comparison between patient five's angiography and the same after superimposing the modelled aorta with the device.*

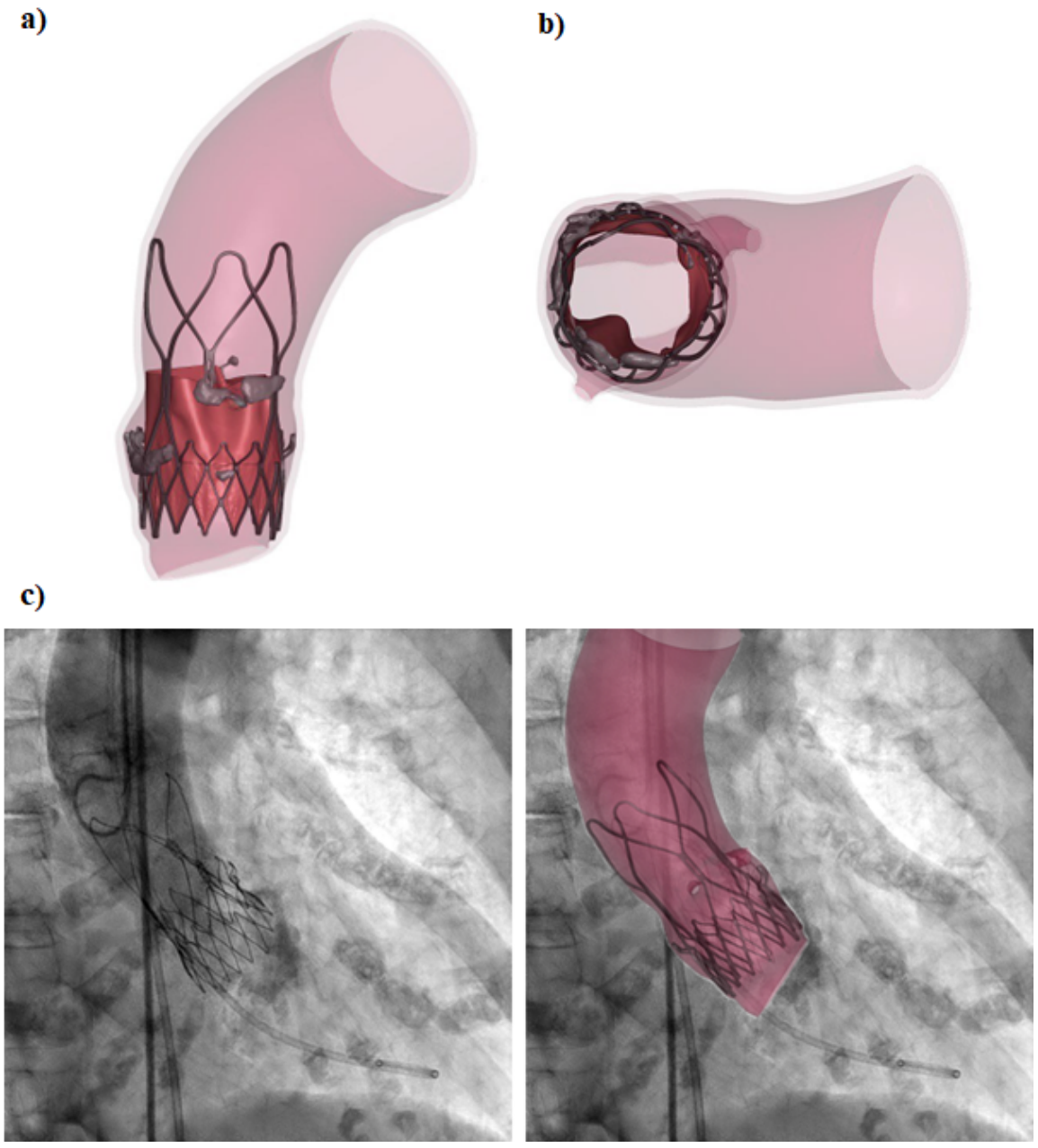

Figure 6.14: *a) Patient six, side view; b) Patient six, top view; c) Comparison between patient six's angiography and the same after superimposing the modelled aorta with the device.*

From the angiographies, the correct positioning of the device was maintained even after the deployment phase. The simulations therefore took place correctly, adequately respecting the actual implantation. After all six implants of the Acurate neo2 valves in the patients have been simulated in LS-Dyna, the results have been analysed in META v22.1.2 (BETA CAE Systems, Switzerland). Among the entire simulation, only the last configuration, i.e. the complete deployment inside the aorta. has been studied, because it represents the

effective situation inside the patient, thus being the one of clinical interest.

6.4.1. First principal stress on the aortic wall

The first result that has been analysed is the first principal stress (1^{st} Princ σ over the aorta's wall, caused by the stent in its opened configuration.
Due to the conformation of the anatomy, the stresses will be higher in correspondence with the Valsalva's sinuses, as expected. Three different planes have been considered (Figure 6.15), at which a horizontal section was made. The first plane (called 'a' in the figures) lies at the connection between the lower and upper parts of the stent. The second (called 'b') lies at the side hooks, while the third ('c') lies in correspondence with the main contact points of the lower cage.

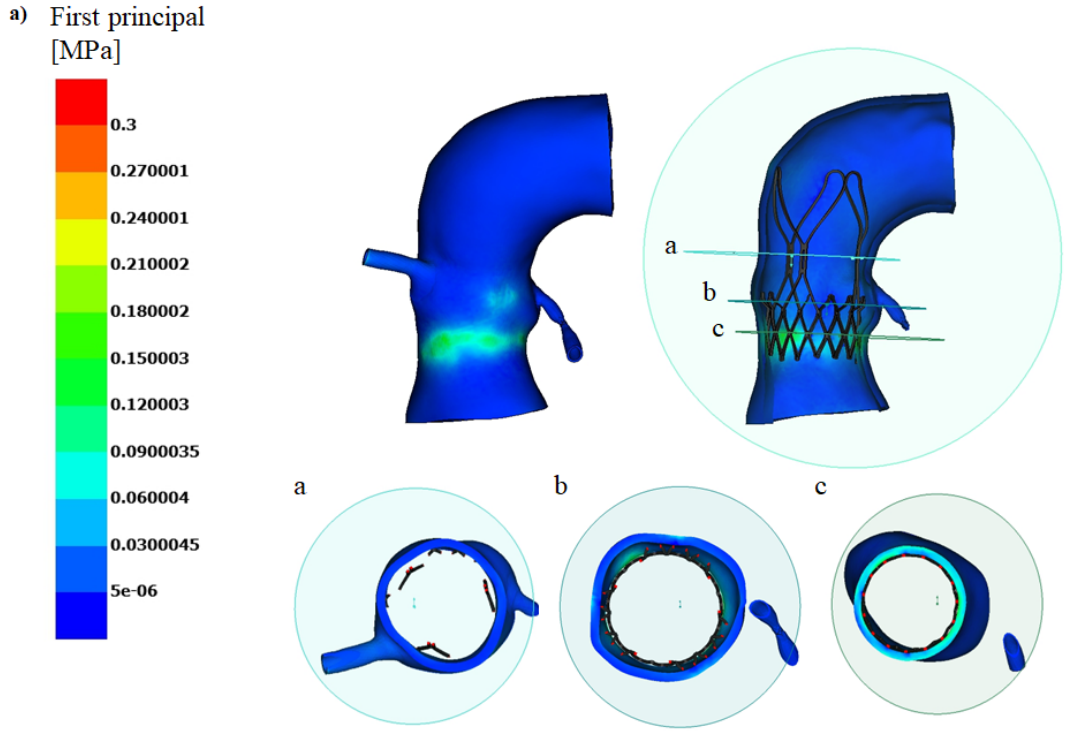

b) First principal [MPa]

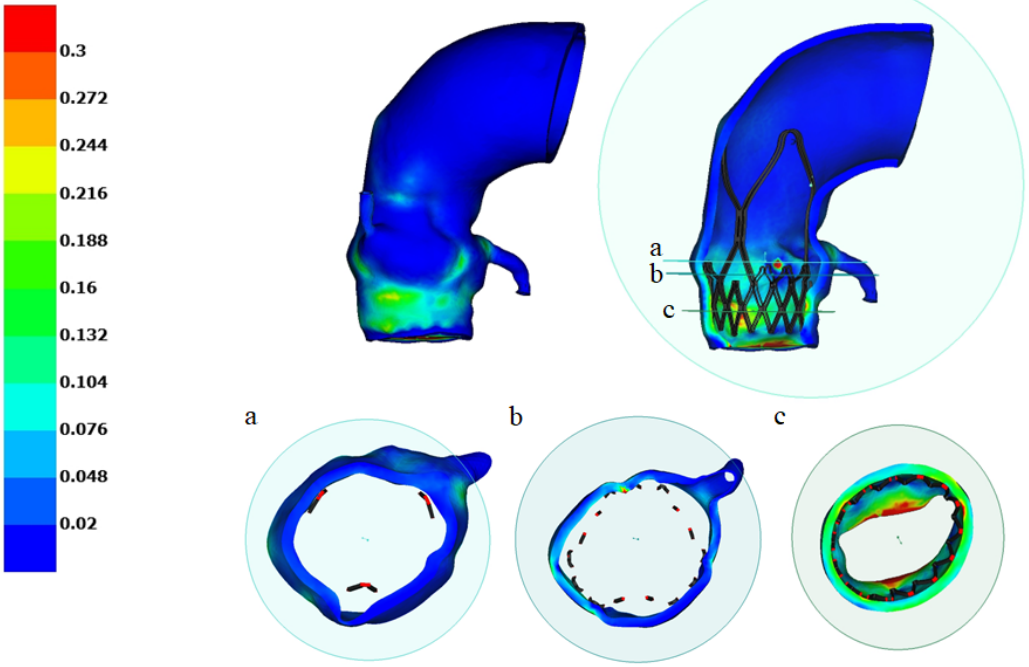

c) First principal [MPa]

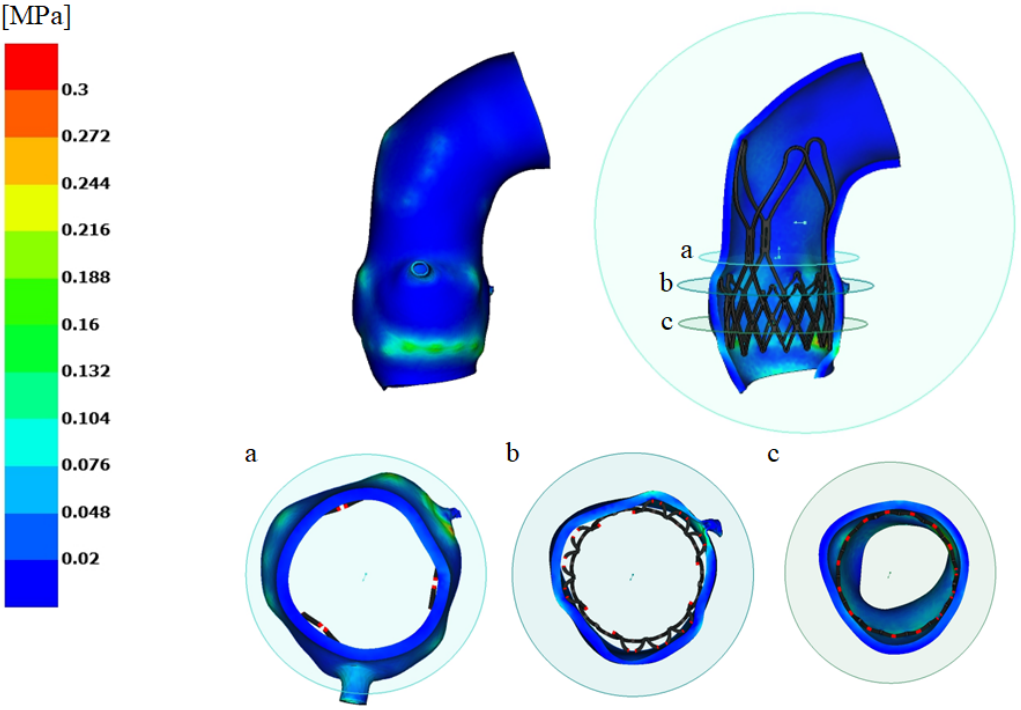

d) First principal [MPa]

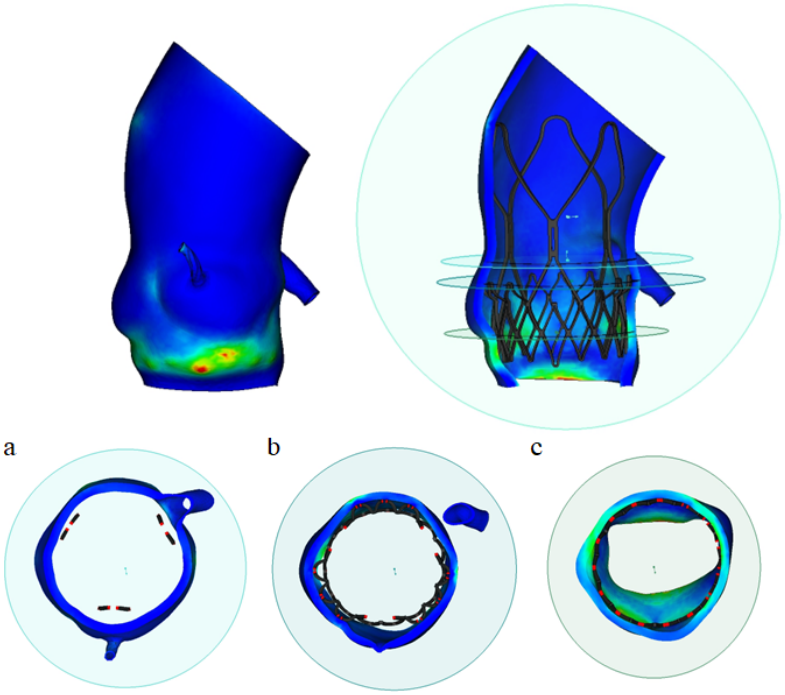

e) First principal [MPa]

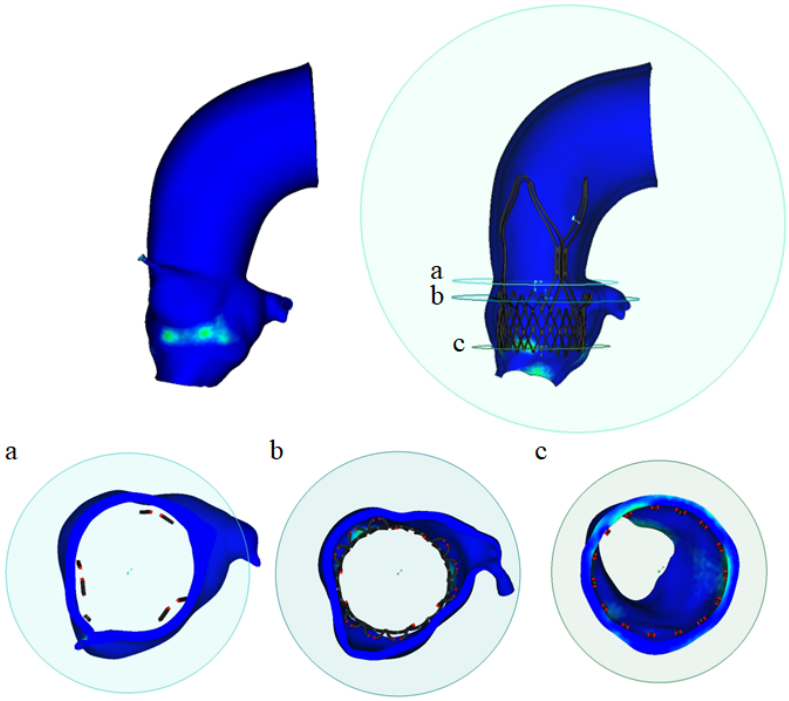

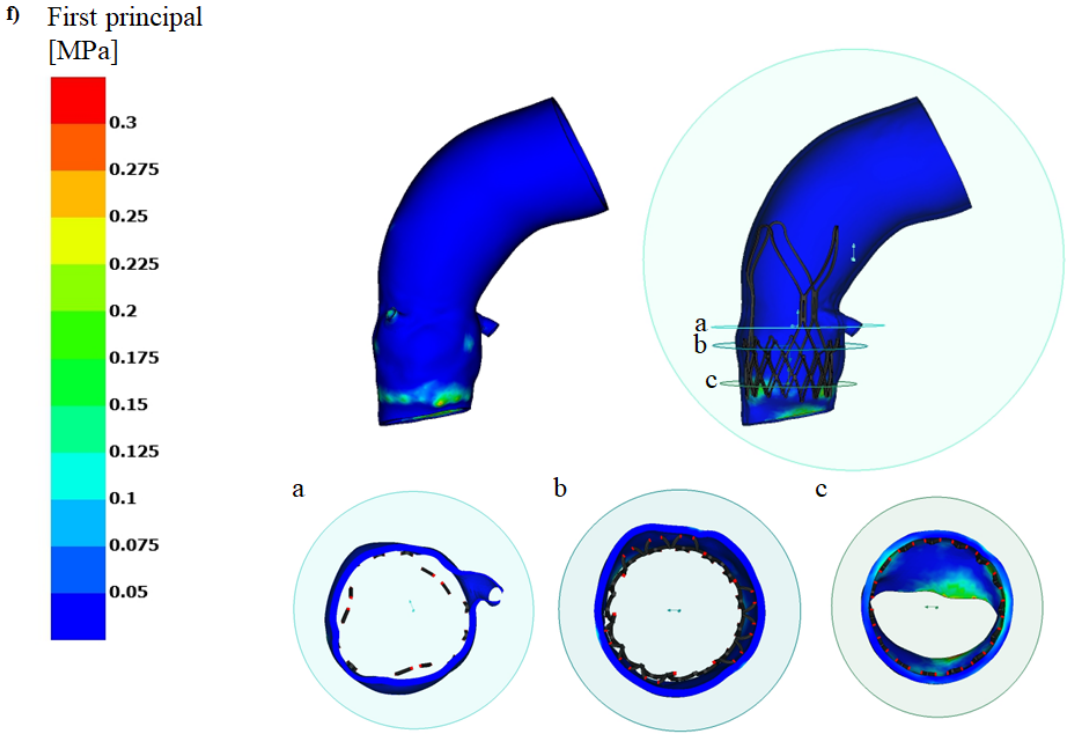

Figure 6.15: *First principal stress on the aortic wall found for each patient (from a) to f)).*

Among the results obtained, uniformity in the distribution of stresses can be seen. The highest values can be reasonably found in all patients in correspondence of the lower cage of the stent, where the device adheres to the inside of the aortic root.
In case of patient number two (Figure 6.15.b), there are different results compared to the other patients, with a larger stress area visible in the lateral area of the aortic sinus. These values are caused by the compression of calcifications of considerable size alongside the aortic wall.
For what concerns patient number four (Figure 6.15.d), the contours show a peak of the stresses in two really localised points, that can be both found below Valsalva's sinuses. It is also possible to notice that in all patients except number one (Figure 6.15.a), the results along the lower edge of the aorta are not reliable, as they are influenced by the boundary conditions applied.

Number of the patient	*Maximum* 1^{st} *Princ* σ *[MPa]*
1	0.3040
2	2.8300
3	0.7210
4	0.4255
5	0.3300
6	0.6580

Table 6.1: *Maximum values of the first principal stress found in each patient.*

Of the values in the table, the only one that differs significantly from the others belongs to patient number two (Figure 6.15.b). This is caused by a high compression on a little zone inside the aortic wall, as there is a small protuberance in that area. This is due to the lateral hooks that are applying pressure at the edge of this anatomic peculiarity.
The maximum stress value of patient six (Figure 6.15.f) is instead located in an element on the edge of one of the two coronary arteries and is probably due to the boundary conditions applied there, as it differs from the remaining values that can be seen in the corresponding contour. The same phenomenon occurs in patient five (Figure 6.15.e), although the maximum stress reached is less different from the other values in the rest of the aorta.

6.4.2. Aortic Root deformation

The second parameter that has been evaluated is the aortic root deformation caused by the Acurate neo2 valve.

a) Deformation

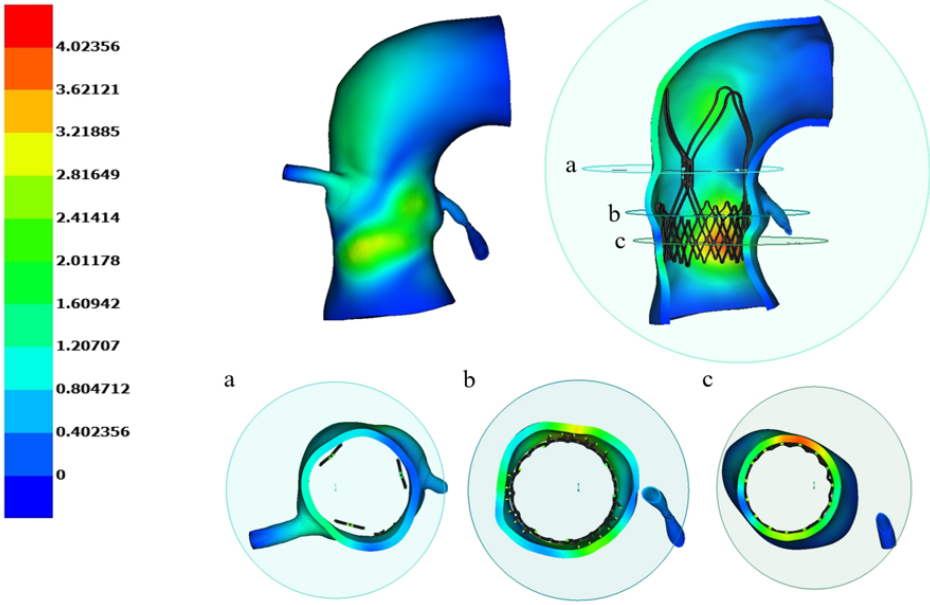

b) Deformation

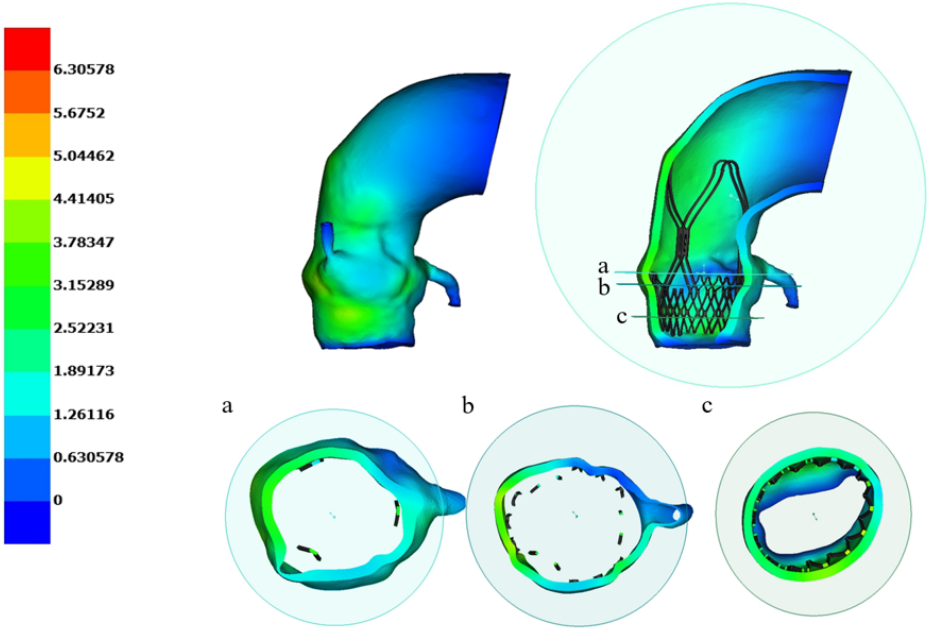

c) Deformation

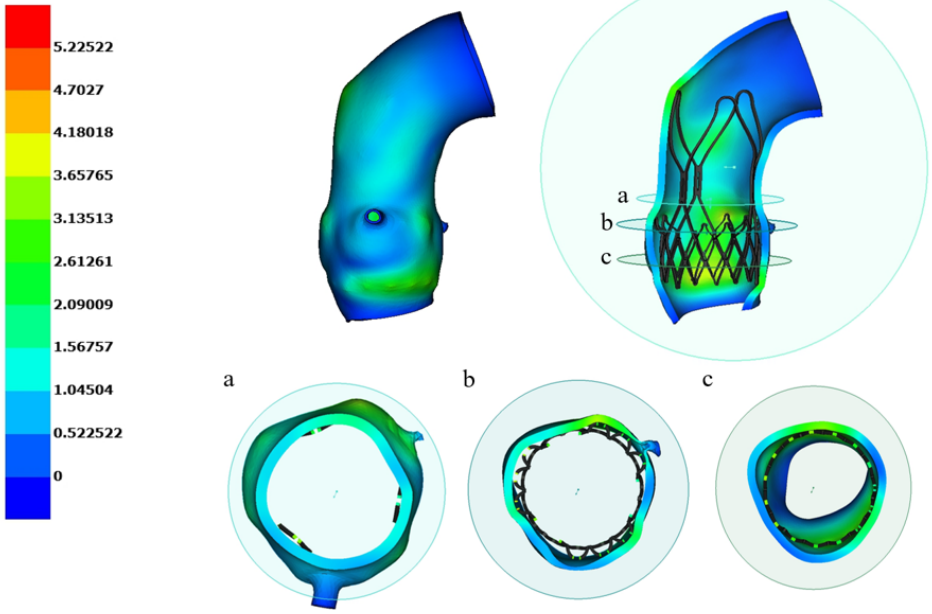

d) Deformation

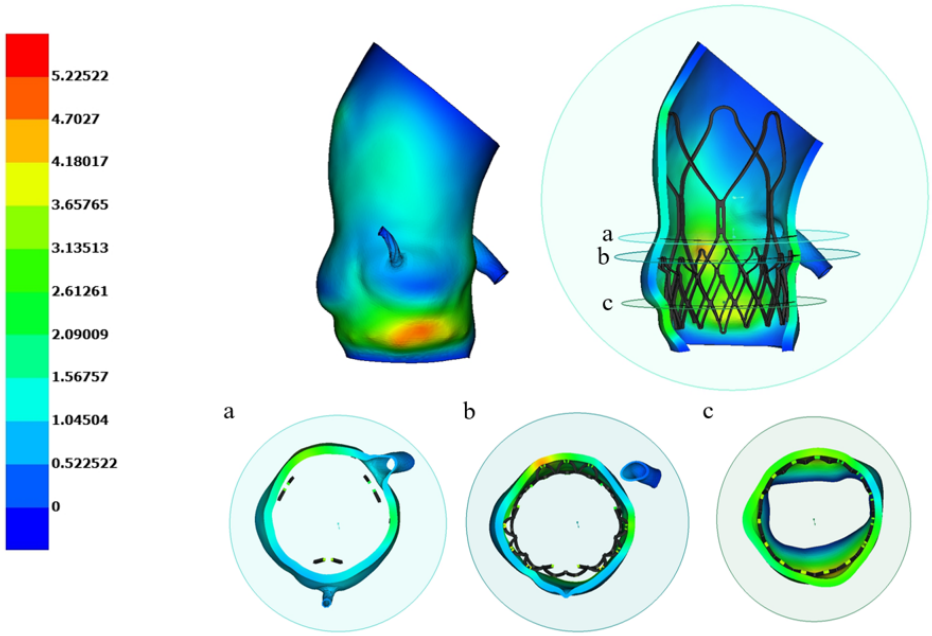

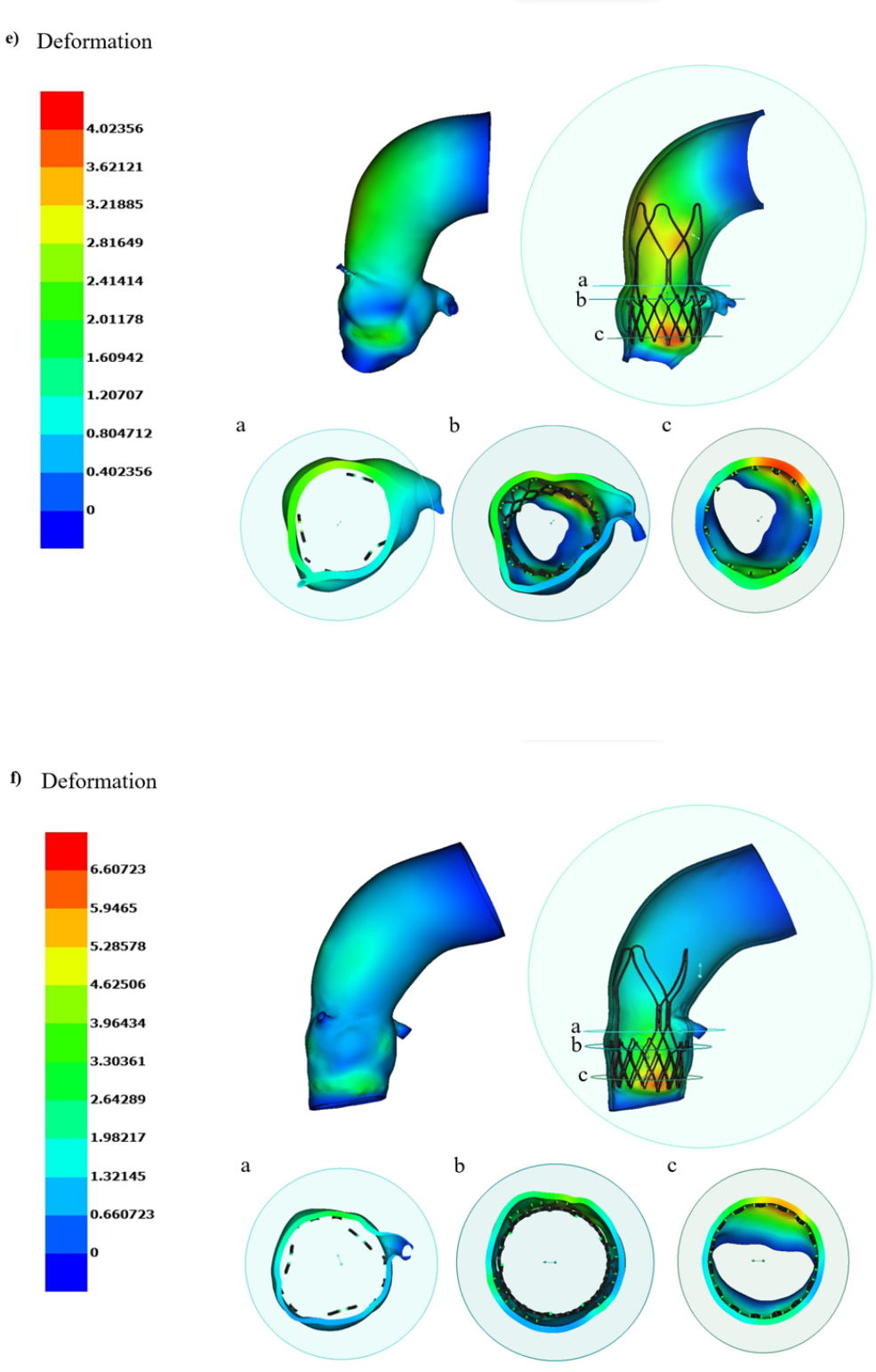

Figure 6.16: *Deformation of the aorta found for each patient (from a) to f)).*

All results agree and show that the most deformed areas are those in correspondence of

the prosthesis. The images representing section "c", which contains the contact between the lower portion of the stent and the aorta's wall, show greater deformation than the other areas. Patients one, four, five and six (Figure 6.16.a, d, e, f) show relatively greater peaks of deformation than the other three patients. Patient five (Figure 6.16.e) is also the only one with a high deformation in the part where the upper cage lies.

6.4.3. Stent's Von Mises stress

The third quantity that has been analysed in the results is the Von Mises stress (σ_{VM}) on the stent. There is a greater variety of results here, due to the different anatomies and patient-specific analyses. Smaller aortic dimensions result in greater pressure on the stent cages, while a larger aortic width allows the aorta to apply less pressure and thus the device to be less stressed. In figure 6.17, it has been decided to highlight in the box next to the valve the most stressed point.

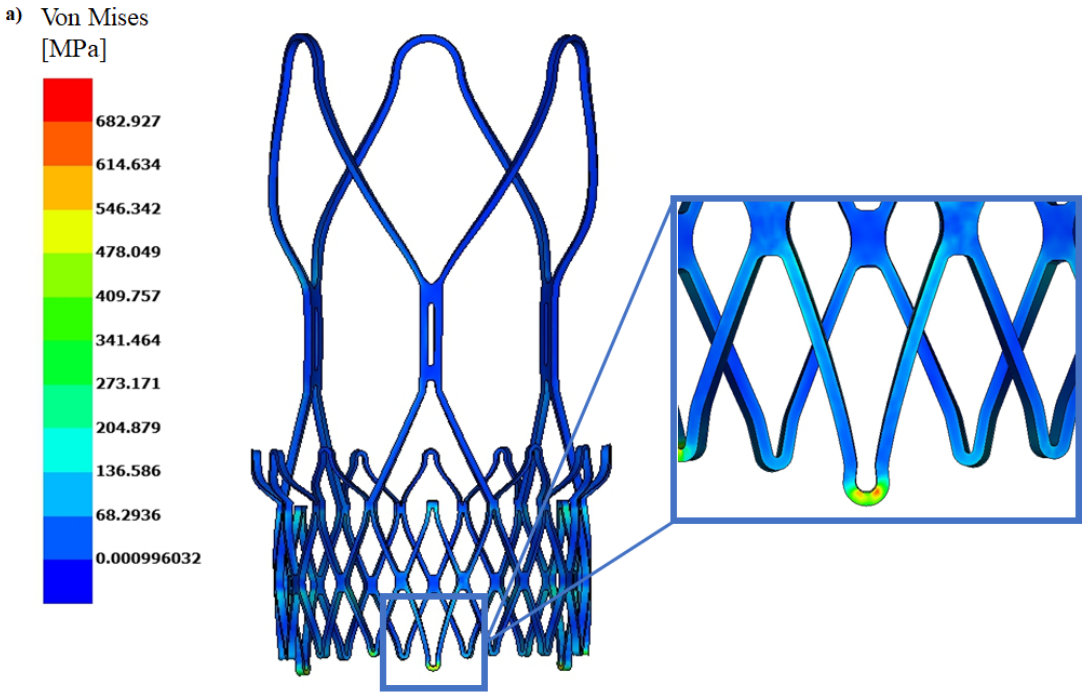

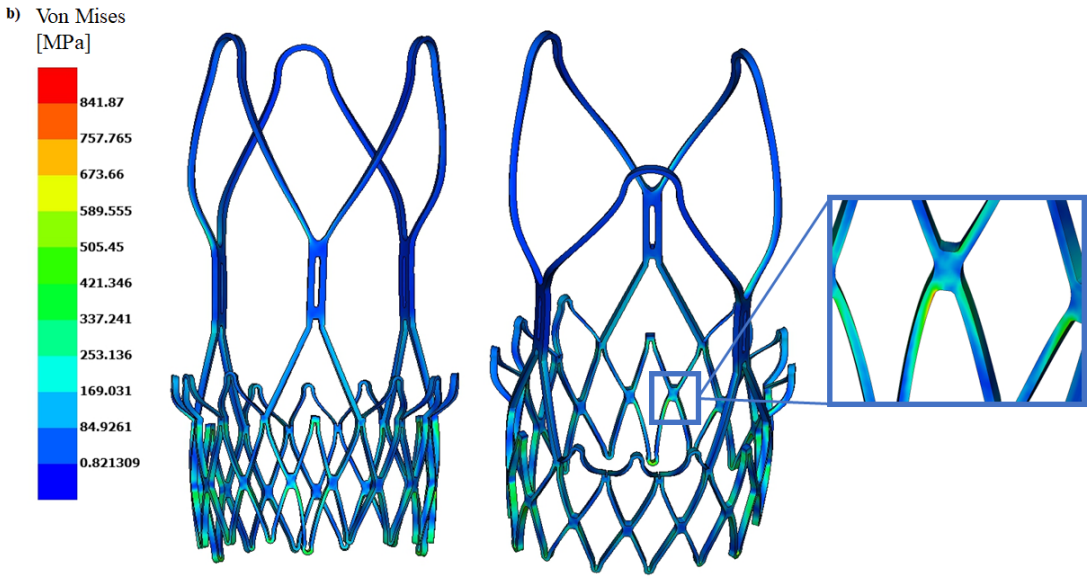
b) Von Mises
[MPa]
841.87
757.765
673.66
589.555
505.45
421.346
337.241
253.136
169.031
84.9261
0.821309

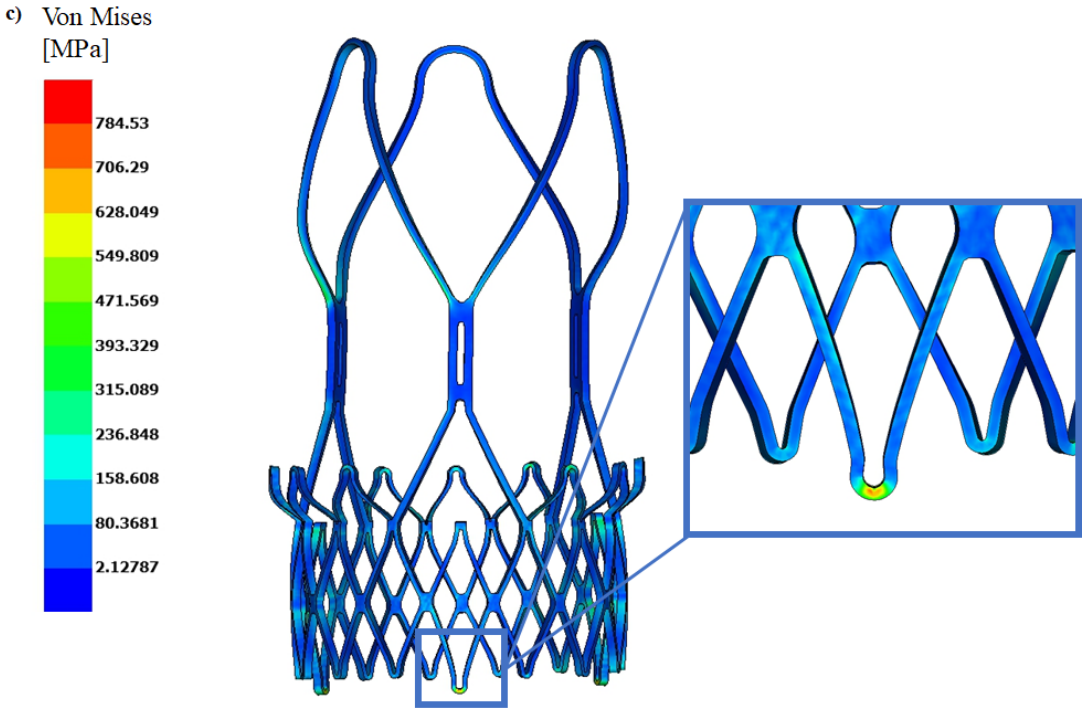
c) Von Mises
[MPa]
784.53
706.29
628.049
549.809
471.569
393.329
315.089
236.848
158.608
80.3681
2.12787

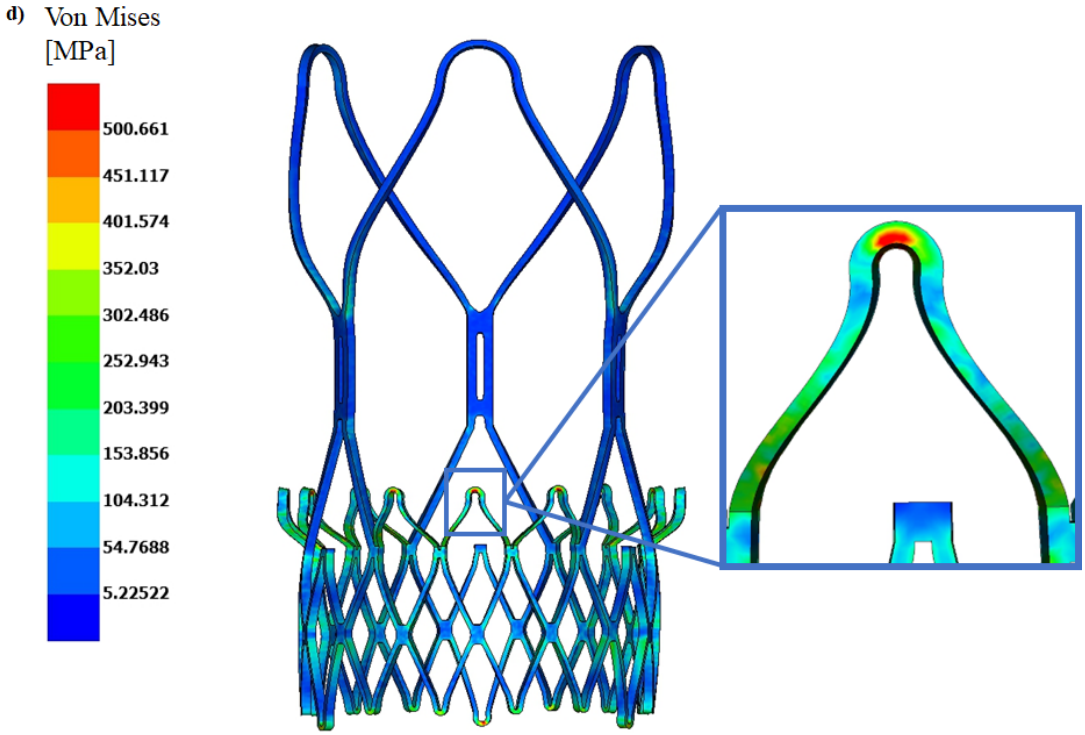
d)
Von Mises
[MPa]
500.661
451.117
401.574
352.03
302.486
252.943
203.399
153.856
104.312
54.7688
5.22522

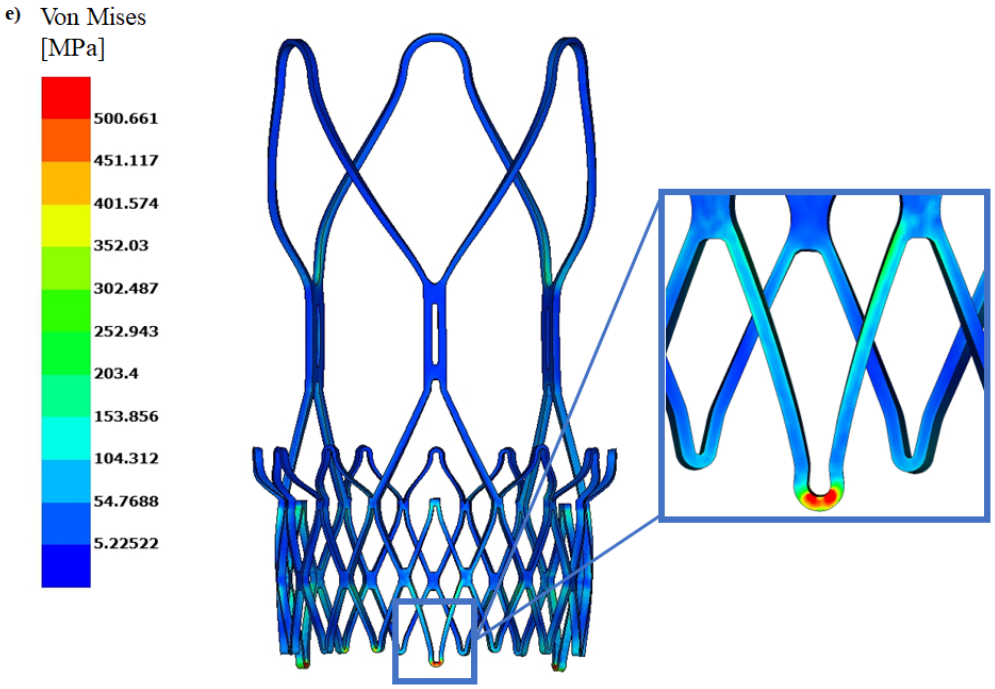
e)
Von Mises
[MPa]
500.661
451.117
401.574
352.03
302.487
252.943
203.4
153.856
104.312
54.7688
5.22522

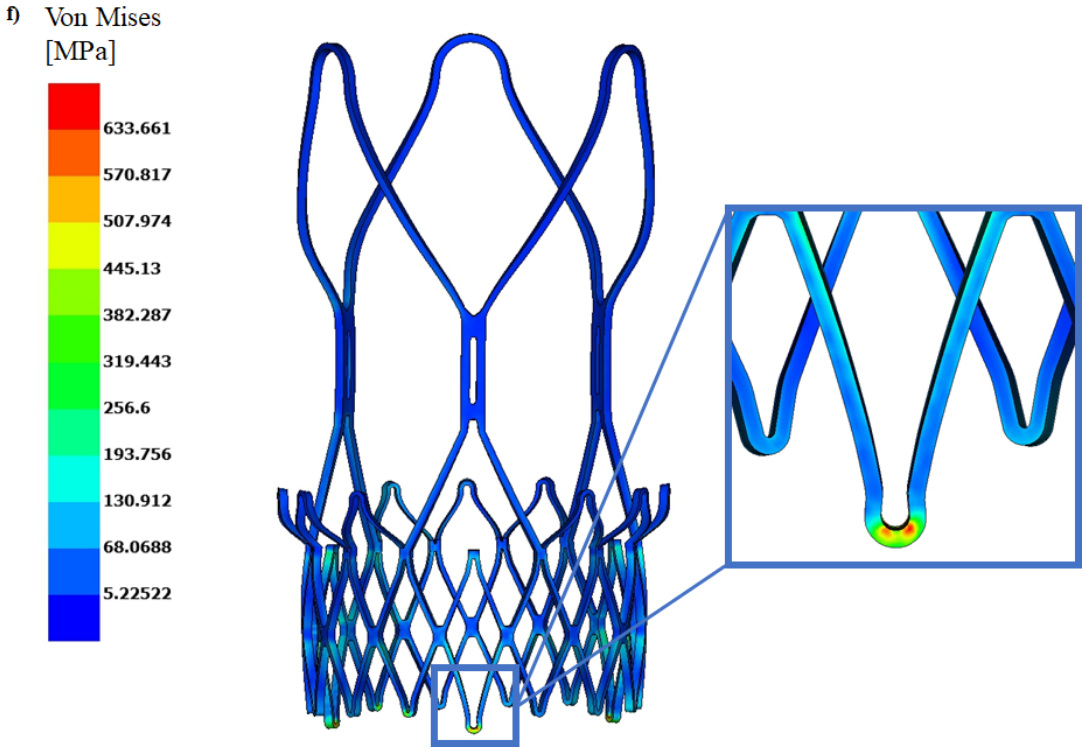

Figure 6.17: *Von Mises stress on the stent found for each patient (from a) to f)).*

As can be seen, the positions vary between different cases. For patients number one, three, five and six (Figure 6.17.a, c, e, f), the point of greatest stress is located within the lower arches of the stent. For patient number four (Figure 6.17.d), on the other hand, the area of greatest stress is located at a lateral hook. Patient number two (Figure 6.17.b), instead, suffers from the geometry of the aortic root. Due to the limited space available, the opening of the prosthetic valve was more difficult, which results in greater stresses at the lower cage, in correspondence of a connection between two cells, and in a slight distortion of the latter.

All the maximum values of the Von Mises stresses found for each patient are higher than 850 MPa. The precise values are shown in the table 6.2.

Number of the patient	*Maximum σ_{VM} [MPa]*
1	859.4
2	860.7
3	936.9
4	872.0
5	877.6
6	883.7

Table 6.2: *Maximum values of the Von Mises stress found in each patient.*

6.4.4. Distance

The last analysis refers to the distance between the stent and the aortic root.

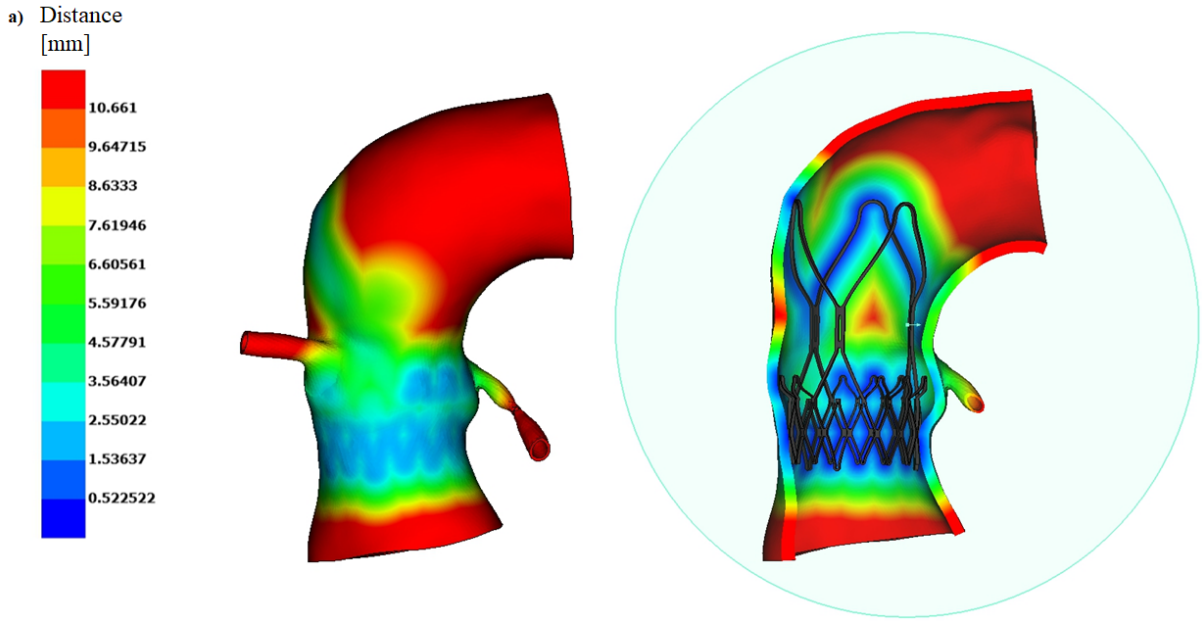

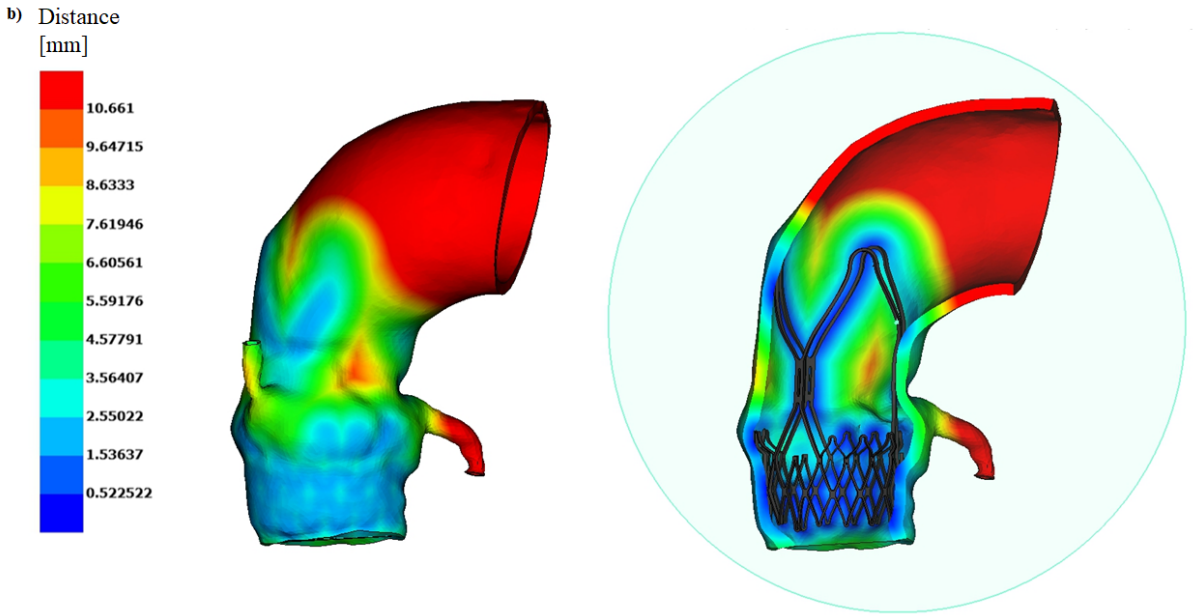
b)
Distance
[mm]
10.661
9.64715
8.6333
7.61946
6.60561
5.59176
4.57791
3.56407
2.55022
1.53637
0.522522

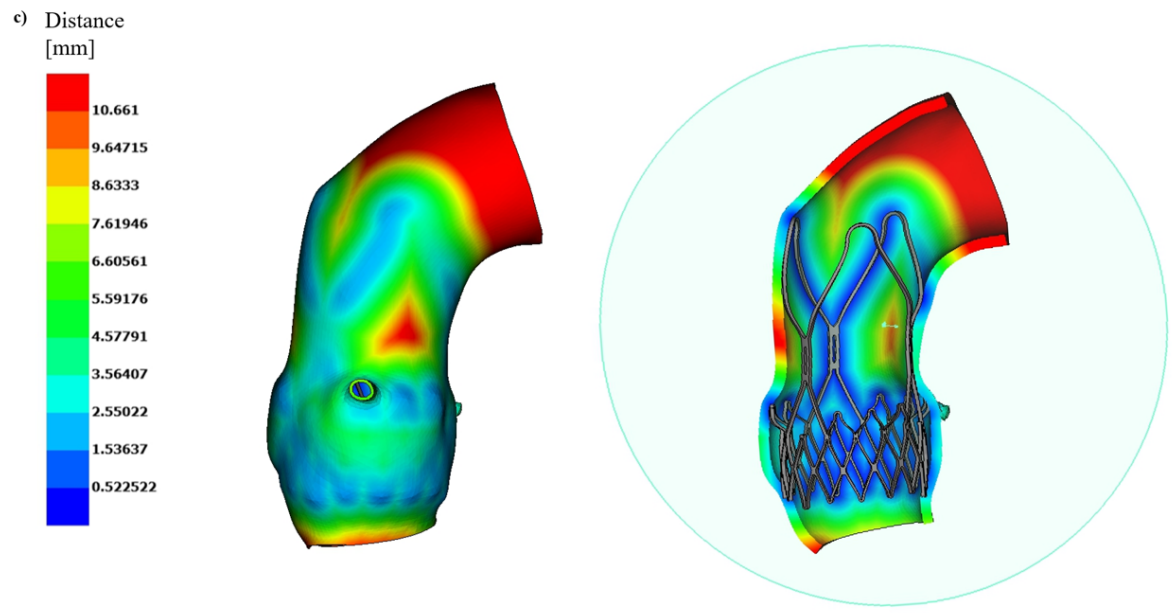
c)
Distance
[mm]
10.661
9.64715
8.6333
7.61946
6.60561
5.59176
4.57791
3.56407
2.55022
1.53637
0.522522

d) Distance [mm]

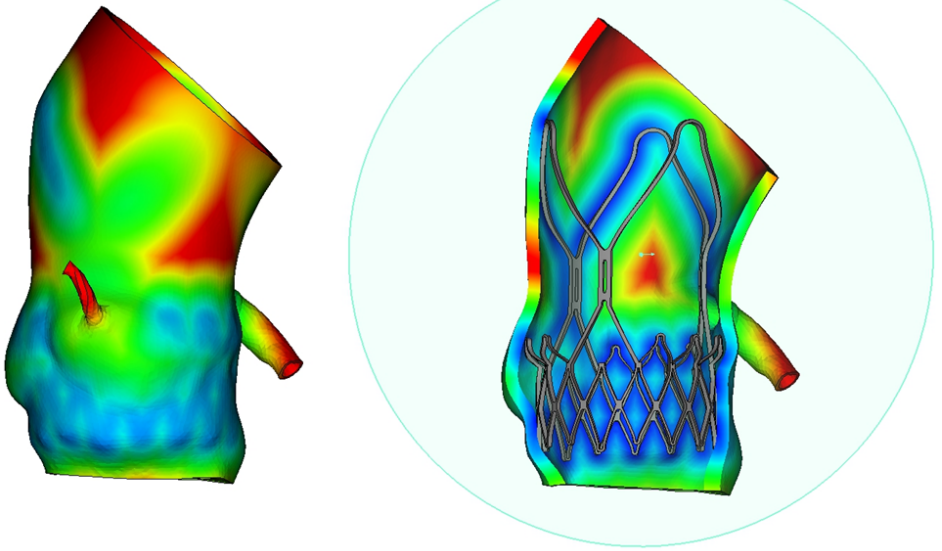

e) Distance [mm]

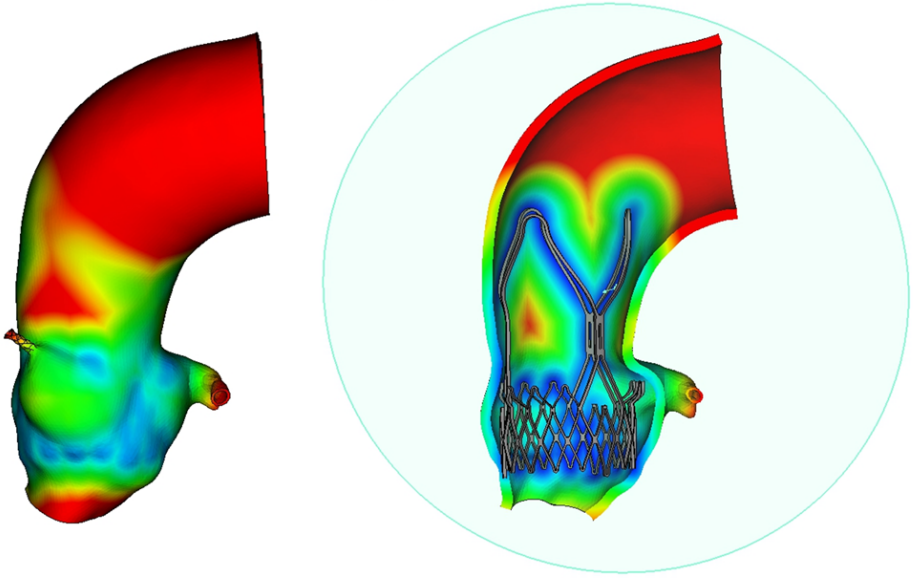

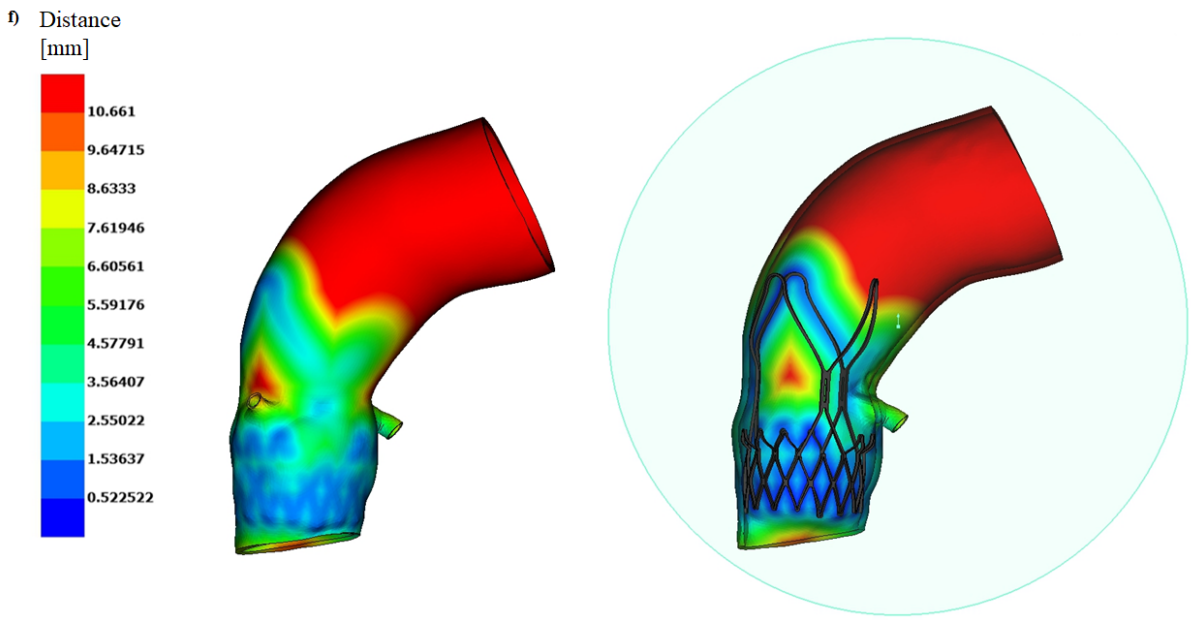

Figure 6.18: *Distance between the stent and the aorta found for each patient (from a) to f)).*

In all patients it can be seen that the stent reaches up to the beginning of the curvature of the aorta and that there is good adhesion of the lower part of the valve. The only differences are present in patients three, four and five (Figure 6.18.c, d, e), where there is a detachment of the lower cage, due to the morphology of their aortic sinuses.
In the upper area, on the other hand, there is less adhesion in correspondence with the upper cage cell placed at the beginning of the curvature of the aorta. In general, the upper cage exhibits different behaviours according to the various anatomies. As can be seen in patients two and three (Figure 6.18.b, c), in fact, the three upper crowns adhere almost perfectly to the curvature of the aorta, while in the others the resulting distance is greater, especially in patient number eight.

7 | Conclusions

7.1. Conclusions

The aim of this thesiswas to develop a computational structural model of an aortic valve prosthetic device and its implant inside the aortic root in order to assess the biomechanics associated with the TAVI procedure and the interaction of this device with six different anatomies. The device that has been studied is the Acurate neo2 valve, made by Boston Scientific. A three-dimensional CAD model, including the pericardium parts, i.e. the skirt and the leaflets, has been recreated in SolidWorks. The device was then discretized in ANSA with solid hexahedral elements for the stent and with shell elements for the skirt and the leaflets. With regard to the patients' pre-implant anatomies, they have been segmented starting from CT images and subsequently discretized in ANSA.
In particular, six patient-specific simulations were developed, fourwith a size S valve, one with a size M valve and the last one with a size L. The correct positioning of the device was made possible with the help of angiographies obtained during the actual operations. Once the meshing of all the components was done, the material properties were modelled in order to best reflect the real mechanical behaviour of the various components, but without overcomplicating the resulting simulation.
The *in silico* model developed considered the two main stages of the procedure, namely the crimping of the prosthetic valve onto the catheter and its subsequent deployment inside the aortic root.
The modelling of the device and the anatomy of the patients - aorta, natural valve and calcifications – allowed to obtain structural finite element simulations that could reproduce and study the influence of the anatomical characteristics of the various patients on the procedure. In fact, the valve was able to adapt in different ways to the geometry of the aorta and the presence of calcifications, taking advantage of its particular design, characterised by the presence of a few lateral hooks. The results of the simulations were then analysed in META.
First, the first principal stresses on the aorta's wall have been analysed. It was possible to understand that the most stressed areas were the lower parts of the sinuses of Valsalva.

This is due to their morphology and the fact that in all six cases the lower cage of the stent, which is also the one with the most cells, adhered to the wall of the aorta precisely at this anatomical point, thus causing these stresses in the aortic tissue. In one case the area involved was larger than the others, due to the presence of a calcification of considerable size, which was crushed on the sinus wall by the stent. In the same patient, the highest value of first principal stress was observed due to the compression of a portion of the aorta between two lateral hooks.
Then the deformation of the aorta was analysed: it was established that the most deformed area is also in this case the lower sinuses area, due to the presence of the lower stent cage. A less intense, but larger area of deformation was also found in the upper part of the aorta due to the presence of the upper device's cage. The importance of obtaining mild deformations makes it possible to avoid damages to the aorta's wall, which would obviously lead to very serious consequences for the patient.
The third analysis looked at the Von Mises stresses on the stent. It was possible to observe the presence of two great stress areas, i.e. the characteristic curvatures of some of the cells of the lower cage and the upper area of the lateral hooks. This can be reconducted to the geometry of these two areas, which are very small and particular, and will therefore reasonably be subjected to very high stresses in order to ensure the correct opening and adhesion of the device within the aortic root. The resistance of these particular areas under high stress is very important, as their rupture would result in irreversible damage to the stent, causing malfunction of the prosthetic valve and the presence of metal debris within the blood stream.
Finally, the distance between the stent and the aorta was assessed. It was observed that in all patients the lower part of the prosthesis is fully adhered to the wall of the patient's anatomy, while the upper part exhibits slightly different behaviour according to specific anatomies. in some cases, in fact, the three upper crowns adhere almost perfectly to the curvature of the aorta, while in others the resulting distance may be greater. This factor must be considered, as the presence of a metal structure in the middle of the aorta could lead to an obstruction of blood passage, and in the worst cases to the formation of clots or haemolysis of red blood cells.
For all analysed quantities, their distribution was consistent in all six patients, except for a few particularities, due precisely to the different anatomical geometry of the various simulations.
In conclusion, the patient-specific computational simulations for the transcatheter aortic valve implantation procedure developed in this study showed that for cardiac surgery is crucial to be aware of each patient's specific anatomy, in line with what has been analysed in previous literature. In fact, each patient has different anatomy and morphology that

could make the TAVI outcomes prediction difficult without the use of additional tools, such as *in silico* simulations. In addition to choosing the correct size device, correct positioning is also of prime importance. As shown in chapter six, different geometries and placements are associated with different stress and deformation responses.
Once again, the great versatility of *in silico* studies is also evident, as it was possible to adapt the modelling of this procedure to six different patient-specific cases, thus confirming the importance of respecting these two aspects in order to accurately reproduce this surgical procedure and its outcomes.
Studies of this kind, if carried out prior to surgery or during the validation of a product, can highlight possible weaknesses or criticalities of an aortic device and its implant.

7.2. Limitations

Our FE model is not absent from limitations. For what concerns the measurement phase, the main limitation of this study is due to the use of ImageJ. In fact, using a photograph of the device placed next to a graph paper, which was used as a scale, in order to obtain all the measurements necessary for the development of a CAD of the neo2 accuracy, it is possible that there were inaccuracies in the measurement. It is therefore important to remember that measurements, being indirect, are not completely reliable, as the resolution of the images themselves did not allow for a perfectly accurate reproduction of the correct dimensions of the real device.
Furthermore, given the geometric conformation of the device and the curvature of the stent, it was not possible to detect any differences (which, if present, would be minimal) in the nitinol cage thickness between the lower and upper parts. The connection zone between the two parts of the stent was recreated with a hole, based on what is present in the literature and on what could be observed from the patients' angiographies, as the product could not be damaged to open the skirt to see its actual geometry. For this reason, the dimensions of this area in particular have been assumed and may therefore not reflect the true dimensions.
With regard to the patient-specific anatomies, as it was not possible to derive the geometry of natural aortic valves from CT images, the leaflet surfaces were created by following reference points describing the geometry of the Valsalva sinuses. This may not be the case in real patient anatomy.
The positioning of the Acurate neo2 inside the aortic roots in the simulations was carried out from the information obtained from the angiographies taken during the respective patient's operation. However, not all the available images were clear enough to be certain

of a correct positioning.
The modelling of material properties is not without limitations. the assumption of linear elasticity for the pericardium of the Acurate neo2, for the natural valve and for the calcifications is widely used in the literature but does not reflect the actual and true behaviour of these components, thus introducing possible errors in the results. The mechanical properties could therefore be improved by introducing more complex models, even though there is not much data available in the literature, particularly for the pericardium and the natural valve. For the latter, it would also be appropriate to use a higher elastic modulus, closer to the real one. The same applies to the aorta, for which a hyperelastic isotropic material was chosen, thus neglecting its true anisotropic nature. An important development could also be to use data for the properties of these patient domain' materials from pathological aortic roots.
The last major limitation of these simulations is their high computational cost. In fact, their durations range from about fifteen to almost twenty-four hours.

7.3. Future developments

The development of these six patient-specific structural computational simulations with the Acurate neo2 device opens up a vast range of future perspectives.
Starting from the beginning, i.e. the creation of the CAD of the prosthetic valve, future studies could develop parametric models of this device. In fact, the use of parameters could allow to study the influence of individual aspects on the behaviour of the Acurate neo2 when implanted in the patient-specific anatomy. There are several quantities that can be investigated as they could potentially change the response of the anatomy and the device, starting with the thickness of the leaflets and skirt, the number, height and general size of the cells, the thickness of the stent mesh, and the orientation angle of the side hooks, i.e. the middle cage, that characterise this device. In addition, the development of a parametric model would make it possible to avoid scaling in order to obtain the various sizes, which, as pointed out in the previous paragraph, is one of the limitations of this study. In this way, it would be possible to obtain the three sizes more accurately and quickly.
A further development of our work could be the creation of a one-dimensional model of the device, which can then be discretized using 1D beam-type elements. This step is fundamental in order to decrease the computational cost of extremely complex simulations such as those developed in this thesis, while maintaining satisfactory quality of results and accuracy.
Decreasing the complexity of this model becomes very important, especially to allow what

is the natural continuation of a structural computational thesis, namely the development of fluid-structure models (FSI). As already pointed out in chapter three, FSI models are in fact the most complex but also the most comprehensive in the study and analysis of TAVI in all its aspects, thanks to the introduction of the fluid domain composed, in this case, of blood. FSI simulations would allow the study of all parameters of great interest in the clinical field, such as paravalvular regurgitation, peak blood flow velocity and pressure gradient. In this way it would be possible to evaluate the fluid-dynamics outcomes of this procedure in the six patients and validate them with the measurements that can be obtained from diagnostic tests.

Bibliography

[1] M. R. Dweck, N. A. Boon, and D. E. Newby, "Calcific aortic stenosis: a disease of the valve and the myocardium," *Journal of the American College of Cardiology*, vol. 60, no. 19, pp. 1854–1863, 2012.

[2] O. M. Rotman, M. Bianchi, R. P. Ghosh, B. Kovarovic, and D. Bluestein, "Principles of tavr valve design, modelling, and testing," *Expert review of medical devices*, vol. 15, no. 11, pp. 771–791, 2018.

[3] X. Liu, W. Zhang, P. Ye, Q. Luo, and Z. Chang, "Fluid-structure interaction analysis on the influence of the aortic valve stent leaflet structure in hemodynamics," *Frontiers in Physiology*, p. 910, 2022.

[4] S. Wald, A. Liberzon, and I. Avrahami, "A numerical study of the hemodynamic effect of the aortic valve on coronary flow," *Biomechanics and modeling in mechanobiology*, vol. 17, no. 2, pp. 319–338, 2018.

[5] R. P. Ghosh, G. Marom, M. Bianchi, K. D'souza, W. Zietak, and D. Bluestein, "Numerical evaluation of transcatheter aortic valve performance during heart beating and its post-deployment fluid–structure interaction analysis," *Biomechanics and modeling in mechanobiology*, vol. 19, no. 5, pp. 1725–1740, 2020.

[6] G. Luraghi, F. Migliavacca, C. Chiastra, A. Rossi, B. Reimers, G. G. Stefanini, and J. F. R. Matas, "Does clinical data quality affect fluid-structure interaction simulations of patient-specific stenotic aortic valve models?," *Journal of Biomechanics*, vol. 94, pp. 202–210, 2019.

[7] G. Luraghi, F. Migliavacca, A. García-González, C. Chiastra, A. Rossi, D. Cao, G. Stefanini, and J. F. Rodriguez Matas, "On the modeling of patient-specific transcatheter aortic valve replacement: a fluid–structure interaction approach," *Cardiovascular engineering and technology*, vol. 10, no. 3, pp. 437–455, 2019.

[8] A. A. Basri, M. Zuber, E. I. Basri, M. S. Zakaria, A. F. Aziz, M. Tamagawa, and K. A. Ahmad, "Fluid structure interaction on paravalvular leakage of transcatheter aortic

valve implantation related to aortic stenosis: a patient-specific case," *Computational and mathematical methods in medicine*, vol. 2020, 2020.

[9] H. S. Kandail, S. D. Trivedi, A. C. Shaikh, T. K. Bajwa, P. Daniel, A. Jahangir, and J. F. LaDisa Jr, "Impact of annular and supra-annular corevalve deployment locations on aortic and coronary artery hemodynamics," *Journal of the mechanical behavior of biomedical materials*, vol. 86, pp. 131–142, 2018.

[10] J. Li, W. Yan, W. Wang, S. Wang, and L. Wei, "Comparison of balloon-expandable valve and self-expandable valve in transcatheter aortic valve replacement: A patient-specific numerical study," *Journal of Biomechanical Engineering*, vol. 144, no. 10, p. 104501, 2022.

[11] S. Pasta, S. Cannata, G. Gentile, M. Di Giuseppe, F. Cosentino, F. Pasta, V. Agnese, D. Bellavia, G. M. Raffa, M. Pilato, *et al.*, "Simulation study of transcatheter heart valve implantation in patients with stenotic bicuspid aortic valve," *Medical & Biological Engineering & Computing*, vol. 58, no. 4, pp. 815–829, 2020.

[12] A. Caballero, W. Mao, R. McKay, and W. Sun, "The impact of balloon-expandable transcatheter aortic valve replacement on concomitant mitral regurgitation: a comprehensive computational analysis," *Journal of the Royal Society Interface*, vol. 16, no. 157, p. 20190355, 2019.

[13] A. J. Weinhaus and K. P. Roberts, "Anatomy of the human heart," in *Handbook of cardiac anatomy, physiology, and devices*, pp. 51–79, Springer, 2005.

[14] F. H. Netter, *Netter Atlas of Human Anatomy.*

[15] N. Piazza, P. de Jaegere, C. Schultz, A. E. Becker, P. W. Serruys, and R. H. Anderson, "Anatomy of the aortic valvar complex and its implications for transcatheter implantation of the aortic valve," *Circulation: Cardiovascular Interventions*, vol. 1, no. 1, pp. 74–81, 2008.

[16] R. H. Anderson, "Clinical anatomy of the aortic root," *Heart*, vol. 84, no. 6, pp. 670–673, 2000.

[17] M. Rozeik, D. Wheatley, and T. Gourlay, "The aortic valve: structure, complications and implications for transcatheter aortic valve replacement," *Perfusion*, vol. 29, no. 4, pp. 285–300, 2014.

[18] M. Loukas, E. Bilinsky, S. Bilinsky, C. Blaak, R. S. Tubbs, and R. H. Anderson, "The anatomy of the aortic root," *Clinical anatomy*, vol. 27, no. 5, pp. 748–756, 2014.

[19] S. A. Akhter, "The heart and pericardium," *Thoracic Surgery Clinics*, vol. 21, no. 2, pp. 205–217, 2011.

[20] S. Y. Ho, "Structure and anatomy of the aortic root," *European journal of echocardiography*, vol. 10, no. 1, pp. i3–i10, 2009.

[21] L. Zocchi, *Principi di Fisiologia*. Edises, 2012.

[22] https://my.clevelandclinic.org/health/diseases/17600-valve-disease-types.

[23] https://www.heartfoundation.org.nz/your-heart/heart-conditions/heart-valve-disease.

[24] R. V. Freeman and C. M. Otto, "Spectrum of calcific aortic valve disease: pathogenesis, disease progression, and treatment strategies," *Circulation*, vol. 111, no. 24, pp. 3316–3326, 2005.

[25] M. Bäck, T. C. Gasser, J.-B. Michel, and G. Caligiuri, "Biomechanical factors in the biology of aortic wall and aortic valve diseases," *Cardiovascular research*, vol. 99, no. 2, pp. 232–241, 2013.

[26] B. Iung and A. Vahanian, "Epidemiology of valvular heart disease in the adult," *Nature Reviews Cardiology*, vol. 8, no. 3, pp. 162–172, 2011.

[27] J. J. Thaden, V. T. Nkomo, and M. Enriquez-Sarano, "The global burden of aortic stenosis," *Progress in cardiovascular diseases*, vol. 56, no. 6, pp. 565–571, 2014.

[28] C. Rostagno, "Heart valve disease in elderly," *World Journal of Cardiology*, vol. 11, no. 2, p. 71, 2019.

[29] A. Vahanian, F. Beyersdorf, F. Praz, M. Milojevic, S. Baldus, J. Bauersachs, D. Capodanno, L. Conradi, M. De Bonis, R. De Paulis, *et al.*, "2021 esc/eacts guidelines for the management of valvular heart disease: developed by the task force for the management of valvular heart disease of the european society of cardiology (esc) and the european association for cardio-thoracic surgery (eacts)," *European heart journal*, vol. 43, no. 7, pp. 561–632, 2022.

[30] H. Baumgartner, J. Hung, J. Bermejo, J. B. Chambers, T. Edvardsen, S. Goldstein, P. Lancellotti, M. LeFevre, F. Miller Jr, C. M. Otto, *et al.*, "Recommendations on the echocardiographic assessment of aortic valve stenosis: a focused update from the european association of cardiovascular imaging and the american society of echocardiography," *European Heart Journal-Cardiovascular Imaging*, vol. 18, no. 3, pp. 254–275, 2017.

[31] F. E. Peeters, S. J. Meex, M. R. Dweck, E. Aikawa, H. J. Crijns, L. J. Schurgers, and B. L. Kietselaer, "Calcific aortic valve stenosis: hard disease in the heart: a biomolecular approach towards diagnosis and treatment," *European heart journal*, vol. 39, no. 28, pp. 2618–2624, 2018.

[32] J. Ross Jr and E. Braunwald, "Aortic stenosis," *Circulation*, vol. 38, no. 1s5, pp. V–61, 1968.

[33] B. Iung, A. Cachier, G. Baron, D. Messika-Zeitoun, F. Delahaye, P. Tornos, C. Gohlke-Barwolf, E. Boersma, P. Ravaud, and A. Vahanian, "Decision-making in elderly patients with severe aortic stenosis: why are so many denied surgery?," *European heart journal*, vol. 26, no. 24, pp. 2714–2720, 2005.

[34] G. A. Fishbein, F. J. Schoen, and M. C. Fishbein, "Transcatheter aortic valve implantation: status and challenges," *Cardiovascular Pathology*, vol. 23, no. 2, pp. 65–70, 2014.

[35] A. Cribier, H. Eltchaninoff, A. Bash, N. Borenstein, C. Tron, F. Bauer, G. Derumeaux, F. Anselme, F. Laborde, and M. B. Leon, "Percutaneous transcatheter implantation of an aortic valve prosthesis for calcific aortic stenosis: first human case description," *Circulation*, vol. 106, no. 24, pp. 3006–3008, 2002.

[36] https://www.euroscore.org/index.php?id=37&lang=en.

[37] N. Piazza, R. Lange, G. Martucci, and P. W. Serruys, "Patient selection for transcatheter aortic valve implantation: patient risk profile and anatomical selection criteria," *Archives of cardiovascular diseases*, vol. 105, no. 3, pp. 165–173, 2012.

[38] W. C. Members, C. M. Otto, R. A. Nishimura, R. O. Bonow, B. A. Carabello, J. P. Erwin III, F. Gentile, H. Jneid, E. V. Krieger, M. Mack, *et al.*, "2020 acc/aha guideline for the management of patients with valvular heart disease: a report of the american college of cardiology/american heart association joint committee on clinical practice guidelines," *Journal of the American College of Cardiology*, vol. 77, no. 4, pp. e25–e197, 2021.

[39] L. A. Goeddel, J. Serini, J. W. Steyn, A. S. Evans, S. Dwarakanath, H. Ramakrishna, J. Augoustides, and M. B. Brady, "Transcatheter aortic valve replacements: Current trends and future directions," in *Seminars in Cardiothoracic and Vascular Anesthesia*, vol. 23, pp. 282–292, SAGE Publications Sage CA: Los Angeles, CA, 2019.

[40] K. Hayashida, T. Lefèvre, B. Chevalier, T. Hovasse, M. Romano, P. Garot, D. My-

lotte, J. Uribe, A. Farge, P. Donzeau-Gouge, *et al.*, "Transfemoral aortic valve implantation: new criteria to predict vascular complications," *JACC: Cardiovascular Interventions*, vol. 4, no. 8, pp. 851–858, 2011.

[41] M. Chiarito, A. Spirito, J. Nicolas, A. Selberg, G. Stefanini, A. Colombo, B. Reimers, A. Kini, S. K. Sharma, G. D. Dangas, *et al.*, "Evolving devices and material in transcatheter aortic valve replacement: What to use and for whom," *Journal of Clinical Medicine*, vol. 11, no. 15, p. 4445, 2022.

[42] 1. https://www.heartvalves.com/gb/edwards-sapien-3-tavi/edwards-sapien-3-ultra-valve.

[43] D. H. Adams, J. J. Popma, M. J. Reardon, S. J. Yakubov, J. S. Coselli, G. M. Deeb, T. G. Gleason, M. Buchbinder, J. Hermiller Jr, N. S. Kleiman, *et al.*, "Transcatheter aortic-valve replacement with a self-expanding prosthesis," *New England Journal of Medicine*, vol. 370, no. 19, pp. 1790–1798, 2014.

[44] W. F. Fearon, S. Kodali, D. Doshi, M. P. Fischbein, A. C. Yeung, E. M. Tuzcu, C. S. Rihal, V. Babaliaros, A. Zajarias, H. C. Herrmann, *et al.*, "Outcomes after transfemoral transcatheter aortic valve replacement: a comparison of the randomized partner (placement of aortic transcatheter valves) trial with the nrca (nonrandomized continued access) registry," *JACC: Cardiovascular Interventions*, vol. 7, no. 11, pp. 1245–1251, 2014.

[45] D. Mahtta, I. Y. Elgendy, and A. A. Bavry, "From corevalve to evolut pro: reviewing the journey of self-expanding transcatheter aortic valves," *Cardiology and therapy*, vol. 6, no. 2, pp. 183–192, 2017.

[46] M. J. Reardon, "The acurate neo™ and neo2™ valve systems," *Heart International*, 2021.

[47] H. Möllmann, D. M. Holzhey, M. Hilker, S. Toggweiler, U. Schäfer, H. Treede, M. Joner, L. Søndergaard, T. Christen, D. J. Allocco, *et al.*, "The acurate neo2 valve system for transcatheter aortic valve implantation: 30-day and 1-year outcomes," *Clinical Research in Cardiology*, vol. 110, no. 12, pp. 1912–1920, 2021.

[48] L. Petrini and F. Migliavacca, "Biomedical applications of shape memory alloys," *Journal of Metallurgy*, vol. 2011, 2011.

[49] T. W. Duerig, "Superelastic nitinol for medical device.," *Medical Plastics and Biomaterials.*, pp. 31–42, 1997.

[50] https://jenavalve.com/jenavalve-receives-ce-mark/.

[51] H. Treede, F.-W. Mohr, S. Baldus, A. Rastan, S. Ensminger, M. Arnold, J. Kempfert, and H.-R. Figulla, "Transapical transcatheter aortic valve implantation using the jenavalve™ system: acute and 30-day results of the multicentre ce-mark study," *European Journal of Cardio-Thoracic Surgery*, vol. 41, no. 6, pp. e131–e138, 2012.

[52] G. Marom, "Numerical methods for fluid–structure interaction models of aortic valves," *Archives of Computational Methods in Engineering*, vol. 22, no. 4, pp. 595–620, 2015.

[53] G. Luraghi, J. F. Rodriguez Matas, and F. Migliavacca, "In silico approaches for transcatheter aortic valve replacement inspection," *Expert Review of Cardiovascular Therapy*, vol. 19, no. 1, pp. 61–70, 2021.

[54] M. Toma, S. Singh-Gryzbon, E. Frankini, Z. Wei, and A. P. Yoganathan, "Clinical impact of computational heart valve models," *Materials*, vol. 15, no. 9, p. 3302, 2022.

[55] Z. A. Wei, S. J. Sonntag, M. Toma, S. Singh-Gryzbon, and W. Sun, "Computational fluid dynamics assessment associated with transcatheter heart valve prostheses: a position paper of the iso working group," *Cardiovascular engineering and technology*, vol. 9, no. 3, pp. 289–299, 2018.

[56] https://www.bostonscientific.com/en-EU/products/transcatheter-heart-valve/acurateneo2-tavi-valve-system.html.

[57] S. Morganti, N. Brambilla, A. Petronio, A. Reali, F. Bedogni, and F. Auricchio, "Prediction of patient-specific post-operative outcomes of tavi procedure: The impact of the positioning strategy on valve performance," *Journal of biomechanics*, vol. 49, no. 12, pp. 2513–2519, 2016.

[58] F. Auricchio, S. Morganti, and D. Vella, "Transcatheter aortic valve implantation: from clinical data to finite element models,"

[59] A. N. Azadani, S. Chitsaz, P. B. Matthews, N. Jaussaud, J. Leung, T. Tsinman, L. Ge, and E. E. Tseng, "Comparison of mechanical properties of human ascending aorta and aortic sinuses," *The Annals of thoracic surgery*, vol. 93, no. 1, pp. 87–94, 2012.

[60] G. A. Holzapfel, G. Sommer, and P. Regitnig, "Anisotropic mechanical properties of tissue components in human atherosclerotic plaques," *Journal of biomechanical engineering*, vol. 126, no. 5, pp. 657–665, 2004.

List of Figures

List of Tables